The Optimal Design of Laminated Plates for Maximum Buckling Load using Finite Element and Analytical Methods

by

Mark Walker

Submitted to the Department of Mechanical Engineering
in partial fulfillment of the requirements for the degree of

Doctor of Philosophy

at the

UNIVERSITY OF NATAL

December 1994

The Optimal Design of Laminated Plates for Maximum Buckling Load using Finite Element and Analytical Methods

by

Mark Walker

Submitted to the Department of Mechanical Engineering
on December 13, 1994, in partial fulfillment of the
requirements for the degree of
Doctor of Philosophy

Abstract

In the first part of the study, finite element solutions are presented for the optimal design of symmetrically laminated rectangular plates subject to a combination of simply supported, clamped and free boundary conditions. The design objective is the maximisation of the biaxial buckling load by determining the fibre orientations optimally with the effects of bending-twisting coupling taken into account. The finite element method coupled with an optimisation routine is employed in analysing and optimising the laminated plate designs. The effect of boundary conditions, the number of layers and bending-twisting coupling on the optimal ply angles and the buckling load are numerically studied.

Optimal buckling designs of symmetrically laminated rectangular plates under in-plane uniaxial loads which have a nonuniform distribution along the edges are presented in the second part of the study. In particular, point loads, partial uniform loads and nonuniform loads are considered in addition to uniformly distributed in-plane loads which provide the benchmark solutions. Poisson's effect is taken into account when in-plane restraints are present along the unloaded edges. Restraints give rise to in-plane loads at unloaded edges which lead to biaxial loading, and may cause premature instability. The laminate behavior with respect to fiber orientation changes significantly in the presence of Poisson's effect as compared to that of a laminate where this effect is neglected. This change in behavior has significant implications for design optimisation as the optimal values of design variables with or without restraints differ substantially. In the present

study, the design objective is the maximisation of the uniaxial buckling load by optimally determining the fiber orientations. Numerical results, determined using the finite element method, are given for a number of boundary conditions and for uniformly and non-uniformly distributed buckling loads.

In the third part of the study, finite element solutions are presented for the optimal design of symmetrically laminated rectangular plates with central circular cut-outs subject to a combination of simply supported, clamped and free boundary conditions. The design objective is the maximisation of the biaxial buckling load by determining the fiber orientations optimally. The effect of boundary conditions and bending-twisting coupling on the optimal ply angles and the buckling load are numerically studied. The results are compared to those for laminates without holes.

The fourth part of the present study gives optimal designs of symmetrically laminated angle-ply plates, which are obtained with the objective of maximising the initial postbuckling stiffness. The design involves optimisation over the ply angles and the stacking sequence to obtain the best laminate configuration. The stacking sequence is chosen from amongst five candidate designs. It is shown that the best configuration depends on the ratio of the in-plane loads in the x and y directions. Results are also given for two additional configurations which do not exhibit bending-twisting coupling.

The final section of the present study deals with the optimal design of uniaxially loaded laminated plates subject to elastic in-plane restraints along the unloaded edges for a maximum combination of prebuckling stiffness, postbuckling stiffness and buckling load. This multiobjective study illustrates that improved buckling and postbuckling performance can be obtained from plates which are designed in this fashion. The multiobjective results are also compared to single objective design results.

Preface

The five design optimisation studies contained in this thesis were done by myself, and have not been submitted (in part, or in whole) to any other University.

The research work was supervised by Professor Sarp Adali and Professor Victor Verijenko.

Well, as before, *pushing back the old frontiers of science and technology* has been tiring, but I guess it was worth it in the end.

Dedication

This Doctoral thesis is dedicated to my parents, Emma and Neville Walker

Acknowledgments

The author is indebted to the following:

Professor Sarp Adali

For his close guidance and encouragement

Professor Victor Verijenko

For his help

The staff at the Departments of Mechanical Engineering, Technikon Natal and the University of Natal

Contents

Chapter 1

Literature Survey

1.1 Introduction

Laminated composite materials are used with increasing frequency in various technical applications, particularly in the fields of automotive, aerospace and marine engineering. This is primarily due to the high specific strength and stiffness values that these materials offer. Structures composed of composite materials often contain components which may be modelled as rectangular plates. A common type of composite plate is the symmetrically laminated angle ply configuration which avoids strength reducing bending-stretching effects by virtue of mid-plane symmetry. An important failure mode for these plates is buckling under in-plane loading. The buckling resistance of fiber composite plates can be improved by using the ply angle as a design variable, and determining the optimal angles to maximise the buckling load. Optimal design of composite plates is necessary to

realise the full potential of fiber-reinforced materials.

A large amount of research into the buckling of laminated plates has been carried out by numerous workers, but there remains much to be done on the optimal design of these plates. One phenomenon associated with symmetric angle-ply configurations is the occurrence of bending-twisting coupling which may cause significantly different results as compared to cases in which this coupling is exactly zero. The effect of bending-twisting coupling becomes even more pronounced for laminates with few layers. Due to this coupling, closed-form solutions cannot be obtained for any of the boundary conditions and this situation led to neglecting bending-twisting coupling in several studies involving the optimisation of symmetric laminates under buckling loads. In actual fact, closed-form solutions for symmetric laminates are not available even for the simplified models where this coupling is neglected except if the boundary conditions are simply supported all around.

The first part of the present study adopts a numerical approach to include the effect of bending-twisting coupling and to obtain the optimal design solutions of laminated plates for a variety of boundary conditions. The finite element formulation, which is used in conjunction with an optimisation routine to compute the optimal fiber orientations, is based on Mindlin type theory for thin laminated composite plates. Numerical results are given for various combinations of boundary conditions and optimal designs with and without bending-twisting coupling are compared.

Poisson's effect manifests itself as in-plane loads if the unloaded edges of a uniaxially loaded plate are restrained from translating freely. This in turn transforms a uniaxial buckling problem into a biaxial one and causes a reduction in the buckling load, as compared to the *classic* case, where the unloaded plate edges are free from restraint. Moreover, the optimal values of design variables change as compared to the classic case. In many practical situations, transverse movement of unloaded edges is restricted by adjacent panels, supports or stiffeners, inducing a transverse in-plane compressive force. In these cases, the buckling of uniaxially compressed rectangular plates is affected by the so-called *Poisson Plate Instability* phenomenon.

The second part of the present study deals with the optimal design of uniaxially loaded symmetrically laminated rectangular plates subject to in-plane restraints along the unloaded edges taking the ply angle as the design variable to maximise the buckling load. The results are obtained for uniformly and nonuniformly distributed in-plane loads. In particular, point loads, partial uniform loads and nonuniform loads are considered in addition to a full uniform load. Taken into account also are the effects of bending-twisting coupling, as well as various combinations of free, simply supported and clamped boundary conditions. These effects rule out the possibility of an analytical solution and thus the finite element method is used to analyse the problem and to determine the buckling loads. Optimal designs are compared with those obtained for plates without in-plane restraints. This study also illustrates that optimal designs for maximum buckling

load based on classical analysis becomes irrelevant and leads to totally erroneous results in the presence of in-plane restraints. Furthermore, an approximation of nonuniform loads by uniform ones again leads to inaccurate buckling loads and non-optimal ply angles.

Plates with central cut-outs have decreased buckling resistance, and the use of values determined in optimal design studies of plates without holes can lead to non-optimal designs. The presence of holes in laminated plates complicates the modelling, and as such, little work has concentrated on the study of such problems. Even less dealing with the optimal design of such plates has been reported in the literature. In the third part of the present study, numerical results are given for biaxially loaded laminated plates with central circular cut-outs having various combinations of boundary conditions, and optimal designs of these plates are compared to those for plates without holes.

Quite often, composite structures are required to carry loads beyond their buckling limit. In these cases, the postbuckling stiffness has to be maximised to improve the load carrying capability beyond the critical buckling load. This is the objective of the fourth part of the present study in which symmetric angle-ply laminates are designed for maximum postbuckling stiffness. In this study, a method is proposed to determine the optimal fiber orientation and stacking sequence of rectangular laminates by considering the initial post-buckling stiffnesses in *both* the x and y directions. Design optimisation involves the comparison of the postbuckling performance of several laminate configurations with optimal

ply angles. Finally, the post-buckling performance of two laminated plates having in-plane and bending orthotropy are studied.

The last section of the present study deals with the optimal design of uniaxially loaded laminates plates subject to elastic in-plane restraints along the unloaded edges for a maximum combination of prebuckling and postbuckling stiffnesses, and buckling load. This multiobjective study illustrates that improved buckling and postbuckling performance can be obtained from plates which are designed in this fashion. The multiobjective results are also compared to single objective design results.

1.2 The finite element method

The finite element method is a numerical analysis technique for obtaining approximate solutions to engineering problems. Although it was originally developed to study the stresses in complex airframes, it has since been extended and applied to continuum mechanics.

It is in general necessary to obtain approximate numerical solutions to engineering problems rather than analytical solutions. The governing equations and boundary conditions of these problems may be readily available, however there is usually no simple analytical solution to these problems. The difficulty, for example may arise as a result of a complex geometry or some other features of the problem which is either irregular or complicated.

One possibility is to make some simplifying assumptions that make the problem easier to solve. In some cases, this may be acceptable. Often, however, this approach results in serious inaccuracies or wrong answers. An alternative way to solve these problems is to keep the complexities of the problem and try to find an approximate solution using a numerical technique. Over the years, several approximate numerical analysis methods have been developed. One of the most commonly used methods is the general finite difference scheme [1], [2]. The finite difference model of a problem gives a pointwise approximation to governing equations which is improved as more points are included. This method may be used to solve fairly difficult problems.

If irregular geometries or unusual boundary conditions are considered, the finite difference techniques become difficult to implement. Another numerical method which has been developed for use in engineering is the finite element method. Unlike the finite difference method, which considers the solution region as an array of grid points, the finite element method considers the solution region as a complete part of many small, interconnected parts or elements. A finite element model of a problem gives a piecewise approximation to the governing equations. These small pieces or elements can be assembled together in many ways to cover the solution region, even for very complex geometries.

1.2.1 The Concept of the Finite Element Method

The finite element discretization procedures reduce the problem to one of a finite number of unknowns by dividing the solution region into small elements and the final solution is defined in terms of assumed approximating functions for each element. The approximating functions (or interpolation functions) are defined at specified points called nodes or nodal points. Nodes are usually placed on the element boundaries. In addition to boundary nodes an element may also have interior nodes. For the finite element representation of a problem, the nodal values of the field variables become the new unknowns. The degree of approximation does not only depend on the size and number of the elements, but also on the interpolation functions selected. The functions cannot be chosen arbitrarily, because special conditions should be satisfied. The functions are usually chosen so that the field variable or its derivatives are continuous across adjoining element boundaries. An important advantage of the finite element method which is different from other approximate numerical methods is its ability to formulate expressions for individual elements before assembling them together to model the entire problem. The steps listed below are useful in explaining how the finite element method works [3].

1. Discretize the continuum. The fist step is to divide the continuum or solution region into elements. It is not only desirable but also may be necessary to use different types of elements in the same solution. The number and the

types of elements to be used in a given problem are matters of engineering judgment.

2. Select interpolation functions. The next step is to assign nodes to each element and then choose the type of interpolation function to represent the variation of the field variable over the element. Polynomials are usually selected as interpolation functions for the field variable, since they are easily integrated and differentiated.

3. Find the element properties. Once the finite element model has been established (the elements and interpolation functions have been selected) the matrix equations are determined to express the properties of the individual elements.

4. Assemble the element properties to obtain the system equations. The matrix equations are combined to express the behaviour of the elements and formed to express the behaviour of the entire solution system.

5. Solve the system equations.

1.2.2 Advantages of the Finite Element Method

One of the main advantages of the finite element method is that the method can handle irregular geometries routinely which is useful since, if irregular geometries are present, closed-form analytical solutions, in general, are not available.

Another advantage of the method is that a variable spacing of the nodes is also routinely handled. When a body is discretized using finite elements, the nodes are said to form a mesh. When the nodes are not equally spaced, the mesh is said to be graded. Another advantage of the finite element method over analytical solution techniques is its ability to handle non-homogeneous and anisotropic materials. There is little extra effort required in the finite element method formulation when these types of materials are modeled. The sizes and shapes of the elements can be selected to create highly irregular geometric forms. Triangular elements are particularly flexible in this respect, while rectangular elements can be simpler in other cases. The element size can be varied, so areas of steep stress gradients can be approximated in particular detail (Figure 1). Any type of external load can be considered. Distributed loads are replaced by equivalent concentrated nodal point loads. The choice of boundary conditions is variable and it is possible to examine the effects of nonlinear properties of materials. A study of the progress of plastification in a notched plate subjected to increasing axial load is an example of this subject [4]. The finite element technique is also used for studying the solution of complex buckling [5] and vibration problems, as well as crack and fatigue effects [6].

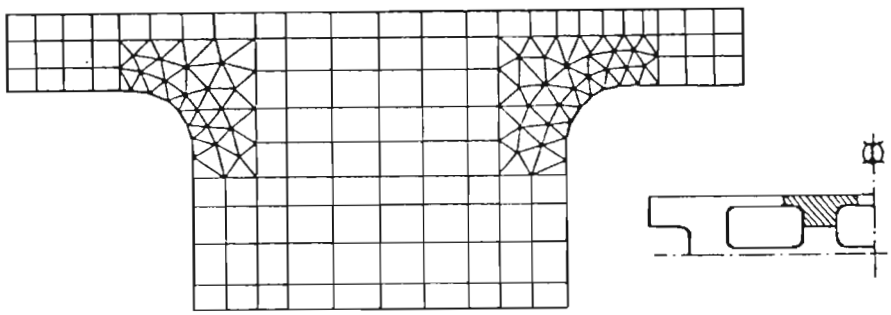

Figure 1. Combinations of triangular and rectangular elements in a typical complex structural model.

1.2.3 A Brief History of The Finite Element Method

The finite element method was developed simultaneously in the fields of applied mathematics and engineering. The first study to use piecewise continuous functions defined over triangular domains appear in the applied mathematics literature with the work of Courant [7] in 1943,who motivated by Euler's [8] paper, used an assemblage of triangular elements and the principle of minimum potential energy to study the St. Venant torsion problem. Polya [9], [10], Hersch [11] and Weinberger [12], [13] worked on finding bounds on eigenvalues using this method. In 1959, Grenestadt [14], motivated by Morse & Feshback [15], made an approach involving cells instead of points, dividing the solution domain into sub domains. In his theory, he describes a procedure for representing the unknown functions by a series of functions. Using continuity requirements, continuous problem are then

discretized. This theory allows for irregularly shaped cell meshes and contains many of the essential and fundamental ideas of finite elements. White [16] and Friedrichs [17] used triangularly shaped elements, in regular meshes, to develop difference equations from variational principles. Numerous studies concerning discretization errors, rates of convergence and stability for different types of finite element approximations have appeared in the literature [18 - 39]. The finite element method has also been applied to nonlinear problems [40]. The development of suitable function approximations to field variables has been considered in the literature on spline functions [41 - 54].

The earliest study in the engineering literature appears to be that of Hrenikoff [55], who assumed a continuum structure to be divided into elements or structural sections. McHenry [56] in 1943 and Newmark [57] in 1949 further developed this concept of discretization. Argyris and collaborators [58 - 64] published a series of papers on linear structural analysis and efficient solution techniques suited for automatic digital computation. In 1956, Turner *et al* [65] published a paper on the solution of plane stress problems by means of triangular elements whose properties were determined from the equations of elasticity theory. This study introduced the direct stiffness method for determining finite element properties. A further study on the plane elasticity problem was presented by Clough [66]. Besseling [67], Melosh [68], Fraeijs de Veubeke [69] and Jones [70] recognized that the finite element method was a form of the Ritz method and confirmed it as a general technique to handle elastic continuum problems. Zienkiewicz & Cheung

part at infinity [72].

Problem Statement

Consider some domain D bounded by the surface Σ. Let ϕ be a scalar function defined in the interior of D such that the behaviour of ϕ in D is given by

$$L(\phi) - f = 0 \tag{1.1}$$

where f is a known scalar function of the independent variables and L is a linear or nonlinear differential operator. It is assumed that the physical parameters in the differential operator are known constants or functions. In n dimensions, second-order differential operators can usually be reduced, by a suitable transformation, to the form

$$L(\ ) = \sum_{i=1}^{n} A_i \frac{\partial^2(\ )}{\partial x_i^2} + \sum_{i=1}^{n} B_i \frac{\partial(\ )}{\partial x_i} + (\ )C + D \tag{1.2}$$

where coefficients , A_i, B_i and C and the term D may be functions. The operator as given in equation (1.2) is linear if A_i, B_i, C and D are functions only of the independent variables (x_1, x_2, x_3, ..., x_n), and quasilinear if A_i, B_i, C and D are functions of x_i; and the dependent parameter, as well as first derivatives of the dependent parameter. An operator is linear only if

$$L(f + g) = L(f) + L(g) \tag{1.3}$$

[71] reported that the finite element method is applicable to all field problems which can be put into variational form.

Numerous papers may be found in the literature, dealing with all aspects of the finite element method and its applications to areas such as static and dynamic structural analysis, fluid flow and heat transfer.

1.2.4 Theoretical Formulation

Continuum Problems

In the *continuum* or Eulerian approach to nature, all processes are characterized by field quantities that are defined at every point in space. The independent variables in continuum problems are the coordinates of space and time. Continuum problems are concerned with fields of temperature, stress, mass concentration, displacement, electromagnetic and acoustic potentials, etc. These problems arise from the phenomena in nature that are approximately characterized by partial differential equations and their boundary conditions.

Continuum problems of mathematical physics are often referred to as boundary value problems because their solution is sought in some domain defined by a given boundary, on which certain conditions called *boundary conditions* are specified. The boundary is said to be closed if conditions affecting the solution of the problem are specified everywhere on the boundary and open if part of the boundary extends to infinity and no boundary conditions are specified on the

The general definition of the operator $L(\ )$ in equation (3.19) precludes a discussion of appropriate boundary conditions. However, without boundary conditions, equation (3.19) does not describe a specific problem.

Some Methods for Solving Continuum Problems

From equation (3.19), it is seen that the general problem is to find the unknown function ϕ that satisfies equation (3.19) and the associated boundary conditions specified on Σ. There are many alternative approaches to the solution of linear and nonlinear boundary value problems and they range from completely analytical to completely numerical. These can be listed as follows:

1. Direct integration (exact solutions).

a. Separation of variables.

b. Similarity solutions.

c. Fourier and Laplace transformations.

2. Approximate solutions.

a. Perturbation.

b. Power series.

c. Probability schemes.

d. Method of weighted residuals (MWR).

e. Finite difference techniques.

f. Ritz method.

g. Finite element method.

The Variational Approach

Often continuum problems have the different, but equivalent, differential and variational formulations. In the differential equation formulation, the problem is to integrate a differential equation or a system of differential equations subject to given boundary conditions. In the *classical variational formulation*, the problem is to find the unknown function or functions that extremize or make stationary a functional such as $I(\phi)$ or system of functionals subject to the same boundary conditions. The two problem formulations are equivalent because the functions which satisfy the differential equations and their boundary conditions also *extremize* or make *stationary* the functionals. The classical variational formulation of a continuum problem often has advantages over the differential equation formulation from the viewpoint of obtaining an approximate solution.

Firstly, the functional, which may actually represent some physical quantity in the problem, contains derivatives of order lower than that of the differential operator and an approximate solution can be sought in a larger class of functions.

Secondly, the problem may possess reciprocal variational formulations, that is, one functional must be minimized and another one of a different form must be maximized.

Third, the variational formulation allows us to treat very complicated boundary conditions as *natural boundary conditions.*

Fourth, from a mathematical viewpoint the variational formulation is helpful because it can sometimes be used to prove the existence of a solution by using calculus of variations.

This approach is especially convenient when it is applicable; but before it can be used, a variational statement for the continuum problem must be formulated, which means that the problem must be posed in a variational form.

Historically, variational methods are among the oldest means of obtaining solutions to problems in physics and engineering. One general method for obtaining approximate solutions to problems expressed in variational form is known as the Ritz method. This method is basically a forerunner of the finite element procedure. In fact, the finite element method is a special case of the Ritz method when the interpolation functions satisfy certain continuity requirements.

The Ritz Method

The Ritz method consists of assuming the form of the unknown solution in terms of known functions (trial functions) with unknown adjustable parameters. (The trial functions are also called coordinate functions.) The procedure is to substitute the trial functions into the functional and thereby express the functional in terms of the adjustable parameters. The functional is then differentiated with respect to each parameter and the resulting equation is set equal to zero. If there are n unknown parameters, there will be n simultaneous equations to be solved for these parameters. The accuracy of the approximate solution depends on the

choice of trial functions. The trial functions are defined over the whole solution domain and they satisfy at least some and usually all of the boundary conditions. If the exact solution is contained in the family of trial solutions, the Ritz procedure gives the exact solution. Generally, the approximation improves as the size of the family of trial functions and the number of adjustable parameters increase. The process of including more and more trial functions leads to a series of approximate solutions which converges to the true solution. Often a family of trial functions is constructed from polynomials of successively increasing degree, but in certain cases other kinds of functions may also offer advantages [73].

Relation of FEM to the Ritz Method

The finite element method and the Ritz method are essentially equivalent. Each method uses a set of trial functions as the starting point for obtaining an approximate solution; both methods take linear combinations of these trial functions and both models seek the combination of the trial functions that makes a given functional stationary. The major difference between the methods is that the assumed trial functions in the finite element method are not defined over the whole solution domain and they have to satisfy no boundary conditions but only certain continuity conditions. Because the Ritz method uses functions defined over the whole domain, it can be used only for domains of relatively simple geometric shape. In the finite element method the same geometric limitations exist, but only for the elements. Due to the fact that elements with simple shapes can be

assembled to represent quite complex geometries, the finite element is far more versatile and flexible than the Ritz method.

Generalising the definition of an element

The mathematical interpretation of the finite element requires the generalisation of the definition of an element which is in less physical terms. The elements are interconnected only at imaginary node points at the boundaries or surfaces of the elements. For the solid mechanics problems, in general, elements do not deform or change shape. They are defined as regions of space where a displacement field exists. The nodes of an element are located in space where the displacement and possibility of its derivatives are known or sought. The mathematical interpretation of a finite element mesh is that it is a spatial subdivision rather than a material subdivision [74].

Once the element mesh for the solution domain has been decided, the behaviour of the unknown field variable over each element is approximated by continuous functions expressed in terms of the nodal values of its derivatives up to a certain degree. The functions defined over each finite element are called *interpolation functions, shape functions*, or field variable models. The collection of the interpolation functions for the whole solution domain provides a piecewise approximation to the field variable.

Element Equations from the Variational Principle

The finite element solution to the problem involves determining the nodal values of ϕ so as to make the functional $I(\phi)$ stationary. To make $I(\phi)$ stationary with respect to the nodal values of ϕ, it is required that

$$\partial I(\phi) = \sum_{i=1}^{n} \frac{\partial I}{\partial \phi_i} \delta \phi_i = 0 \tag{1.4}$$

where n is the total number of discrete values of ϕ assigned to the solution domain. Since the $\delta \phi_i$'s are independent, equation (1.4) can be satisfied only if

$$\frac{\partial I}{\partial \phi_i} = 0, i = 1, 2, ..., n \tag{1.5}$$

The functional $I(\phi)$ may be written as a sum of individual functionals defined for all elements of the assemblage, that is,

$$I(\phi) = \sum_{e=1}^{M} I^{(e)}(\phi^{(e)}) \tag{1.6}$$

where M is the total number of elements and the superscript (e) denotes an element. From equation (1.6), it follows that

$$\delta I = \sum_{e=1}^{M} \delta I^{(e)} = 0 \tag{1.7}$$

where the variation of $I^{(e)}$ is taken only with respect to the nodal values associated

with the element (e). Equation (1.7) implies that

$$\{\frac{\partial I^{(e)}}{\partial \phi}\} = \frac{\partial I}{\partial \phi_j} = 0,\ j = 1, 2, ..., r \tag{1.8}$$

where r is the number of nodes assigned to element (e). Equation (1.8) comprises a system of r equations that characterize the behavior of element (e). Equation (1.8) for element (e) can always be written as [75]

$$\{\frac{\partial I^{(e)}}{\partial \phi}\} = [K]^{(e)}\{\phi\}^{(e)} - \{F\}^{(e)} = \{0\} \tag{1.9}$$

where $[K]^{(e)}$ is a square matrix of constant *stiffness* coefficients, $\{\phi\}^{(e)}$ is the column vector of nodal values and $\{F\}$ is the vector of resultant nodal actions. Symbolically, the complete set of equations can be written as

$$\frac{\partial I}{\partial \phi_i} = \sum_{e=1}^{M} \frac{\partial I^{(e)}}{\partial \phi_i} = 0,\ i, 1, 2, ..., n \tag{1.10}$$

or

$$\{\frac{\partial I}{\partial \phi}\} = \{0\} \tag{1.11}$$

The problem is solved when the set of n equations (2.8) is solved simultaneously for the n nodal values of ϕ. If there are Q nodes in the solution domain where ϕ is specified by boundary conditions, there will be $n - q$ equations to be solved for the $n - q$ unknowns.

Requirements for Interpolation Functions

Approximate solutions converge to the correct solution where an increasing number of elements are used, that is, when the element mesh is refined. Mathematical proofs of convergence assume that the process of mesh refinement occurs in a regular fashion, defined by three conditions [76].

1. the elements must be made smaller in such a way that every point of the solution domain can always be within an element, regardless of how small the element may be;

2. all previous meshes must be contained in the refined meshes;

3. the form of interpolation functions must remain unchanged during the process of mesh refinement.

These three conditions are shown in Figure 2.

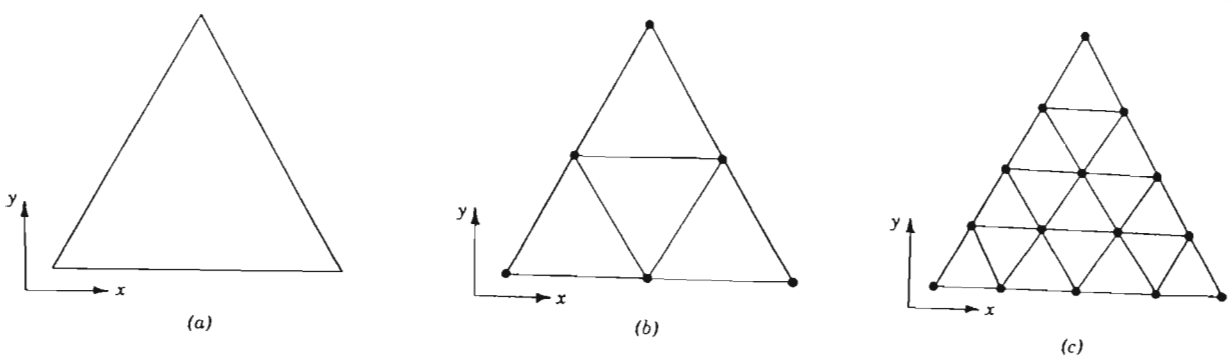

Figure 2. An example of successive mesh refinements.

a). Original solution domain b). Discretization with four triangular elements

c). Discretization with sixteen triangular elements

To guarantee monotonic convergence in the sense just described and to make the assembly of the individual equations meaningful, it is required that the interpolation functions $N^{(e)}$ in the expressions

$$\phi^{(e)} \left[N^{(e)}\right] \{\phi\}^{(e)}, \; e = 1, 2, ..., M \tag{1.12}$$

where $\left[N^{(e)}\right]$ is the row vector of interpolation functions that are functions of the coordinates of the nodes and $\{\phi\}^{(e)}$ is the column vector. Equation (3.1) is chosen so as to satisfy the following general requirements:

1. At element interfaces (boundaries) the field variable ϕ and any of its partial derivatives up to one order less than the highest order derivative appearing in $I(\phi)$ must be continuous.

2. All uniform states of ϕ and its partial derivatives up to one order less than the highest order derivative appearing in $I(\phi)$ should have representation in $\phi^{(e)}$ when, in the limit, the element size shrinks to zero.

These requirements were given by Felippa & Clough [76] and justified by Oliveira [77]. The first one is known as the *compatibility* requirement, and the second as the *completeness* requirement. Elements whose interpolation functions satisfy the first requirement are called *compatible* elements, those satisfying the second requirement, *complete* elements.

In addition to satisfying these requirements, it is also required that the field variable representation within an element and hence the polynomial expansion for the element remain unchanged under a linear transformation from one Cartesian coordinate system to another. Polynomials that exhibit this invariance property are said to posses *geometric isotropy.*

Domain Discretization

The first task in a finite element solution consists of discretizing the continuum by dividing it into a series of elements. The type of element that should be used depends on the problem being considered. Often only one type of element is used to represent the continuum, unless the circumstances dictate otherwise. It is easy to imagine the problem for which several different types of elements would be necessary. An example from solid mechanics would be an elastic body supported by pin connected bars. In this case the elastic body would be represented by three dimensional solid elements such as *bricks,* and the bars would be approximated by one dimensional elements. The most popular and versatile elements, because of the ease with which they can be assembled to fit complex geometries, are triangular elements in two dimensions.

A uniform element mesh is easy to construct, but it may not always provide a good representation of the continuum. More elements should be used in regions where the boundary is irregular than in regions where it is smooth.

The ratio of elements smallest dimension to its largest dimension should be

near unity. Long narrow elements should be avoided because they lead to a solution with direction bias that may lead to inaccurate results.

When solving a particular type of problem for the first time, it is good practice to obtain several solutions with different numbers of element. By comparing the results, it is possible to see whether enough elements are being used in the solution. This is known as convergence testing.

1.2.5 Derivation of Finite Element Equations using the Method of Weighted Residuals

The method of weighted residuals is a technique for obtaining approximate solutions to linear and non-linear partial differential equations. The method offers another means of formulating the finite element equations.

Applying the method of weighted residuals involves basically two steps. The first is to assume the general functional behavior of the dependent field variable to approximately satisfy the given differential equation and boundary conditions. Substitution of this approximation into the original differential equation and boundary conditions then results in some error called a *residual.* This residual is required to vanish in some average sense over the entire solution domain.

The second step is to solve the equations resulting from the first step and specialize the general function form to a particular function, which then becomes the approximate solution sought.

A typical example given below is to find an approximate functional representation for a field variable ϕ governed by the differential equation

$$\mathrm{L}(\phi) - f = 0 \tag{1.13}$$

in the domain D bounded by the surface Σ. The function f is a known function of the independent variables and it is assumed that proper boundary conditions are prescribed on Σ.

First the unknown exact solution ϕ is approximated by $\tilde{\phi}$ where either the functional behavior of $\tilde{\phi}$ is completely specified in terms of unknown parameters, or the functional dependence on all but one of the independent variables is specified while the functional dependence on the remaining independent variables is left unspecified. Thus the dependent variable is approximated by

$$\phi \approx \tilde{\phi} = \sum_{i=1}^{m} N_i C_i \tag{1.14}$$

where N_i are the assumed functions and the C_i are either the unknown parameters or unknown functions of one of the independent variables. The upper limit on the summation, m, is the number of unknowns, C_i. The m functions N_i are usually chosen to satisfy the global boundary conditions.

When $\tilde{\phi}$ is substituted in equation (3.2), viz.

$$\mathrm{L}(\tilde{\phi}) - f = R \tag{1.15}$$

where R is the residual or error that results from approximating ϕ by $\tilde{\phi}$. The method of weighted residuals seeks to determine the m unknowns C_i in such a way that error R over the entire solution domain is small. This is accomplished by forming a weighted average of the error and specifying that the weighted average vanishes over the solution domain. Hence m linearly independent weighting functions W_i are chosen and the weighted average is computed as

$$\int_D [\mathrm{L}(\tilde{\phi}) - f] W_i dD = \int_D R W_i dD = 0, \; i = 1, 2, ..., m \tag{1.16}$$

In this case $R = 0$.

The form of the error distribution principle expressed in equations (1.16) depends on the choice of the weighting functions. Once the weighting functions are specified, equations (1.16) represent a set of m equations, other algebraic or ordinary differential equations to be solved for the coefficients of C_i. The second step is to solve equations (1.16) for C_i and hence obtain an approximate representation of the unknown field variable ϕ via equations (1.14).

There is a variety of weighted residual techniques available because of the broad choice of weighting functions or error distribution functions that can be

used. The error distribution principle most often used to derive finite element equation is known as the *Galerkin criterion.* According to the *Bubnow-Galerkin* method, the weighting functions are chosen to be the same as the approximating functions used to represent ϕ, that is $W_i = N_i$ for $i = 1, 2, ..., m$. Thus Galerkin's method requires that

$$\int_D [\mathrm{L}(\phi^{(e)}) - f^{(e)}] N_i^{(e)} dD^{(e)} = 0, \; i = 1, 2, ..., r \tag{1.17}$$

where the superscript (e) restricts the range to one element, $\phi^{(e)} = \left\lfloor N^{(e)} \right\rfloor \{\phi\}^{(e)}$, $f^{(e)}$ is a forcing function defined over the element (e) and r is a number of unknown parameters assigned to the elements.

Elements and Interpolation Functions

A standard definition and notation to express the degree of continuity of a field variable at element interfaces are given next. If the field variable is continuous at element interfaces it is said that there is C^0 continuity. If the field variable is continuous for the first derivatives there is C^1 continuity; if second derivatives are also continuous there is C^2 continuity and so on.

The functions appearing under the integrals in the element equations contain derivatives up to $(r + 1)th$ order. Following requirements must be satisfied to have assurance of convergence as element size decreases.

Compatibility requirements: At element interfaces there must be C^r continuity.

Completeness requirements: Within an element there must be C^{r+1} continuity.

These requirements hold whether the element equations were derived using the variational method, the Galerkin method or some other method.

Basis Element Shapes

The continuum or solution domain of arbitrary shape can be accurately modeled by an assemblage of simple shapes. Most finite elements are geometrically simple.

For one-dimensional problems with only one independent variable, the elements are line segments (Figure 3).

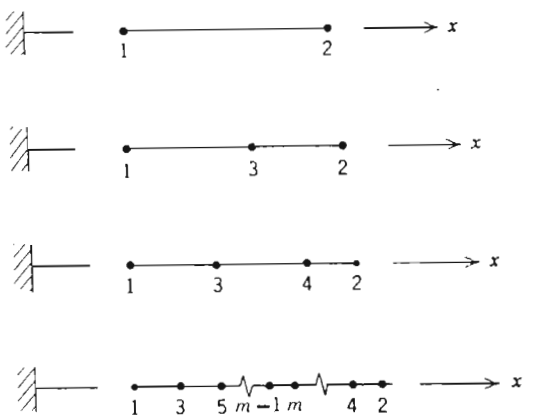

Figure 3. A family of one-dimensional line elements

The number of nodes assigned to a particular element depends on the type of nodal variables, the type of interpolation function and the degree of continuity required. For some one-dimensional problems the finite element method is the most rational approach, foe example, frame analysis in solid mechanics and flow network analysis in fluid mechanics. In elasticity problems where spars are used as

stiffeners, one-dimensional elements can represent the spars while being connected to other two- or three-dimensional elements that represent the rest of the elastic solid.

Common two-dimensional element shapes are shown in Figure 4.

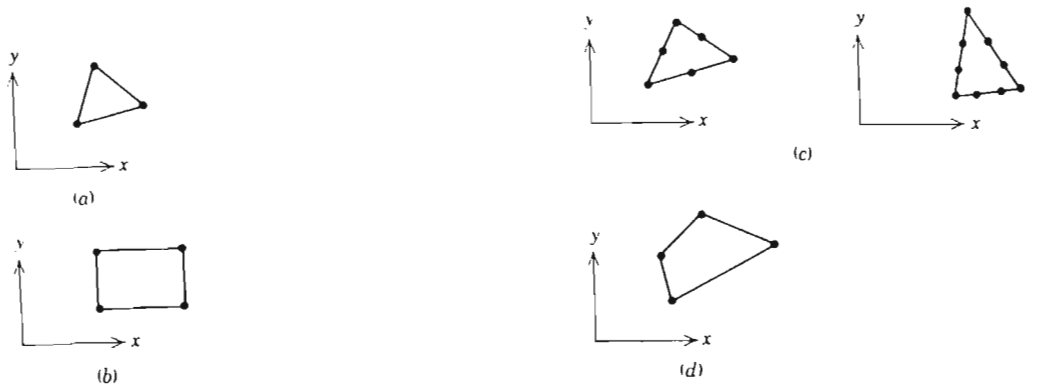

Figure 4. Examples of two dimensional elements

a). Three node triangle b). Rectangle c). Triangles with six and ten nodes d). General quadrilateral

The three-node flat triangular element (Figure 4a) is the simplest two-dimensional element and it enjoys the distinction of being the first and most often used basic finite element. The reason is that an assemblage of triangles can always represent a two-dimensional domain of any shape. A simple but less useful two-dimensional element is the four node rectangle (Figure 4b) whose sides are parallel to the global coordinate system. This type of element is easy to construct automatically by computer because of its regular shape, but is not well suited for approximating curved boundaries.

In addition to the simplest triangle and the rectangle, other common two-

dimensional elements are six-node triangle (Figure 4c), and the general quadrilateral (Figure 4d). Quadrilateral elements may be formed directly or developed by combining two or four basic triangle elements as shown in Figure 5.

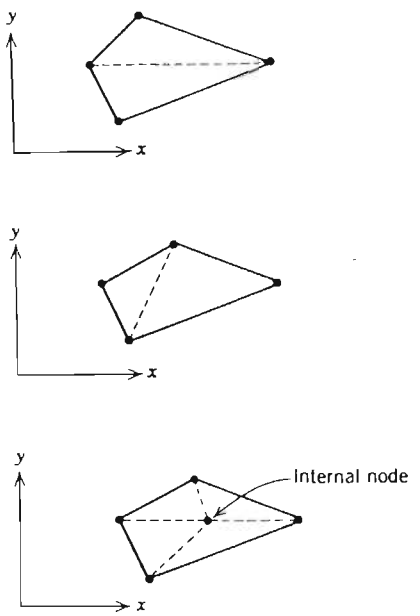

Figure 5. The quadrilateral element formed by combining triangles

Other types of elements that are actually three-dimensional but described by only one or two independent variables are axisymmetric or ring-type elements (Figure 6). These elements are useful when treating problems that possess axial symmetry in cylindrical coordinates.

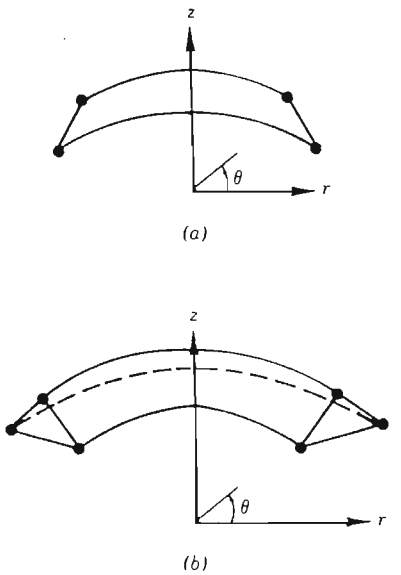

Figure 6. Examples of axisymmetric ring elements

a). One-dimensional ring element b). Two-dimensional triangular ring element

The four-node tetrahedron element in three-dimensions (Figure 7a) is the simplest and the most useful element in three-dimensional problems. Another simple three-dimensional element is the right hand prism shown in Figure 7b. A general hexahedron (Figure 7c) may be constructed from five tetrahedra. Elements which are constructed with curved boundaries are known as isoparametric elements. These, some examples of which are shown in Figure 8 are most useful when it is desirable to approximate curved boundaries with only a few elements. They have been useful in the solution of three-dimensional problems, where it is necessary to reduce the computations by using fewer elements.

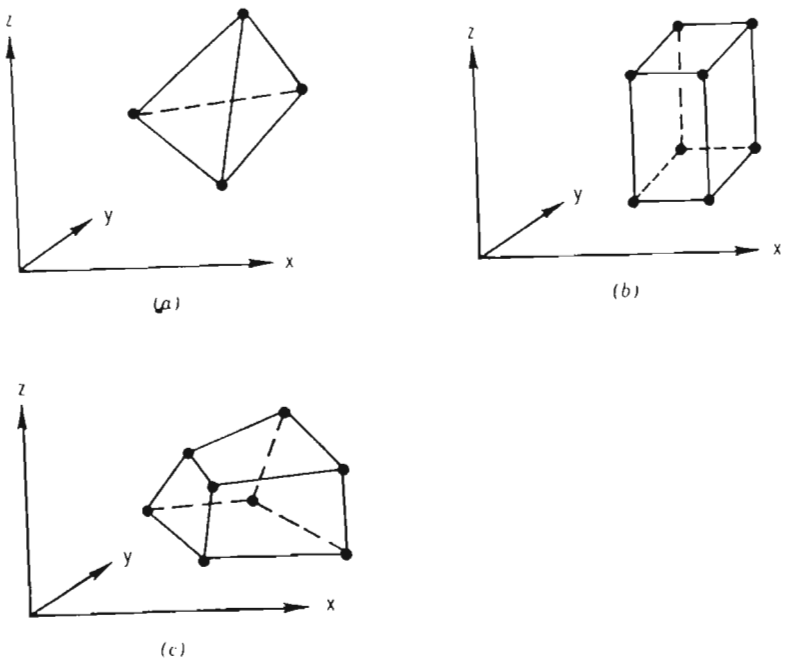

Figure 7. Three dimensional elements

a). Tetrahedron b). Right prism c). General hexahedron

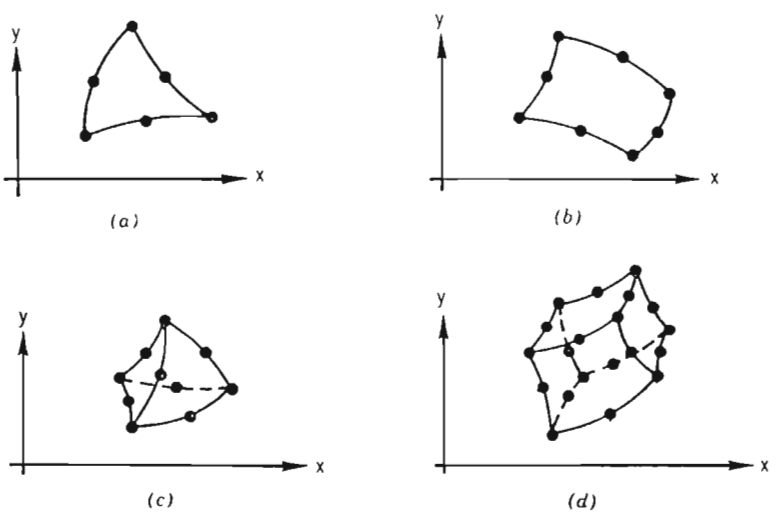

Figure 8. Common isoparametric elements

a). Triangle b). Quadrilateral c). Tetrahedron d). Hexahedron

Basic Element Shape Functions

Interpolation Functions - Polynomials

Although it is conceivable that many types of functions could serve as interpolation functions, only polynomials have received widespread use. They can be integrated or differentiated without difficulty.

One independent variable

In one dimension a general complete n^{th}-order polynomial may be written as

$$P_n(x) = \sum_{i=0}^{T_n^{(1)}} \alpha_i x^i \tag{1.18}$$

where the number of terms in the polynomial is $T_n^{(1)} = n + 1$. For $n = 1$, $T_1^{(1)} = 2$ and $P_1(x) = \alpha_o + \alpha_1 x$; for $n = 2$, $T_2^{(1)} = 3$ and $P_2(x) = \alpha_o + \alpha_1 x + \alpha_2 x^2$; and so on.

Two independent variables

In two dimensions a complete n^{th}-order polynomial may be written as

$$P_n(x,y) = \sum_{k=0}^{T_n^{(2)}} \alpha_k x^i y^j, \; i + j \leq n \tag{1.19}$$

where the number of terms in the polynomial is $T_n^{(2)} = (n + 1)(n + 2)/2$. For $n = 1$, $T_1^{(2)} = 3$ and $P_1(x,y) = \alpha_1 + \alpha_2 x + \alpha_3 y$; for $n = 2$, $T_2^{(2)} = 6$ and $P_2(x,y) = \alpha_1 + \alpha_2 x + \alpha_3 y + \alpha_4 xy + \alpha_5 x^2 + \alpha_6 y^2$; and so on. Figure 9 shows the array of terms in a complete polynomial in two-dimensions.

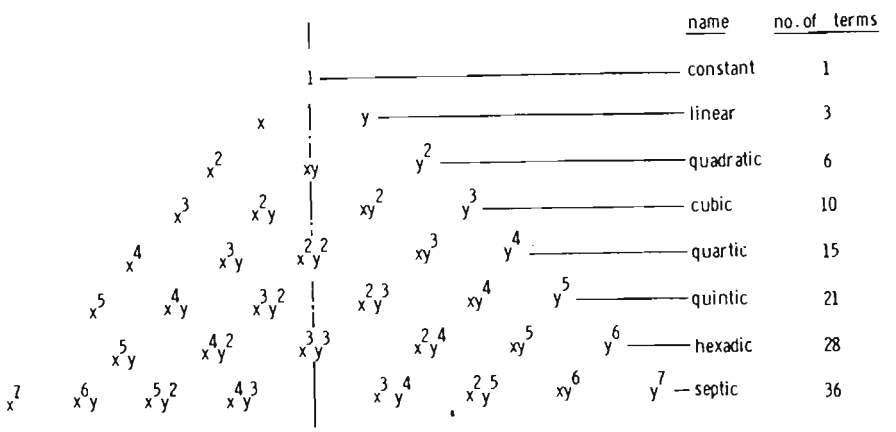

Figure 9. Array of terms in a complete polynomial in two dimensions

Three independent variables

In three dimensions a complete n^{th}-order polynomial may be written as

$$P_n(x,y,z) = \sum_{l=0}^{T_n^{(3)}} \alpha_l x^i y^j z^k, \; i+j+k \leq n \tag{1.20}$$

where the number of terms in the polynomial is

$$T_n^{(3)} = \frac{(n+1)(n+2)(n+3)}{6} \tag{1.21}$$

For $n = 1$, $T_1^{(3)} = 4$ and $P_1(x,y,z) = \alpha_1 + \alpha_2 x + \alpha_3 y + \alpha_4 z$; for $n = 2$, $T_2^{(3)} = 10$ and $P_2(x,y,z) = \alpha_1 + \alpha_2 x + \alpha_3 y + \alpha_4 z + \alpha_5 xy + \alpha_6 xz + \alpha_7 yz + \alpha_8 x^2 + \alpha_9 y^2 + \alpha_{10} z^2$; and so on. The array of terms in a complete polynomial in three dimensions is

shown in Figure 10.

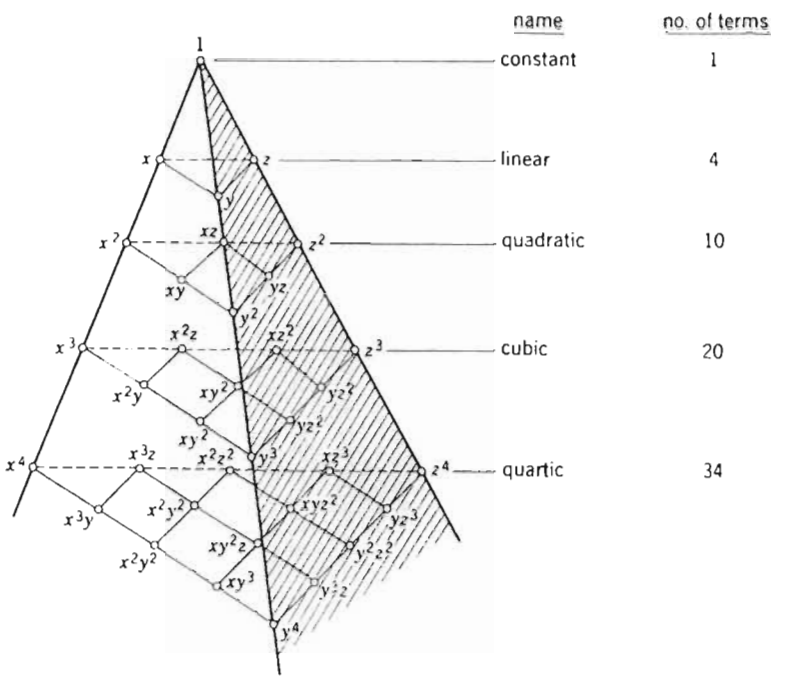

Figure 10. Array of terms in a complete polynomial in three dimensions

Two-Dimensional Problems

Elements for C^0 problems

The number of elements capable of satisfying C^0 continuity is infinite since nodes and degrees of freedom may be added to the elements to form ever increasing higher-order elements. In general, as the complexity of the elements is increased by adding more nodes and more degrees of freedom and using higher-order polynomials, the number of elements and total number of degrees of freedom needed to achieve a given accuracy in a given problem are less than would be required if simpler elements were used. None the less, this does not suggest that

higher-order elements always be used in preference to lower order elements.

There is no general guideline for choosing the optimum element for a given problem, because the type of element that yields good accuracy with low computing time is problem dependent. For C^0 problems, elements that require polynomials of order greater than three are rarely used, since little additional accuracy is gained for the extra effort expended. If a complicated boundary is to be modeled, it is more advantageous to use a large number of simple elements than a few complex elements.

Triangular elements

Figure 11 shows a portion of the family of higher-order elements obtained by assigning additional external and interior nodes to triangles. Each element in this series has a sufficient number of nodes to specify a complete polynomial of the order necessary to give C^0 continuity. The compatibility, completeness and geometric isotropy requirements are satisfied.

For the three-node triangular element, the linear variation of ϕ is written as

$$\phi(x,y) = \alpha_1 + \alpha_2 x + \alpha_3 y = [1 \; x \; y]\{\alpha\} = [P]\{\alpha\} \tag{1.22}$$

and by evaluating this expression at each node, we obtain

$$\{\phi\} = [G]\{\alpha\} \tag{1.23}$$

According to the procedure of deriving interpolation functions, this can be written as

$$\phi = [P][G]^{-1}\{\alpha\} = [N]\{\phi\}$$
$$[N] = [P][G]^{-1} \tag{1.24}$$

where the elements of $[N]$, $N_i = L_i$ are the area coordinates for the triangle.

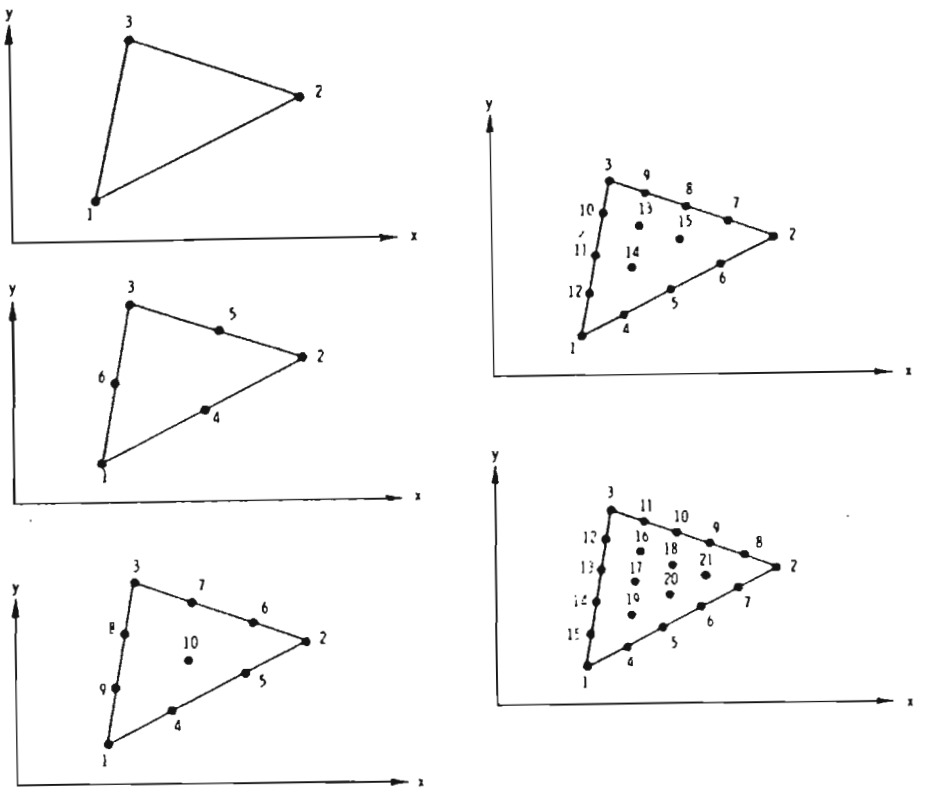

Figure 11. Linear and higher order triangular elements with ϕ specified at nodes (the nodes along any line are equally spaced)

Rectangular elements

Interpolation functions for rectangular elements with sides parallel to the global axes are easily developed using Lagrangian interpolation concepts. For example, the four interpolation functions for the four node rectangle are derived

in Figure 12. After the local coordinates are defined in Figure 12, it can be written as

$$\phi(\xi,\eta) = N_1(\xi,\eta)\phi_1 + N_2(\xi,\eta)\phi_2 + N_3(\xi,\eta)\phi_3 + N_4(\xi,\eta)\phi_4 \tag{1.25}$$

where

$$\begin{aligned} N_1(\xi,\eta) &= L_1(\xi)L_1(\eta), \\ N_2(\xi,\eta) &= L_2(\xi)L_2(\eta), \\ &\text{etc} \end{aligned} \tag{1.26}$$

and the L_i are the Lagrange polynomials. Interpolation functions formed as products in this way satisfy the requirements of possessing unit value at the node for which they are defined and zero at the other nodes.

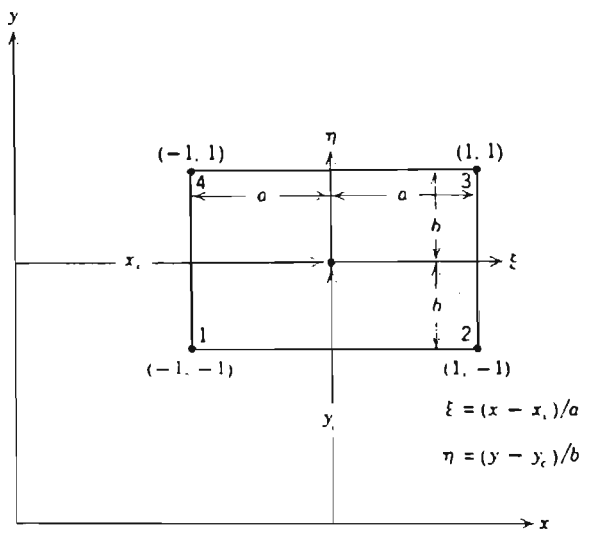

Figure 12. Rectangular element showing the relation between local and global coordinates

Elements for C^1 Problems

Constructing two-dimensional elements that can be used for problems requiring continuity of the field variable ϕ as well as its normal derivative $\frac{\partial \phi}{\partial n}$ along element boundaries is far more complicated than constructing elements for C^0 continuity alone. The field variable ϕ and $\frac{\partial \phi}{\partial n}$ are uniquely specified along the element boundaries by the degrees of freedom assigned to the nodes along a particular boundary. According to Felippa & Clough [76], the difficulties arise from the following principles:

1. The interpolation functions must contain at least some cubic terms, because the three nodal values ϕ, $\frac{\partial \phi}{\partial x}$ and $\frac{\partial \phi}{\partial y}$ must be specified at each corner of the element.

2. For non rectangular elements C^1 continuity requires the specification of at least the six nodal values, ϕ, $\frac{\partial \phi}{\partial x}$, $\frac{\partial \phi}{\partial y}$, $\frac{\partial^2 \phi}{\partial x^2}$, $\frac{\partial^2 \phi}{\partial y^2}$ and $\frac{\partial^2 \phi}{\partial x \partial y}$. at the corner nodes. For a rectangular element with sides parallel to the global axes it is necessary to specify at the corner nodes only ϕ, $\frac{\partial \phi}{\partial x}$, $\frac{\partial \phi}{\partial y}$ and $\frac{\partial^2 \phi}{\partial x \partial y}$.

Three Dimensional Elements

Elements for C^o problems

Constructing three-dimensional elements to give C^0 continuity at element interfaces follows immediately from a natural extension of the corresponding elements in two dimensions. Instead of requiring continuity of the field variable

along the edge of the element, continuity is required on the faces of the elements.

Hexahedral elements

The concept of Lagrange and Hermite interpolation for two-dimensional elements extend also to hexahedral elements in three dimension. The first three members of the Lagrange hexahedral family (right prisms) are shown in Figure 13. Interpolation functions for this family of elements may be written as the product of the Lagrange polynomials in all of the orthogonal coordinate directions ξ, η, ζ, (origin at the centroid of the element). Hence for node k

$$N_k(\xi, \eta, \zeta) = L_k(\xi), L_k(\eta), L_k(\zeta) \tag{1.27}$$

where it is understood that each function L_k is properly formed to account for number of subdivisions (nodes) in the particular coordinate direction. Zienkiewicz *et al* [71] generated the series of such elements shown in Figure 14. The interpolation functions for these serendipity elements are incomplete polynomials and are derived by inspection.

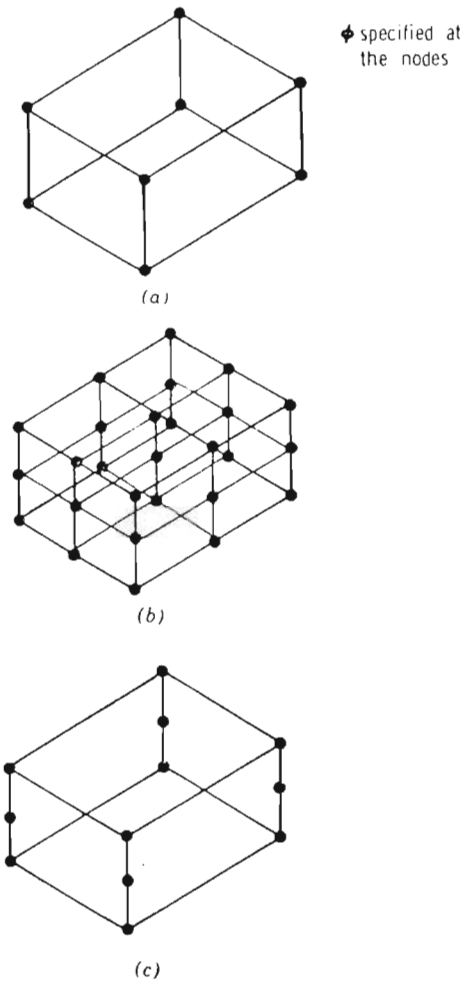

Figure 13. Some hexahedral elements of the Lagrange family

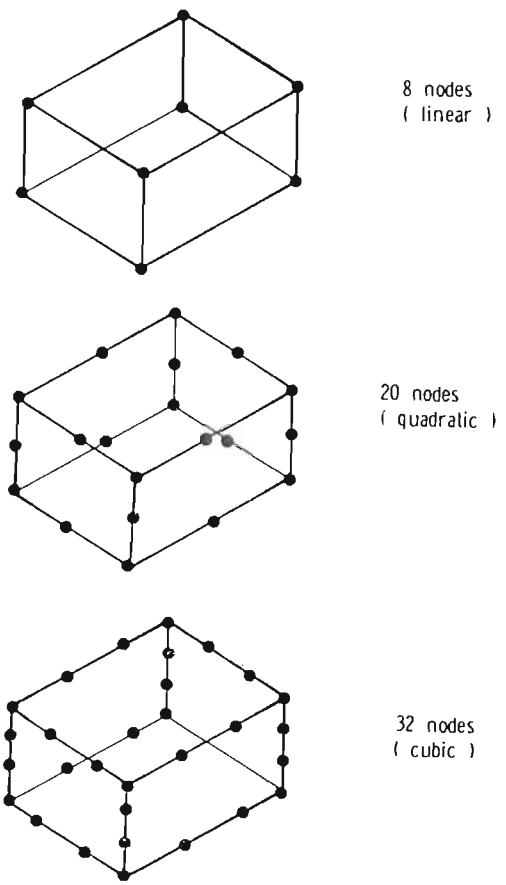

Figure 14. Hexahedral elements of the serendipity family containing only exterior nodes

Linear element

Equation 8-node linear element shown in Figure 14 is written as

$$N_i = \frac{1}{8}(1 + \xi\xi_i)(1 + \eta\eta_i)(1 + \xi\xi_i) \tag{1.28}$$

Higher-order elements of this family are seldom considered because interior nodes must be introduced to continue the construction of the interpolation functions.

Triangular prisms

Modeling complex-shape, three-dimensional solution domains with hexahedral elements can cause some difficulties because these *brick*-shaped elements may not fit the boundary. Rather than using a large number of small *bricks*, it is advantageous to mix hexahedra and triangular prisms to obtain a good fit. Lagrange hexahedra or serendipity hexahedra are shown in Figure 15.

For the quadratic prism of the serendipity type (Figure 15b);

Corner nodes:

$$N_i = \frac{1}{2}L_i(2L_i - 1)(1 + \xi) - \frac{1}{2}L_i(1 - \xi^2) \tag{1.29}$$

Midsides of triangles

$$N_i = 2L_iL_j(1 + \xi) \tag{1.30}$$

Midsides of rectangles

$$N_i = L_i(1+\xi)^2 \tag{1.31}$$

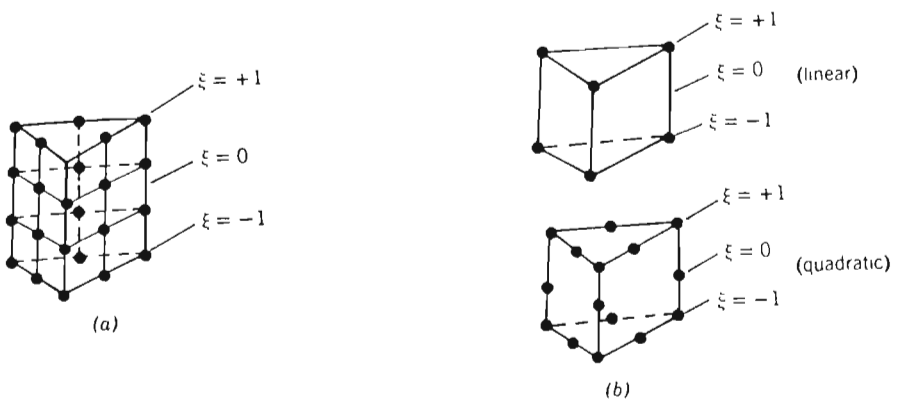

Figure 15. Families of triangular prism elements.

a). One member of the Lagrange b). Two members of the serendipity family.

1.2.6 Elasticity Problems

An Introduction to Elasticity Problems

Most applications of the finite element method to solid mechanics problems use a variational principle to derive the necessary element properties or equations. The three most commonly used variational principles are the principle of minimum potential energy, the principle of complementary energy and Reissner's principle.

Model	Variational principle	Inside each element	Along Interelement boundary	Unknown in final equations
Compatible	Minimum potential energy	Continuous displacements	Displacement compatibility	Nodal displacements
Equilibrium	Minimum complementary energy	Continuous and equilibrating stresses	Equilibrium boundary tractions	Stress parameters Generalized nodal displacements
Hybrid 1	Modified complementary energy	Continuous and equilibrating stresses	Assumed compatible displacements	Nodal displacements
Hybrid 2	Modified potential energy	Continuous displacements	Assumed equilibrating boundary tractions	Displacement parameters and boundary forces
Hybrid 3	Modified potential energy	Continuous displacements	Assumed boundary tractions for each element and assumed boundary displacements	Nodal displacements
Mixed (Plate-bending problems)	Reissner's principle	Continuous stresses and displacements	Combinations of boundary displacements and tractions	Combination of boundary displacements and tractions

Table 1. Classification of finite element methods in elasticity.

When the potential energy principle is used, the form of the displacement field within each element must be assumed. This is sometimes called the *displacement method* or the *compatibility method* in the finite element analysis. When the complementary energy method is used, the form of the stress field is assumed

and this is called the *force method* or *equilibrium method.* Pian and Tong [78] tabulated (Table 1) these and other variational bases of the finite element method in solid mechanics. For particular problems, one principle may be more suitable than another, but for a large class of problems the displacement method is the simplest to apply and the most widely used.

General Formulation for Two-dimensional Problems

The variational principle

The potential energy of a two-dimensional elastic body acted upon by surface and body forces and in equilibrium can be written as:

$$\begin{aligned}\Pi(u,v) = \tfrac{1}{2}\int\int_A [\left\lfloor\tilde{\delta}\right\rfloor [B]^T[C]\{\delta\} - 2\left\lfloor\tilde{\delta}\right\rfloor [B]^T[C]\{\epsilon_0^*\}]tdA \\ - \int\int_A \lfloor\delta\rfloor\, tdA - \int_{C_1}[T^*]\{\delta\}dS\end{aligned} \tag{1.32}$$

where $t = t(x,y)$ is the thickness of the body,

$\{\delta\} = \begin{Bmatrix} u(x,y) \\ v(x,y) \end{Bmatrix}$: column matrix of the components of the displacement field measured from some datum,

$[B] = \begin{bmatrix} \partial/\partial x & 0 \\ 0 & \partial/\partial y \\ \partial/\partial x & \partial/\partial y \end{bmatrix}$ is the matrix relating strains and displacements,

$[C]$ is the material stiffness which takes different forms according to the problem considered,

$\{\epsilon_0^*\}$ is the column vector of initial strains which may be due to nonuniform

temperature distributions, shrink fits etc.

$\lfloor F^* \rfloor = \lfloor X^*, Y^* \rfloor$ are the body force components due to gravity, centrifugal action, and the like,

$\lfloor T^* \rfloor = \left\lfloor T_x^*, T_y^* \right\rfloor$ are the boundary traction components acting on portion C_1 of the boundary; these are defined per unit length for a unit thickness.

The asterisk superscript denotes known quantities. At equilibrium the displacement field (u, v) in the body is such that the total system potential energy assumes a minimum value.

After using a suitable variational principle, general finite element equations for the elastic continuum may be developed. First the continuum will be subdivided into elements of some shape, then the form of displacement function is assumed over each element. For the general formulation, it is not needed to specify the type of element nor the particular displacement function. Firstly the equations for the general case can be developed. Subsequently they are specialised for particular cases.

Requirements for the Displacement Interpolation Functions

It is assumed that the area A (Figure 16) is divided into M discrete elements. The potential energy of the elements is the sum of the potential energies of all elements provided that the interpolation functions expressing the variation of the displacement within each element satisfy the compatibility and completeness

requirements. In other words to write

$$\Pi(u,v) = \sum_{e=1}^{M} \Pi^{(e)}(u,v) \tag{1.33}$$

and to be assured of convergence as element mesh size decreases, the interpolation must satisfy the compatibility and completeness requirements.

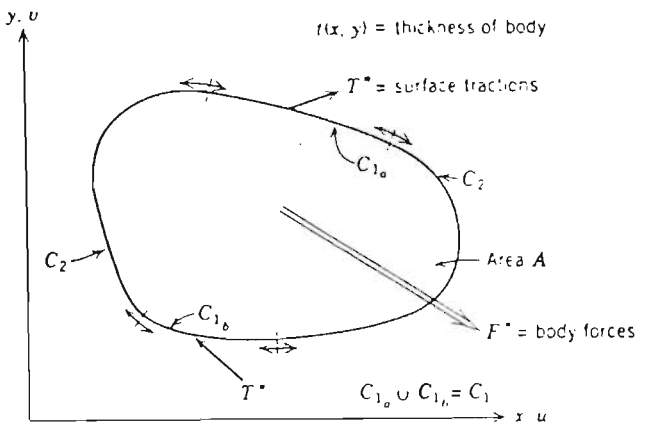

Figure 16. Arbitrary two-dimensional elastic body experiencing surface tractions and body forces.

For plane stress and plane strain as well as three-dimensional elasticity problems polynomial interpolations satisfy the compatibility and completeness requirements when the polynomials contain at least a constant and linear terms.

To express $\Pi^{(e)}(u,v)$, which is the potential energy function for one element, in terms of discrete values of displacement components, it is assumed that within each element having r nodes, the displacement field is approximately related

to its nodal values by r interpolating functions $N_i(x,y)$. Thus the distributed displacement field can be expressed as

$$\{\tilde{\delta}\}^{(e)} = \begin{Bmatrix} u(x,y) \\ v(x,y) \end{Bmatrix}^{(e)} = \begin{Bmatrix} \sum_{i=1}^{r} N_i(x,y)u_i \\ \sum_{i=1}^{r} N_i(x,y)v_i \end{Bmatrix} = \begin{Bmatrix} \lfloor N \rfloor \{u\} \\ \lfloor N \rfloor \{v\} \end{Bmatrix}(e) = [N]\{\delta\}^{(e)} \quad (1.34)$$

where $\{\delta\}^{(e)}$ denotes the element nodal displacements.

Element Stiffness Equations

Since the displacement field for the element has been expressed in terms of known interpolation functions and unknown displacements, the potential energy functional will be similarly expressed. Thus for element (e), the discretised functional is

$$\Pi^{(e)}(\{\delta\}^{(e)}) = \Pi^{(e)}(u_1, u_2, ..., u_r, v_1, v_2, ..., v_r) \quad (1.35)$$

or more explicitly

$$\begin{aligned} \Pi^{(e)}(\{\delta\}^{(e)}) = \tfrac{1}{2} \int\int_{A^{(e)}} [\lfloor \delta \rfloor^{(e)} [B]^{T^{(e)}} [C]^{(e)} [B]^{(e)} \{\delta\}^{(e)} \\ -2 \lfloor \delta \rfloor^{(e)} [B]^{T^{(e)}} [C]^{(e)} \{\epsilon_0^*\}^{(e)}] t^{(e)} dA^{(e)} \\ - \int\int_{A^{(e)}} \lfloor F^* \rfloor^{(e)} \{\delta\}^{(e)} t^{(e)} dA^{(e)} \\ - \int_{C_1^{(e)}} \lfloor T^* \rfloor^{(e)} \{\delta\}^{(e)} dS^{(e)} \end{aligned} \quad (1.36)$$

At equilibrium, the potential energy of the system assumes a minimum value

when the first variation of the functional vanishes, that is

$$\delta\Pi(u,v) = \sum_{e=1}^{M} \delta\Pi^{(e)}(u,v) = 0 \tag{1.37}$$

where

$$\delta\Pi(u,v) = \sum_{i=1}^{r} \frac{\delta\Pi^{(e)}}{\delta u_i}\delta u_i + \sum_{i=1}^{r} \frac{\delta\Pi^{(e)}}{\delta v_i}\delta v_i = 0 \tag{1.38}$$

But the δu_i and the δv_i are independent variations and equation (1.38) is satisfied only if

$$\frac{\delta\Pi^{(e)}}{\delta u_i} = \frac{\delta\Pi^{(e)}}{\delta v_i} = 0, \; i = 1,2,...,r \tag{1.39}$$

for every element (e) of the system.

Equation (1.39) expresses the condition we use to find the element equations. A typical equation in submatrix form is

$$\left[[k]^{q1}[k]^{q2}...[k]^{qp}...[k]^{qr}\right]\begin{bmatrix} u_1 \\ v_1 \\ - \\ . \\ . \\ . \\ - \\ u_q \\ v_q \\ - \\ . \\ . \\ . \\ - \\ u_r \\ v_r \end{bmatrix} = \{F\}^q,\ q = 1,2,...,r \qquad (1.40)$$

where $p = 1,2,...,r$ and r is the number of element nodes. A typical 2×2 submatrix $[k]^{qp}$ denotes the stiffness relationship between nodes q and p and

$\{F\}^q$ is the resultant external load vector at node q.

$$\begin{aligned}\frac{\delta\Pi^{(e)}}{\delta u_q}\Big/\frac{\delta\Pi^{(e)}}{\delta u_v} = \{0\} = &\int\int_{A^{(e)}}[B]_q^{T^{(e)}}[C]^{(e)}[B]_p^{(e)}\{\delta\}^q t^{(e)}dA^{(e)} \\ &- \int\int_{A^{(e)}}[B]_q^{T^{(e)}}[C]^{(e)}\{\epsilon_0^*\}_q^{(e)}t^{(e)}dA^{(e)} \\ &- \int\int_{A^{(e)}} N_q\{F^*\}_q^{(e)}t^{(e)}dA^{(e)} - \int_{C_i^{(e)}} N_q\{T^*\}_q^{(e)}dS_q^{(e)}\end{aligned} \tag{1.41}$$

where

$$\{\delta\}^q = \begin{Bmatrix} u_q \\ v_q \end{Bmatrix} \tag{1.42}$$

is the column vector of the two displacement components at node q.

$$[B]_q^{(e)} = \begin{bmatrix} \delta N_q/\delta x & 0 \\ 0 & \delta N_q/\delta y \\ \delta N_q\delta y & \delta N_q/\delta x \end{bmatrix} \quad q = 1, 2, ..., r \tag{1.43}$$

The definition of $[B]_q^{(e)}$ in equation (1.43), for a two-dimensional elastic follows from the definitions of the three nonzero strain components ε_x, ε_y, and γ_{xy}. Since the traction vector $\{T^*\}$ is a boundary effect, the last term of equation (1.41) applies only if element (e) lies on the boundary where traction is specified.

Equation (1.41) is the force-displacement relation for node q. In matrix notation it can be written as

$$[k]^{qp}\{\delta\}^q = \{F_0\}^q + \{F_B\}^q + \{F_T\}^q = \{F\}^q \tag{1.44}$$

where

$$[k]^{qp} = \int\int_{A^{(e)}} [B]_q^{T^{(e)}} [C]^{(e)} \{\epsilon_0^*\}_q^{(e)} t^{(e)} dA^{(e)} \tag{1.45}$$

is the initial force vector at node q,

$$\{F_B\}^q = \int\int_{A^{(e)}} N_q(x,y) \{F^*\}_q^{(e)} t^{(e)} dA^{(e)} \tag{1.46}$$

is the nodal body force vector and

$$\{F_T\}^q = \int\int_{C_1^{(e)}} N_q(x,y) \{T^*\}_q^{(e)} dS_q^{(e)} \tag{1.47}$$

is the nodal force vector due to surface loading (present only for boundary elements).

$$\{F\}^q = \text{ resultant external load vector at node } q \tag{1.48}$$

Equation (1.43) expresses the stiffness submatrices associated with a typical node, but since each element has r nodes, the complete stiffness for the element

is a $2r \times 2r$ matrix of the form

$$[K]^{(e)} = \begin{bmatrix} [k]^{11} & [k]^{12} & \dots & [k]^{1r} \\ [k]^{21} & [k]^{22} & \dots & [k]^{2r} \\ \vdots & \vdots & \vdots & \vdots \\ [k]^{q1} & [k]^{q2} & \dots & [k]^{qr} \\ \vdots & \vdots & \vdots & \vdots \\ [k]^{r1} & [k]^{r2} & \dots & [k]^{rr} \end{bmatrix} \tag{1.49}$$

The arrangement of terms in the element stiffness matrix implies that the column matrix of discrete nodal displacements for the elements has the form

$$\{\delta\}^{(e)} = \begin{Bmatrix} \{\delta\}^1 \\ \{\delta\}^2 \\ \vdots \\ \{\delta\}^r \end{Bmatrix} = \begin{Bmatrix} u_1 \\ v_1 \\ u_2 \\ v_2 \\ \vdots \\ u_r \\ v_r \end{Bmatrix} \tag{1.50}$$

thus the force-displacement equations for the element take the standard form

$$[K]^{(e)}\{\delta\}^{(e)} = \{F\}^{(e)} \tag{1.51}$$

where

$$\{F\}^{(e)} = \begin{Bmatrix} \{F\}^1 \\ \{F\}^2 \\ \vdots \\ \{F\}^q \\ \vdots \\ \{F\}^r \end{Bmatrix} \tag{1.52}$$

It is important to note that $\{\delta\}^{(e)}$, defined by equation (1.50), is the column vector of discrete nodal displacements for element (e), whereas $\{\tilde{\delta}\}^{(e)}$ is the column vector of the continuous displacement field within the element.

The System Equations

Equation (1.49) with its components given by equation (1.11) is the general form of the element stiffness matrix for two-dimensional elasticity problems. The *system* equations have the same form as the *element* equations except that they are expanded in dimension to include all nodes. Hence, when the discretised system has m nodes, the system equations become

$$\underset{[K]}{(2m \times 2m)} \quad \underset{\{\delta\}}{(2m \times 1)} = \underset{\{F\}}{(2m \times 1)} \tag{1.53}$$

where $\{\delta\}$ is a column vector of nodal displacement components for the entire system and $\{F\}$ is the column vector of the resultant nodal forces.

For the displacement formulation either force or displacement is known in every node of the system. If body forces and initial strains are absent, the vector $\{F\}$ has zero components except for the components corresponding to nodes where concentrated external forces or displacements are specified.

For steady-state problems, once the system equations are solved for the nodal displacements, the basic relations between stress and strain, and strain and displacement, may be defined to find the stress at any point in any of the elements. A general equation for the stress components , including stresses due to displacements and initial strains, can be written as

$$\{\sigma\}^{(e)} = [C]^{(e)}[B]^{(e)}\{\delta\}^{(e)} - [C]^{(e)}\{\epsilon_0^*\}^{(e)} \tag{1.54}$$

If any initial stresses are present, these must also be added.

1.2.7 Bending of Thin Plates: A C_1- Continuity Problem

In the classic theory of plates, certain approximations are introduced initially to simplify the problem to two dimensions. These assumptions concern the linear variation of strains and stresses on lines normal to the plane of the plate. So-called exact solutions of plate theory are only true if these assumptions are valid. This is so when the plates are thin and the deflections small. In the following, the starting point will be based on the classical plate theory assumptions.

The state of deformation of a plate can be described by one quantity. This is the lateral displacement w of the *midplane* of the plate. Continuity conditions between elements have to be imposed not only on this quantity, but also its derivative, in order to ensure that the plate remains continuous, and does not 'kink'. If kinking occurs, the second derivative or curvature becomes infinite and certain infinite terms occur in the energy expression. At each node, therefore, three conditions of and continuity will usually be imposed.

Determination of suitable interpolation functions is thus a more complex task. It is, however, possible to find interpolation functions which, while preserving continuity of w, may violate its slope continuity between elements, although not at the node where such continuity is imposed. If such chosen functions satisfy the *constant strain* criterion, and in addition pass the patch test, then convergence will still be found. These are termed *non-conforming* interpolation functions [75].

The simplest type of element shape is thus the rectangle. The problem of thin plates, where the potential energy function contains *second derivatives* of unknown functions, is characteristic of a large class of physical problems associated with *fourth order differential equations.*

Displacement Formulation of the Plate Problem

The displacement of a plate, under the usual thin plate theory is uniquely specified once the deflection, w, is known at all points.

In general

$$w = Na^{(e)} \tag{1.55}$$

in which the interpolation functions are dependant on Cartesian coordinates x, y, and $a^{(e)}$ list the element (nodal) parameters.

By defining the strain and stress carefully, the product of the two will correspond to the internal work requirements. Thus, the *strain* is defined as

$$\varepsilon = \left\{ \begin{array}{c} -\frac{\partial^2 w}{\partial x^2} \\ -\frac{\partial^2 w}{\partial y^2} \\ 2\frac{\partial^2 w}{\partial xy} \end{array} \right\} \tag{1.56}$$

The corresponding *stresses* are the bending and twisting moments per unit lengths in the x and y directions:

$$\sigma = \left\{ \begin{array}{c} M_x \\ M_y \\ M_{xy} \end{array} \right\} \tag{1.57}$$

Since the true strains and stresses vary linearly across the plate thickness, these can be found from such expressions as:

$$\sigma = \frac{12M_x}{t^3} z, \text{ etc} \tag{1.58}$$

where z is measured from the plate midplane, and t is the thickness of the plate.

As the strains are defined by second derivatives, the continuity criterion requires that the interpolation functions be such that both w and its slope normal to the interface between elements be continuous.

The criterion of constant strain requires that any constant arbitrary value of second derivative should be reproducible within the element. To ensure at least an approximate satisfaction of slope continuity, three displacement components are considered as nodal parameters: the first the actual displacement w_n in the z direction, the second a rotation about the x axis $(\theta_x)_n$, and the third about the y axis $(\theta_y)_n$. Figure 17 shows these rotations with their positive directions determined by the right-hand screw rule.

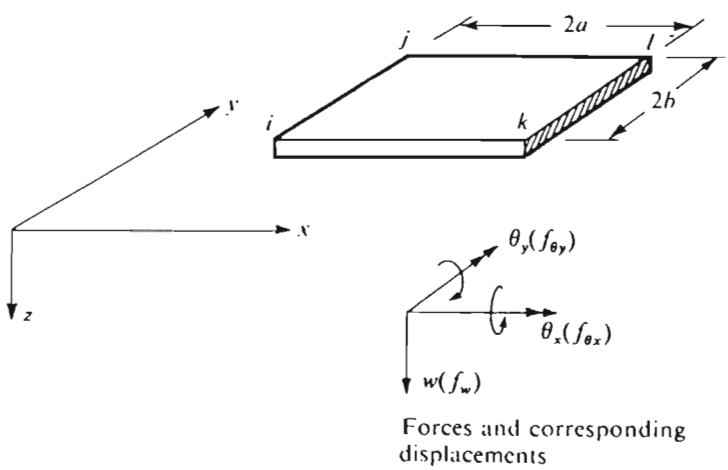

Figure 17. A rectangular plate element

It is obvious that the slopes of w and the rotation are identical (except for the sign), and thus

$$a_i = \left\{ \begin{array}{c} w_i \\ \theta_{xi} \\ \theta_{yi} \end{array} \right\} = \left\{ \begin{array}{c} w_i \\ -\left(\frac{\partial w}{\partial y}\right)_i \\ \left(\frac{\partial w}{\partial y}\right)_i \end{array} \right\} \tag{1.59}$$

The nodal 'forces' corresponding to theses displacements can be interpreted as a direct force and two couples

$$f_i = \left\{ \begin{array}{c} f_{wi} \\ f_{\theta xi} \\ f_{\theta yi} \end{array} \right\} \tag{1.60}$$

as shown in Figure 17.

It follows immediately that

$$B_i = \left\{ \begin{array}{c} -\frac{\partial^2}{\partial x^2} N_i \\ -\frac{\partial^2}{\partial y^2} N_i \\ 2\frac{\partial^2}{\partial xy} N_i \end{array} \right\} \tag{1.61}$$

The elasticity matrix D is given by

$$\sigma \equiv M = D(\varepsilon - \varepsilon_0) + \sigma_0 \tag{1.62}$$

For an *isotropic* plate

$$D = \frac{Et^3}{12(1-\nu^2)} \begin{bmatrix} 1 & \nu & 0 \\ \nu & 1 & 0 \\ 0 & 0 & (1-\nu)/2 \end{bmatrix} \tag{1.63}$$

and for an *orthotropic* slab with principal directions of orthotropy coinciding with the x and y axes, four constants are needed to define the behavior:

$$D = \begin{bmatrix} D_x & D_1 & 0 \\ D_1 & D_y & 0 \\ 0 & 0 & D_{xy} \end{bmatrix} \tag{1.64}$$

Clearly, for a most complete case of anisotropy, six constants at most will need to define D since the matrix has to be symmetric.

Rectangular Elements with Corner Nodes

Interpolation functions

Consider a rectangular element of a plate $ijkl$ coinciding with the $x-y$ plane as shown in Figure 17. At each node, displacements a_n are introduced. These have three components: the first a displacement in the z direction, w_n, the second a rotation about the x axis $(\theta_x)_n$, the third a rotation about the y axis $(\theta_y)_n$.

The nodal displacements are defined by equation (1.59) while the element

displacement will, as usual, be given by the listing of the nodal displacements:

$$a^{(e)} = \begin{Bmatrix} a_i \\ a_j \\ a_l \\ a_k \end{Bmatrix} \tag{1.65}$$

A polynomial expression is conveniently used to define interpolation functions in terms of the twelve parameters. Certain terms must be omitted for a complete fourth order polynomial. Expressing

$$\begin{aligned} w = \alpha_1 + \alpha_2 x + \alpha_3 y + \alpha_4 x^2 + \alpha_5 xy + \alpha_6 y^2 + \\ \alpha_7 x^3 + \alpha_8 x^2 y + \alpha_9 x y^2 + \alpha_{10} y^3 + \alpha_{11} x^3 y + \alpha_{12} x y^3 \end{aligned} \tag{1.66}$$

has some advantages. In particular, along any $x = const$ or $y = const$ line, the displacement w will vary as a cubic. The element boundaries or interfaces are composed of such lines. As a cubic is uniquely defined by four constants, the two end values of slopes displacements at the ends of the boundaries will therefore define the displacements along this boundary uniquely. As such end values are common to adjacent elements, continuity of w will be imposed all along any interface. This function can be shown to be *non-conforming.*

The constants α_1 to α_{12} can be evaluated. For instance

$$\begin{aligned} w_i &= \alpha_1 + \alpha_2 x_i + \alpha_3 y_i + \ldots \\ (-\tfrac{\partial w}{\partial y})_i &= \theta_{x_i} = -\alpha_3 + \ldots \\ (\tfrac{\partial w}{\partial x})_i &= \theta_{y_i} = -\alpha_3 + \ldots \\ &etc. \end{aligned} \tag{1.67}$$

In matrix form

$$a^{(e)} = C\alpha \tag{1.68}$$

where C is a 12×12 matrix depending on the nodal coordinates and α is a vector of the twelve unknown constants. Thus

$$\alpha = C^{-1} a^{(e)} \tag{1.69}$$

It is now possible to write the expression for the displacement in the standard form as

$$u \equiv w = N a^{(e)} = P C^{-1} a^{(e)} \tag{1.70}$$

where

$$P = (1, x, y, x^2, xy, y^2, x^3, x^2y, xy^2, y^3, x^3y, xy^3) \tag{1.71}$$

For any node, in terms of normalised coordinates

$$\begin{aligned} N_i = \tfrac{1}{2}[\zeta_0 + 1](\eta_0 + 1)(2 + \xi_0 + \eta_0 - \xi^2 - \eta^2), \\ a\xi_i(\xi_0 + 1)^2(\xi_0 - 1)(\eta_0 + 1), \\ b\eta_i(\xi_0 + 1)(\eta_0 + 1)^2(\xi_0 - 1)] \end{aligned} \tag{1.72}$$

with

$$\begin{aligned} \xi = (x - x_c)/a \\ \xi = (y - y_c)/b \\ \xi_0 = \xi.\xi_i \\ \eta_0 = \eta.\eta_i \end{aligned} \tag{1.73}$$

The form of B is obtained directly from equations (1.66) or (1.70) using equation (1.61). Thus

$$\varepsilon = \left\{ \begin{array}{ccccc} -2\alpha_4 & -6\alpha_7 x & -2\alpha_8 y & -6\alpha_{11} xy & \\ -2\alpha_6 & -2\alpha_9 x & -6\alpha_{10} y & -6\alpha_{12} y & \\ 2\alpha_5 & 4\alpha_8 x & 4\alpha_9 y & 6\alpha_{11} x^2 & 6\alpha_{12} y^2 \end{array} \right\} \tag{1.74}$$

and

$$\varepsilon = Q\alpha = QC^{-1}a^{(e)} \tag{1.75}$$

and thus

$$B = QC^{-1} \tag{1.76}$$

in which

$$Q = \begin{bmatrix} 0 & 0 & 0 & -2 & 0 & 0 & -6x & -2y & 0 & 0 & -6xy & 0 \\ 0 & 0 & 0 & 0 & 0 & -2 & 0 & 0 & -2x & -6y & 0 & -6xy \\ 0 & 0 & 0 & 0 & 2 & 0 & 0 & 4x & 4y & 0 & 6x^2 & 6y^2 \end{bmatrix} \quad (1.77)$$

Note that the displacement function chosen permits a state of constant strain (curvature) to exist. This satisfies one of the criteria of convergence.

Stiffness and Load Matrices

The stiffness matrix relating the nodal *forces* (given by a lateral force and two moments at each node) to the corresponding nodal displacement is

$$K^{(e)} = \int \int_{v^{(e)}} B^T D B dx dy \quad (1.78)$$

Substituting equation (1.76) and taking t as constant within the element,

$$K^{(e)} = C^{-1T}(\int \int Q^T D Q dx dy) C^{-1} \quad (1.79)$$

An explicit expression for the stiffness matrix K has been evaluated for the case of an orthotropic material and the result is given in Table 2.

$$\mathbf{K} = \frac{1}{60ab}\mathbf{L}\{D_x\mathbf{K}_1 + D_y\mathbf{K}_2 + D_1\mathbf{K}_3 + D_{xy}\mathbf{K}_4\}\mathbf{L}$$

with

$$\begin{Bmatrix} \mathbf{f}_i \\ \mathbf{f}_j \\ \mathbf{f}_k \\ \mathbf{f}_l \end{Bmatrix} = \mathbf{K} \begin{Bmatrix} \mathbf{a}_i \\ \mathbf{a}_j \\ \mathbf{a}_k \\ \mathbf{a}_l \end{Bmatrix}$$

$\mathbf{K}_1 = p^{-2}$

$p^{-2} = \dfrac{b^2}{a^2}$

Symmetrical

60											
0	0										
30	0	20									
30	0	15	60								
0	0	0	0	0							
15	0	10	30	0	20						
−60	0	−30	−30	0	−15	60					
0	0	0	0	0	0	0	0				
30	0	10	15	0	5	−30	0	20			
−30	0	−15	−60	0	−30	30	0	−15	60		
0	0	0	0	0	0	0	0	0	0	0	
15	0	5	30	0	10	−15	0	10	−30	0	20

$\mathbf{K}_2 = p^2$

$p^2 = \dfrac{a^2}{b^2}$

Symmetrical

60											
−30	20										
0	0	0									
−60	30	0	60								
−30	10	0	30	20							
0	0	0	0	0	0						
30	−15	0	−30	−15	0	60					
−15	10	0	15	5	0	−30	20				
0	0	0	0	0	0	0	0	0			
−30	15	0	30	15	0	−60	30	0	60		
−15	5	0	15	10	0	−30	10	0	30	20	
0	0	0	0	0	0	0	0	0	0	0	0

$\mathbf{K}_3 =$

Symmetrical

30											
−15	0										
15	−15	0									
−30	0	−15	30								
0	0	0	15	0							
−15	0	0	15	15	0						
−30	15	0	30	0	0	30					
15	0	0	0	0	0	−15	0				
0	0	0	0	0	0	−15	15	0			
30	0	0	−30	−15	0	−30	0	15	30		
0	0	0	−15	0	0	0	0	0	15	0	
0	0	0	0	0	0	15	0	0	−15	−15	0

Table 2. Stiffness matrix for a Rectangular element

The corresponding stress matrix for the internal moments of all the nodes is given in Table 3.

$6\rho^{-1}D_x + 6\rho D_1$	$-8aD_1$	$8bD_x$	$-6\rho D_1$	$-4aD_1$	0	$-6\rho^{-1}D_x$	0	$4bD_x$	0	0	0
$6\rho D_y + 6\rho^{-1}D_1$	$-8aD_y$	$8bD_1$	$-6\rho D_y$	$-4aD_y$	0	$-6\rho^{-1}D_1$	0	$4bD_1$	0	0	0
$-2D_{xy}$	$4bD_{xy}$	$-4aD_{xy}$	$2D_{xy}$	0	$4aD_{xy}$	$2D_{xy}$	$-4bD_{xy}$	0	$-2D_{xy}$	0	0
$-6\rho D_1$	$4aD_1$	0	$6\rho^{-1}D_x + 6\rho D_1$	$8aD_1$	$8bD_x$	0	0	0	$-6\rho^{-1}D_x$	0	$4bD_x$
$-6\rho D_y$	$4aD_y$	0	$6\rho D_y + 6\rho^{-1}D_1$	$8aD_y$	$8bD_1$	0	0	0	$-6\rho^{-1}D_1$	0	$4bD_1$
$-2D_{xy}$	0	$-4aD_{xy}$	$2D_{xy}$	$4bD_{xy}$	$4aD_{xy}$	$2D_{xy}$	0	0	$-2D_{xy}$	$-4bD_{xy}$	0
$-6\rho^{-1}D_x$	0	$-4bD_x$	0	0	0	$+\frac{6\rho^{-1}D_x}{6\rho D_1}$	$-8aD_1$	$-8bD_x$	$-6\rho D_1$	$-4aD_1$	0
$-6\rho^{-1}D_1$	0	$-4bD_1$	0	0	0	$+\frac{6\rho D_y}{6\rho^{-1}D_1}$	$-8aD_y$	$-8bD_1$	$-6\rho D_y$	$-4aD_y$	0
$-2D_{xy}$	$4bD_{xy}$	0	$2D_{xy}$	0	0	$2D_{xy}$	$-4bD_{xy}$	$-4aD_{xy}$	$-2D_y$	0	$4aD_{xy}$
0	0	0	$-6\rho^{-1}D_x$	0	$-4bD_x$	$-6\rho D_1$	$4aD_1$	0	$+\frac{6\rho^{-1}D_x}{6\rho D_1}$	$8aD_1$	$-8bD_x$
0	0	0	$-6\rho^{-1}D_1$	0	$-4bD_1$	$-6\rho D_y$	$4aD_y$	0	$+\frac{6\rho D_y}{6\rho^{-1}D_1}$	$8aD_y$	$-8bD_1$
$-2D_{xy}$	0	0	$2D_{xy}$	$4bD_{xy}$	0	$2D_{xy}$	0	$-4aD_{xy}$	$-2D_{xy}$	$-4bD_{xy}$	$4aD_{xy}$

Table 3. Rectangular element of Figure 17.

If a distributed load q acts per unit area on an element in the direction of w then the contribution of these forces to each of the nodes is

$$f_i = -\int\int N^T q dx dy \tag{1.80}$$

or by equation (1.70)

$$f_i = -C^{-1T}\int\int P^T q dx dy \tag{1.81}$$

Quadrilateral and Parallelogram Elements

The rectangular element is not easily generalised into the quadrilateral shape. Transformation of coordinates can be performed, but generally results in the violation of the constant curvature criterion. Thus such elements behave badly, but convergence may still occur providing the patch test is passed in the curvilinear coordinates.

Only for the case of the parallelogram is it possible to achieve constant curvature exclusively using functions of ξ and η. For a parallelogram the local coordinates (Figure 18) can be related to the global coordinates by an explicit expression

$$\begin{aligned} \xi &= (x - y\cot\alpha)/a \\ \eta &= \csc\alpha/b \end{aligned} \tag{1.82}$$

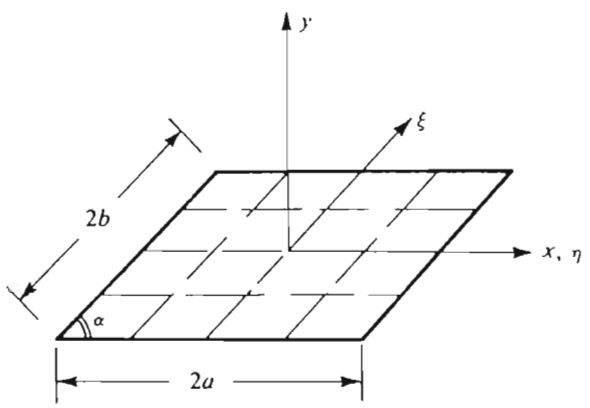

Figure 18. Parallelogram element and skew coordinates

1.3 Buckling of Structures

1.3.1 Introduction

In certain instances, like when subjected to in-plane loads, a structure may have induced within it critical compressive stresses which lead to the development of large distortions. Such structures are said to *buckle*, or become *unstable*, at these

critical loads.

The mathematical formulation of such problems are termed *eigenvalue* problems, as the following example illustrates.

1.3.2 The Mathematical Formulation of a Typical Buckling Problem - Pin Ended-Struts

Consider a pin-ended strut subject to an axial thrust P as shown Figure 19.

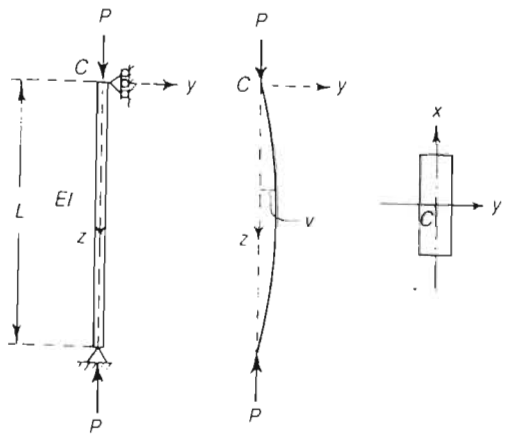

Figure 19. Flexural buckling of a pin ended strut under axial thrust.

Suppose L is the length of the bar and EI, its uniform flexural stiffness for bending in the $y-z$ plane. The bending moment at any section of the bar is then [79]

$$M = Pv \tag{1.83}$$

where v is the deflection. The moment-curvature relation for the beam at any section is also given by

$$M = -EI\frac{d^2v}{dz^2} \tag{1.84}$$

provided the deflection v is small. Thus

$$Pv = -EI\frac{d^2v}{dz^2} \tag{1.85}$$

Consequently

$$Pv + EI\frac{d^2v}{dz^2} = 0 \tag{1.86}$$

Thus

$$P\frac{d^2v}{dz^2} + \frac{d^2}{dz^2}(EI\frac{d^2v}{dz^2}) = 0 \tag{1.87}$$

which is the *Euler-Bernoulli* eigenvalue equation, with the eigenvalue $\lambda = P$.

1.3.3 Solution of the Eigenvalue Problem

The eigenvalue problem can typically be expressed in the general form:

$$(A - \lambda I)X = 0 \tag{1.88}$$

where I the identity matrix, and X the eigenvector. This can be solved for λ by determining the non-trivial values of λ for

$$|A - \lambda I| = 0 \tag{1.89}$$

1.4 Composite Materials

1.4.1 Introduction

Composites are produced when two or more materials are joined to give a combination of properties that cannot be attained in the original materials. Composite materials may be selected to give unusual combinations of stiffness, strength, weight, corrosion resistance, hardness or conductivity.

Fiber reinforced composites incorporate strong, stiff and brittle fibers into a softer, ductile matrix. The matrix material transmits the force to the fibers, which carry most of the load. The reinforcing fibers may be introduced into the matrix in a number of orientations. Short, randomly orientated fibers with small aspect ratios are easily introduced into the matrix, and result in relatively isotropic composite behaviour. Unidirectional arrangement of long fibers produces anisotropic behaviour, with particularly good strength and stiffness parallel to the fibers.

One of the unique characteristics of fiber-reinforced composites is that their properties can be tailored to meet different loading conditions. Long continuous

fibers can be introduced in several directions within the matrix, and this is the basis for laminated composite structures. Such laminates are composed of layer upon layer, within each of which the fibers are arranged at a particular discrete orientation. The resulting mechanical properties can be extremely advantageous, and indeed, laminated composite materials are used with increasing frequency in various technical applications, particularly in the fields of automotive, aerospace and marine engineering. This is primarily due to the high specific strength and stiffness values that these materials offer.

1.4.2 General Theory of Composite Materials

Unidirectional Composites

The fundamental stress-strain relationships, as for isotropic materials, are [80]:

$$\begin{aligned} \epsilon_x &= \frac{1}{E_x}\sigma_x \\ \epsilon_y &= -\frac{\nu_x}{E_x}\sigma_x = -\nu_x\epsilon_x \end{aligned} \tag{1.90}$$

where ϵ_x and ϵ_y are the strains in the x and y directions due to a stress in the x direction σ_x; E_x is the longitudinal Young's modulus and ν_x the longitudinal Poisson's ratio. The shear strain is given by

$$\epsilon_s = \frac{1}{E_s}\sigma_s \tag{1.91}$$

where E_s is the longitudinal shear modulus and σ_s, the shear stress. By applying the principle of superposition, the following is obtained:

$$\begin{aligned} \epsilon_x &= \tfrac{1}{E_x}\sigma_x - \tfrac{\nu_y}{E_y}\sigma_y \\ \epsilon_y &= \tfrac{\nu_x}{E_x}\sigma_x - \tfrac{1}{E_y}\sigma_y \\ \epsilon_s &= \tfrac{1}{E_s}\sigma_s \end{aligned} \tag{1.92}$$

Solving for the stresses in terms of the strain results in:

$$\begin{aligned} \sigma_x &= mE_x[\epsilon_x + \nu_y\epsilon_y] \\ \sigma_y &= mE_y[\nu_x\epsilon_x + \nu_y] \\ \sigma_s &= E_s\epsilon_s \end{aligned} \tag{1.93}$$

where $m = [1 - \nu_x\nu_y]^{-1}$. Components of modulus Q_{ij} are introduced in order to simplify the notation:

$$\begin{pmatrix} \sigma_x \\ \sigma_y \\ \sigma_s \end{pmatrix} = \begin{pmatrix} Q_{xx} & Q_{xy} & 0 \\ Q_{yx} & Q_{yy} & 0 \\ 0 & 0 & Q_{ss} \end{pmatrix} \begin{pmatrix} \epsilon_x \\ \epsilon_y \\ \epsilon_s \end{pmatrix} \tag{1.94}$$

where

$$\begin{aligned} Q_{xx} &= mE_x \qquad Q_{yy} = mE_y \qquad Q_{yx} = m\nu_x E_y \\ Q_{xy} &= m\nu_y E_x \qquad Q_{ss} = E_s \end{aligned} \tag{1.95}$$

Symmetric Laminates

Inplane stiffness

Multidirectional laminates consisting of plies with arbitrary orientations may also be described by components of modulus. A multidirectional laminate is symmetric if there is symmetry around its midplane, or $z = 0$ plane, where z is the dimension through the thickness of the laminate. The upper half of the stacking of layers is thus the same as the lower half, except that the sequence is reversed. This condition is may be written as

$$\theta(z) = \theta(-z) \tag{1.96}$$

The derivation of the stress-strain relation for multidirectional laminates also requires the following assumption:

$$Q_{ij}(z) = Q_{ij}(-z) \tag{1.97}$$

that is, the ply material modulus must also be symmetric with respect to the midplane of the laminate. In addition, the strain across the laminate thickness is

taken to remain constant. The assumed strain components are then denoted by:

$$\begin{aligned} \epsilon_1(z) &= \epsilon_1^0 \\ \epsilon_2(z) &= \epsilon_2^0 \\ \epsilon_6(z) &= \epsilon_6^0 \end{aligned} \tag{1.98}$$

Since the modulus for different layers varies, the actual stress across the laminate is not constant. An average stress is thus defined across the laminate, as

$$\begin{aligned} \bar{\sigma}_1 &= \tfrac{1}{h}\int_{-h/2}^{h/2} \sigma_1 dz \\ \bar{\sigma}_2 &= \tfrac{1}{h}\int_{-h/2}^{h/2} \sigma_2 dz \\ \bar{\sigma}_6 &= \tfrac{1}{h}\int_{-h/2}^{h/2} \sigma_6 dz \end{aligned} \tag{1.99}$$

Substituting the stress-strain relation for any layer, gives:

$$\bar{\sigma}_1 = \frac{1}{h}\int [Q_{11}\epsilon_1 + Q_{12}\epsilon_2 + Q_{16}\epsilon_6] dz \tag{1.100}$$

and using the constant strain assumption

$$\bar{\sigma}_1 = \frac{1}{h}\int [Q_{11}\epsilon_1^0 + Q_{12}\epsilon_2^0 + Q_{16}\epsilon_6^0] dz \tag{1.101}$$

where, for symmetric laminates

$$Q_{11} = Q_{xx}\cos^4\theta + Q_{yy}\sin^4\theta + 2Q_{xy}\sin^2\theta\cos^2\theta + 4Q_{ss}\cos^2\theta\sin^2\theta$$

$$Q_{22} = Q_{xx}\sin^4\theta + Q_{yy}\cos^4\theta + 2Q_{xy}\sin^2\theta\cos^2\theta + 4Q_{ss}\cos^2\theta\sin^2\theta$$

$$Q_{12} = Q_{xx}\sin^2\theta\cos^2\theta + Q_{yy}\sin^2\theta\cos^2\theta + Q_{xy}(\cos^4\theta + \sin^4\theta)$$

$$-4Q_{ss}\cos^2\theta\sin^2\theta$$

$$Q_{66} = Q_{xx}\sin^2\theta\cos^2\theta + Q_{yy}\sin^2\theta\cos^2\theta - 2Q_{xy}\sin^2\theta\cos^2\theta$$

$$+Q_{ss}(\cos^2\theta - \sin^2\theta)^2$$

This can be written as

$$\bar{\sigma}_1 = \frac{1}{h}[A_{11}\epsilon_1^0 + A_{12}\epsilon_2^0 + A_{16}\epsilon_6^0] \tag{1.102}$$

and similarly

$$\begin{aligned}\bar{\sigma}_2 &= \tfrac{1}{h}[A_{21}\epsilon_1^0 + A_{22}\epsilon_2^0 + A_{26}\epsilon_6^0] \\ \bar{\sigma}_6 &= \tfrac{1}{h}[A_{61}\epsilon_1^0 + A_{26}\epsilon_2^0 + A_{66}\epsilon_6^0]\end{aligned} \tag{1.103}$$

where

$$\begin{aligned}A_{11} &= \int Q_{11}dz \\ A_{22} &= \int Q_{22}dz \\ A_{12} &= \int Q_{12}dz\end{aligned} \tag{1.104}$$

and

$$A_{12} = A_{21}$$
$$A_{16} = A_{61} \tag{1.105}$$
$$A_{26} = A_{62}$$

where the bending stiffness A_{ij} is the equivalent inplane modulus for a multidirectional laminate. Defining a stress resultant N_i in terms of the average stresses gives

$$N_1 = h\bar{\sigma}_1$$
$$N_2 = h\bar{\sigma}_2 \tag{1.106}$$
$$N_6 = h\bar{\sigma}_6$$

which may be written as

$$N_1 = A_{11}\epsilon_1^0 + A_{12}\epsilon_2^0 + A_{16}\epsilon_6^0$$
$$N_2 = A_{21}\epsilon_1^0 + A_{22}\epsilon_2^0 + A_{26}\epsilon_6^0 \tag{1.107}$$
$$N_6 = A_{61}\epsilon_1^0 + A_{62}\epsilon_2^0 + A_{66}\epsilon_6^0$$

These stress-strain relations are valid for inplane deformations.

Flexural stiffness

The flexural stiffness for the laminate may be derived by using the moment-curvature relation which describes the flexural behaviour. To take the place of the stress resultant, a moment is defined as follows

$$M_1 = \int \sigma_1 z dz \tag{1.108}$$

In terms of the components of modulus, this becomes

$$M_1 = \int [Q_{11}\epsilon_1 + Q_{12}\epsilon_2 + Q_{16}\epsilon_6] z dz \tag{1.109}$$

It can be shown that the strain can be written in terms of the curvature k, that is

$$\epsilon_1(z) = zk_1 \tag{1.110}$$

and equation (1.109) becomes

$$M_1 = \int [Q_{11}k_1 + Q_{12}k_2 + Q_{16}k_6] z^2 dz \tag{1.111}$$

These curvatures are independent of z thus

$$M_1 = D_{11}k_1 + D_{12}k_2 + D_{16}k_6 \tag{1.112}$$

and

$$\begin{aligned} M_2 &= D_{21}k_1 + D_{22}k_2 + D_{26}k_6 \\ M_6 &= D_{61}k_1 + D_{62}k_2 + D_{66}k_6 \end{aligned} \tag{1.113}$$

where the flexural stiffnesses are given as

$$\begin{aligned} D_{11} &= \int Q_{11} z^2 dz \quad D_{22} = \int Q_{22} z^2 dz \\ D_{12} &= \int Q_{12} z^2 dz \quad D_{66} = \int Q_{66} z^2 dz \\ D_{16} &= \int Q_{16} z^2 dz \quad D_{26} = \int Q_{26} z^2 dz \end{aligned} \tag{1.114}$$

and

$$\begin{aligned} D_{12} &= D_{21} \\ D_{16} &= D_{61} \\ D_{26} &= D_{62} \end{aligned} \tag{1.115}$$

Coupling modulus

General laminates are usually unsymmetric, and their key feature is the presence of an additional degree of coupling. The basic behaviour of this class of laminates is governed by the strain distribution across the thickness of the laminate. Combining the previously assumed strain for both in-plane and flexural deformation, the following is obtained:

$$\begin{aligned} \epsilon_1(z) &= \epsilon_1^0 + z k_1 \\ \epsilon_2(z) &= \epsilon_2^0 + z k_2 \\ \epsilon_6(z) &= \epsilon_6^0 + z k_6 \end{aligned} \tag{1.116}$$

Substituting this into the definition of the stress resultant:

$$\begin{aligned} N_1 &= \int (Q_{11}[\epsilon_1^0 + zk_1] + Q_{12}[\epsilon_2^0 + zk_2] + Q_{16}[\epsilon_6^0 + zk_6])dz \\ &= \int Q_{11}dz\epsilon_1^0 + \int Q_{12}dz\epsilon_2^0 + \int Q_{16}dz\epsilon_6^0 \\ &+ \int Q_{11}zdzk_1 + \int Q_{12}zdzk_2 + \int Q_{16}zdzk_6 \\ &= A_{11}\epsilon_1^0 + A_{12}\epsilon_2^0 + A_{16}\epsilon_6^0 + B_{11}k_1 + B_{12}k_2 + B_{16}k_6 \end{aligned} \tag{1.117}$$

Similarly

$$\begin{aligned} N_2 &= A_{21}\epsilon_1^0 + A_{22}\epsilon_2^0 + A_{26}\epsilon_6^0 + B_{21}k_1 + B_{22}k_2 + B_{26}k_6 \\ N_6 &= A_{61}\epsilon_1^0 + A_{62}\epsilon_2^0 + A_{66}\epsilon_6^0 + B_{61}k_1 + B_{62}k_2 + B_{66}k_6 \end{aligned} \tag{1.118}$$

and the components of the new coupling modulus are

$$\begin{aligned} B_{11} = \int Q_{11}zdz,\ B_{22} = \int Q_{22}zdz,\ B_{12} = \int Q_{12}zdz, \\ B_{66} = \int Q_{66}zdz,\ B_{26} = \int Q_{26}zdz,\ B_{16} = \int Q_{16}zdz, \end{aligned} \tag{1.119}$$

The B_{ij} are also called the 'torsional stiffnesses'.

1.5 Buckling of Laminated Rectangular Plates

1.5.1 Governing equations and boundary conditions

Consider a laminated rectangular plate of length a, width b and thickness H laying in the x, y, z plane, as shown in Figure 20.

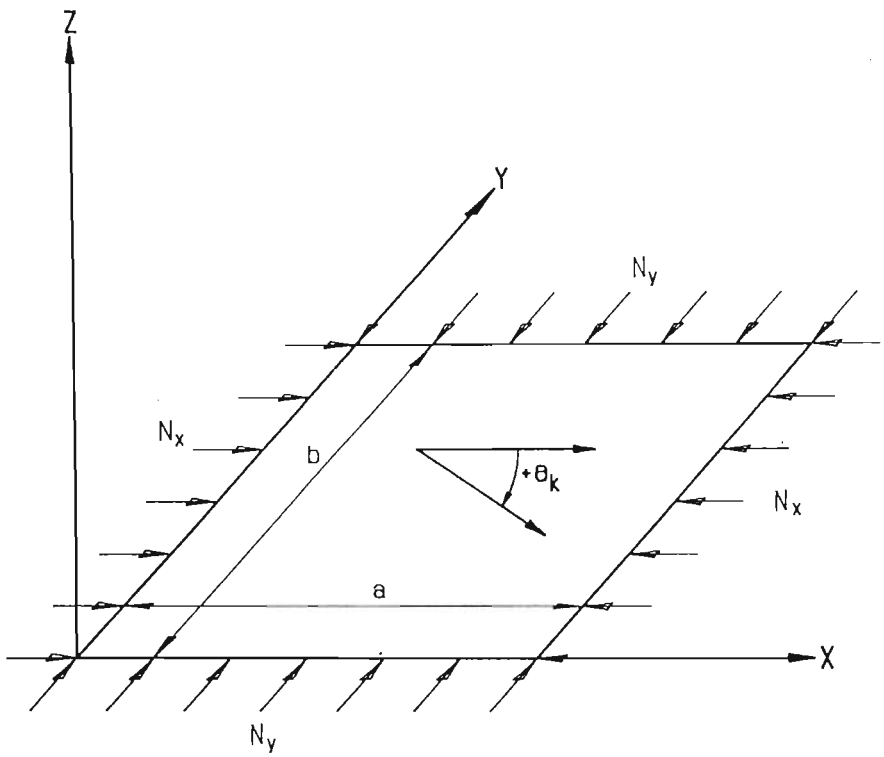

Figure 20. Geometry and loading of the laminated plate

It is constructed of an arbitrary number K of orthotropic layers of thickness H_k and fiber orientation θ_k where $k = 1, 2, ..., K$. An analysis based on the linear stability theory theory and the initial equilibrium position can be used to deter-

mine the buckling load. The equations governing the linear buckling of laminated plates under in-plane loads N_x, N_y and N_{xy} is given by [81]:

$$\begin{aligned} &A_{11}u_{,xx} + 2A_{16}u_{,xy} + A_{66}u_{,yy} + A_{26}v_{,xx} + (A_{12} + A_{66})v_{,xy} + A_{26}v_{,yy} \\ &-B_{11}w_{,xxx} - 3B_{16}w_{,xxy} - (B_{12} + 2B_{66})w_{,xyy} - B_{26}w_{,yyy} = 0 \end{aligned} \tag{1.120}$$

$$\begin{aligned} &A_{16}u_{,xx} + (A_{16} + A_{66})u_{,xy} + A_{26}u_{,yy} + A_{66}v_{,xy} + 2A_{26}v_{,xy} + A_{22}v_{,yy} \\ &-B_{16}w_{,xxx} - (B_{12} + 2B_{66})w_{,xxy} - 3B_{26}w_{,xyy} + B_{22}w_{,yyy} = 0 \end{aligned} \tag{1.121}$$

$$\begin{aligned} &D_{11}w_{,xxxx} + 4D_{16}w_{,xxxy} + 2(D_{12} + 2D_{66})w_{,xxyy} + 4D_{26}w_{,xyyy} + D_{22}w_{,yyyy} \\ &-B_{11}u_{,xxx} - 3B_{16}u_{,xxy} - (B_{12} + 2B_{66})u_{,xyy} - B_{26}u_{,yyy} - B_{16}v_{,xxx} \\ &- (B_{12} + 2B_{66})v_{,xxy} - 3B_{26}v_{,xyy} - B_{22}v_{,yyy} \\ &+ N_x w_{,xx} + 2N_{xy}w_{,xy} + N_y w_{,yy} = 0 \end{aligned} \tag{1.122}$$

where

$$(A_{ij},\ B_{ij},\ D_{ij}) = \int_{-H/2}^{H/2} (\bar{Q}_{ij})_k (1,\ z,\ z^2) dz \tag{1.123}$$

are the bending, torsional and flexural stiifnesses, as defined in eqns. (1.104), (1.119) and (1.114), and u, v and w are the displacements of the middle plane in the x, y and z directions, respectively, and $(\bar{Q}_{ij})_k$ is the plane stress reduced stiffness components of the $k-th$ layer.

Equations (1.120) - (1.122) give the displacement formulation of the buckling equations and their solution as an eigenvalue problem subject to specified

boundary conditions determines the buckling load.

The boundary conditions can be obtained from consideration of the variational formulation of the problem and involve one member of each pair of the following four quantities along a boundary:

$$u_n \text{ or } N_n^r,\ u_s \text{ or } N_{ns}^r,\ w_{,n} \text{ or } M_n^r,\ w \text{ or } M_{ns,s}^r + Q_n + N_n w_{,n} + N_{ns} w_{,s} \quad (1.124)$$

where n and s denote the normal and tangential directions to the plate edge. In equation (3.16), N^r and M^r are stress and moment resultants obtained by integrating the stresses and their moments across the laminate thickness with respect to z. For rectangular plates $n = x$ or $s = y$ or x corresponding to edges parallel to the y or x axis, respectively.

Symmetric cross-ply laminates

In the case of the symmetrically laminated cross-ply plate, the axes of orthotropy are aligned with the $x - y$ coordinates of the plate so that θ_k is either 0^o or 90^o. Due to symmetry, the coupling stiffnesses. B_{ij} are zero. Since Q_{16} and Q_{26} are zero for $\theta = 0^o$ and 90^o, the stiffnesses A_{16}, A_{26}, D_{16} and D_{26} also vanish. The equations (1.120) and (1.121) are uncoupled from eqn. (1.122) which now

becomes

$$D_{11}w_{,xxxx} + 2(D_{12} + 2D_{66})w_{,xxyy} + D_{22}w_{,yyyy} + N_x w_{,xx} + 2N_{xy}w_{,xy} + N_y w_{,yy} = 0 \tag{1.125}$$

For simply supported plates,

$$w = 0, \; M_n^r \tag{1.126}$$

on each boundary. These boundary conditions can be exactly satisfied by a displacement function of the form

$$w(x,y) = \sum_m^M \sum_n^N W_{mn} \sin(m\pi x/a) \sin(n\pi y/b) \tag{1.127}$$

The solution (1.127) represents $M \times N$ possible modes of buckling and a truncated series can be used to obtain the solution of eqn. (1.125). In particular, under biaxial compression with $N_x = \lambda_1 N$, $N_y = \lambda_2 N$ with $N_{xy} = 0$, the buckling load for the half-wave numbers (m,n) is given by

$$N_{mn}(H_k, \theta_k) = \frac{D_{11}\alpha_m^4 + 2(D_{12} + 2D_{66})\alpha_m^2\beta_n^2 + D_{22}\beta_n^4}{\alpha_m^2\lambda_1 + \beta_n^2\lambda_2} \tag{1.128}$$

where $\alpha_m = m\pi x/a$ and $\beta_n = n\pi y/b$. The critical buckling load $N_{cr}(H_k, \theta_k)$ and the corresponding mode shape are determined by minimising N_{mn} over m and n.

Symmetric angle-ply laminates without bending-twisting coupling

In the case of angle-ply laminates, the fiber orientation of the $k-th$ layer is between 0^o and 90^o, and consequently the bending stiffnesses D_{16} and D_{26} are non-zero, giving rise to bending-twisting coupling. This effect can be neglected by assuming D_{16} and D_{26} to be zero. In this case the differential equation governing the buckling of symmetric angle-ply laminates is given by eqn. (1.125) and the buckling load N_{mn} by eqn. (3.35), except that the values of D_{ij} are functions of θ_k. The values of D_{16} and D_{26} are largest for three-layered symmetric laminates $(\theta/\text{-}\theta/\theta)$ and decreases in value for laminates with a stacking sequence of $(\theta/\text{-}\theta/...)_{sym}$ as the number of layers increases [70]. For laminates with several layers, D_{16} and D_{26} can be small in comparison to the other D_{ij}. However, neglecting even small values of D_{16} and D_{26} may lead to erroneous results [70].

Symmetric angle-ply laminates with bending-twisting coupling

The influence of bending-twisting coupling stiffnesses D_{16} and D_{26} on the buckling of symmetric angle-ply laminates has been investigated by Noor *et al* [82], Nemeth [83] and Whitney [81], [84]. A study by Grenestedt [85], carried out using a perturbation approach for a combination of simply supported and clamped boundary conditions shows that when D_{16} and D_{26} are included in the formulation, the axial buckling load decreases. A parametric study of infinitely long laminates by Nemeth [86] indicated that the buckling resistance can be increased

by tailoring the laminate construction so as to increase the twisting stiffness parameter (D_{16} and D_{26})/(D_{11} D_{22})$^{1/2}$. Moreover, the importance of anisotropy generally diminishes as this parameter increases. A detailed discussion of the effect of D_{16} and D_{26} on the axial and shear buckling loads was given by Rohwer [87] where the influence of boundary conditions, the number of layers and ply angles was studied. It was observed that the buckling load reduction under axial loads is the highest for small number of layers and for ply angles around 45° for a combination of simply-supported and clamped edges. Comparison of laminates with and without bending-twisting coupling were given by Sherbourne & Pandey [88] for various boundary conditions and linearly varying uniaxial compressive loads.

1.5.2 Optimal buckling design of symmetric laminates using the layer fiber angle as the design variable: An Overview

Lay-up optimisation of laminates under buckling loads involves the maximisation of the buckling load by determining the optimum values of the layer ply angles [89].

Cross ply laminates

Earlier work carried out on the lay-up optimisation of symmetric cross-ply laminates subject to in-plane buckling loads includes that by Chen & Bert [90], and Bert & Chen [91]. In these studies, the layer thicknesses are taken as constant and various combinations of ply angles for four layer simply supported plates are investigated. For laminates with an aspect ratio $a/b = 3$, subject to a uniaxial load N_x, the stacking sequence in order of increasing buckling load are $(90^o/90^o)_{sym}$, $(0^o/0^o)_{sym}$,$(90^o/0^o)_{sym}$ and $(0^o/90^o)_{sym}$ for glass/epoxy and graphite/epoxy materials. When the same laminates are subject to biaxial compression $N_y/N_x = 0.5$ and 1.0, the stacking sequence in order of increasing buckling load are $(0^o/0^o)_{sym}$, $(0^o/90^o)_{sym}$, $(90^o/90^o)_{sym}$ and $(90^o/0^o)_{sym}$ for boron/epoxy and graphite/epoxy materials.

Symmetric laminates with D_{16} and D_{26} neglected

Studies by Bert & Chen [90], [91] showed that optimum, ply fiber angles are functions of the load ratio N_y/N_x and the material properties. Further studies by Hirano [92], [93], and Joshi & Iyengar [94], [95] gave the optimum ply angle as 45^o for $a/b = 1$, 2 under uniaxial buckling loads. The optimal ply angle is found to be 0^o for aspect ratios of 0.5, 38^o for $a/b = 0.8$, and 50.5^o for $a/b = 1.25$. Similar results were obtained by Nagagiri & Takabatake [96]. Muc [97] using a general theory but assuming Q_{16} and $Q_{26} = 0$ showed that symmetric laminates

give the highest buckling load for simply supported boundaries.

The results for maximum buckling load under shear only were obtained by Hirano [98] without assuming symmetry a priori but taking Q_{16} and $Q_{26} = 0$. Optimum designs produced symmetric layups with optimum ply angles of 45°, 55° and 60° for aspect ratios $a/b = 1$, 1.5 and 3, respectively, which validates the results obtained by Housner & Stein [99]. These results were confirmed by Grenestedt [100] using lamination parameters to compute the optimum ply angles which were observed to be similar for a simply supported and clamped boundary conditions in the interval $a/b = 1$ to $a/b = 3$.

Optimum ply angles of symmetric laminates under axial buckling loads N_x and inplane shear N_y were given by Chao *et al* [101] for glass/epoxy materials and it was observed that θ_{opt} tends to 90° as the aspect ratio increases, which confirmed the results obtained by Crouzet-Pascal [102] for uniaxially compressed plates of the same material. In the study by Chao *et al* [101] the critical aspect ratios are determined such that the laminate fails by buckling at aspect ratios higher than the critical one and by yielding at the lower ones.

Optimisation of symmetrically laminated plates was studied by Tang [103], [104], [105], Pedersen [106], [107], Grenestadt [100], [108], [109], and Cheng & Tang [110] with emphasis on the qualitative aspects of the optimal design. Tang [103], [104] showed that symmetric laminates give the highest buckling load and determined the optimal ply angles under unimodal and bimodal buckling. Tang also established that for these problems the optimisation can be reduced to a

single variable design problem. Pedersen [106], [107] pointed out the importance of the functional

$$\phi = D_{11}(m/a)^4 + 2(D_{12} + 2D_{66})(mn/ab)^2 + D_{22}(n/b)^4 \tag{1.129}$$

in the optimal design of symmetric laminates with buckling, vibration and/or deflection objectives and highlighted its character in terms of the node parameter $\eta_{mn} = mb/na$ for the computation of optimum ply angles. Grenestedt [100], [108] confirmed the results of Tang [103], [104] by showing the sufficiency of one parameter to characterise the optimum configurations of symmetrically laminated plates. Convexity of the feasible region of the lamination parameters was investigated for the most general lay-ups in the study by Grenestedt [109] and the feasible regions were determined for some special cases. Cheng & Tang [110] determined the expressions for optimum ply angles and the intervals where these angles are valid in terms of the mode parameter η_{mn} for symmetric laminates undergoing unimodal or bimodal buckling after establishing that a symmetric laminate gives the highest buckling load.

Symmetric laminate with bending-twisting coupling

Optimum ply angles were determined by Housner & Stein [99] for clamped and simply supported laminates. In the case of simply supported plates under axial loads, θ_{opt} shifts from 0^o to 45^o as the aspect ratio increases from 1 to ∞, while the

shift is from 45^o to about 60^o in the cast of shear loading. For simply supported plates, θ_{opt} is approximately equal to 45^o for all values of the plate aspect ratio, under uniaxial loading, and θ_{opt} is approximately equal to 45^o to 60^o for $a/b = 1 - \infty$, under shear loading which is similar to the clamped case. A concise outline of these results is given by Leissa [111], [112]. The behaviour of optimum ply angles with respect to the aspect ratio was investigated for clamped and simply supported boundary conditions by Kassimaly *et al* [113] for the uniaxial loading case. The optimum ply angles for maximum shear load with and without D_{16} and D_{26} differ only marginally for simply supported and clamped laminates, for the aspect ratios $a/b = 1 - 3$, as shown by Grenestedt [100]. However, the maximum shear load may be higher or lower than that of an orthotropic laminate depending on the direction of the shear load [100].

The effects of the number of layers K and the bending-twisting coupling on the optimum ply angles and the buckling load were investigated by Sawyer [114]. For simply supported laminates of aspect ratios of 1 and 10, and under uniaxial compression, θ_{opt} is 45^o for the stacking sequence $(\theta/\text{-}\theta/...)_{sym}$ with the effect of D_{16} and D_{26} becoming negligible for $K \geq 8$. Qian *et al* [115] determined the optimum ply angles of symmetric laminates with bending-twisting coupling for a combination of simply supported and clamped boundary conditions. In the study by Qian, directional design derivatives were used to derive the optimality condition

$$(Lw)^T[\delta D](L\tilde{w}) = 0 \qquad (1.130)$$

where $(Lw)^T = (w_{,xx}\ w_{,yy}\ 2w_{,xy})$ and $[\delta D]$ represents the matrix of which the elements are given by

$$\delta D_{ij} = \sum_{k}^{K/2} (\frac{\partial D_{ij}}{\partial \theta_k}) \delta\theta_k \tag{1.131}$$

with $\delta\theta_k$ denoting the independant design changes.

In eqn. (1.131), the buckling modes $\tilde{w}(x,y)$ and $w(x,y)$ are equal in the case of unimodal buckling, and are orthonormal in the case of bimodal buckling. Explicit expressions of optimality can be derived for both cases using eqns. (1.130) and (1.131). The problem is solved by an iterative technique in which the designs are updated until convergence is achieved, and the optimality condition (1.130) is satisfied. In the study by Qian [115], numerical results were given by eight ply laminates with a stacking sequence given by $(\theta_2/\text{-}\theta_2/\theta_1/\text{-}\theta_1)_{sym}$. It was found that the optimum ply angles vary around $\pm 45^o$ for various boundary conditions, and aspect ratios when the load is uniaxial, except when the unloaded edges are clamped, and $a/b = 1$, in which case $\theta_{1opt} = \theta_{2opt} = 0^o$. Under biaxial compression with $N_y/N_x = 1$, θ_{1opt} and θ_{2opt} vary around 65° and -70° respectively, for simply supported and around 55^o and -60° for clamped plates when $a/b \geq 1.4$.

Poisson's effect on the optimal design

Buckling analysis of uniaxially compressed plates is generally based on the assumption that the unloaded edges of the plate are free to translate, and thus Poisson's effect can be neglected. This assumption can be expressed by the boundary

conditions $N_n = N_{ns} = 0$ imposed on the unloaded edges. When these edges are restrained, and thus cannot translate freely, the buckling behavior of the laminate changes as the compression becomes biaxial owing to the effect of Poisson's ratio [116]. The inclusion of this effect in the analysis leads to lower buckling loads and considerable difference in the optimum ply angles as compared to the cases where these effects are neglected. As such, the *classic* optimisation results for uniaxially compressed laminated plates become inapplicable in the presence of restrained unloaded edges, as shown in a study by Sherbourne & Pandey [117].

A formulation of the problem may be given as follows. Let uniaxial compression N_x be applied in the x direction, and the unloaded edges $y = 0,\ b$ be restrained from translating in the y direction by setting the in-plane displacement to zero. Then two types of boundary conditions on the unloaded edges are defined with $N_{xy} = 0$ on $y = 0,\ b$,corresponding to free shear deformation, and $\gamma_{xy} = 0$ on $y = 0,\ b$ corresponding to zero shear deformation. In the first case, N_y is given by

$$N_y = (A_{12}A_{66} - A_{16}A_{26})N_x/(A_{11}A_{66} - A_{16}^2) \tag{1.132}$$

In the latter case ($\gamma_{xy} = 0$ on $y = 0,\ b$), N_y and N_{xy} are given by

$$N_y = A_{12}N_x/A_{11},\ N_{xy} = A_{16}N_x/A_{11} \tag{1.133}$$

In the study by Sherboune & Pandey [117], the problem was solved by approximating the displacement $w(x, y)$ by a series of orthogonal polynomials generated by a Gran-Schmidt process [118] and by computing the buckling load using the Rayleigh-Ritz method. In the case of simply supported square plates with $N_{xy} = 0$, on $y = 0, b$, θ_{opt} is 0^o if Poisson's effect is included as apposed to 45^o if it is neglected. The variation of the buckling load with θ is similar to that described by Obraztsov & Vasil'ev [116]. For clamped plates, θ_{opt} is 0^o for $a/b = 1$ and 2 with Poisson's effect included in the analysis, and 0^o and 45^o, respectively, without this effect. The maximum buckling load decreases when the free edges are restrained with the decrease being substantial when the loaded edges are simply supported and relatively small when these edges are clamped.

The study of Sherbourne & Pandey [117] also gives results for bidirectional laminates with a stacking sequence $(\gamma - 30^o, \gamma + 30^o)_{sym}$ where γ denotes the twist angle. Bidirectional laminates differ from laminates with a stacking sequence of $(\theta/\text{-}\theta)_{sym}$ in that the maximum buckling loads when Poisson's effect is included can be higher than those for the classical case. The optimum twist angle is found to be around 45^o for aspect ratios $a/b = 1$ and 2 irrespective of the boundary conditions. This seems to be due to the fact that Poisson's ratio ν_{xy} is negative for γ ranging from 35^o to 55^o which induces a tensile force in the transverse direction, thereby increasing the buckling load and producing the optimum γ in this range.

The effect of cut-outs

The presence of cut-outs significantly affects the buckling behavior and optimum design of laminated plates. Results obtained by Srivatsa & Krishna Murty [119] for symmetric laminates under uniaxial compression indicate that the optimum ply angle depends on the size of the cut-out to a large extent. For simply supported plates square laminates made of graphite/epoxy, θ_{opt} changed from 45^o to 60^o as d/a increases from 0 to 0.6 where d is the diameter of the central hole. For clamped plates this change is between 0^o and 60^o. In the case of clamped loaded edges and simply supported unloaded edges, θ_{opt} varies from 0^o to 45^o as d/a varies from 0 to 0.5.

Parametric studies by Nemeth [120] investigate the relations between the uniaxial buckling load, ply angle and the hole size for symmetrically laminated plates.

A variable fiber angle was proposed by Hyer & Lee [121] to increase the buckling resistance of composite plates with holes. The problem is solved by the finite element method and element fiber orientations are employed as design variables. A sensitivity study indicates the regions which are most affective in improving the buckling resistance. The results obtained using s gradient-search technique show the buckling load can be increased by 2.96 times as compared to a baseline design taken as $(\pm 45^o/0^o)_{sym}$.

Postbuckling of rectangular laminated plates

Frauenthal [122] reported in a study that isotropic structures optimised with respect to buckling strength may exhibit low postbuckling resistance. Consequently, optimisation in the postbuckling rang becomes an important design consideration for laminates which may be exposed to compressive loads higher than the buckling load. Results reported by Obraztsov & Vasil'ev [116] indicate that optimum ply angles for the maximisation of the ultimate load carrying capacity of symmetric angle-ply laminates coincides with the fiber orientations providing maximum strength in the pre-buckled state. Effects of designing for maximum buckling load on the postbuckling behavior as well as optimal designs for maximum postbuckling stiffness were studied by Pandey & Sherbourne [123] for simply supported symmetric laminates. In this study, the initial postbuckling stiffness was used as a measure of the postbuckling strength. a non-linear analysis based on a large deflection theory gives the postbuckling stiffness K_p as

$$K_p = \frac{a_{22} + \mu_{mn}^4 a_{11}}{2a_{11}a_{22}(1 + \lambda\mu_{mn}^2) + (a_{22} + \mu_{mn}^4 a_{11})(a_{11} + \lambda a_{12})} \tag{1.134}$$

where $\mu_{mn} = \beta_n/\alpha_m = na/mb$, $\lambda = N_y/N_x$ and a_{ij} are the in-plane flexibility coefficients given by $a_{ij} = A_{ij}^{-1}$. Eqn. (1.134) is evaluated at critical wavenumbers m and n corresponding to the linear buckling load of the laminate. An examination of eqns. (3.35) and (1.134) shows that the buckling load and the postbuckling stiffness are described by functions of different nature as reflected

by D_{ij} and A_{ij} repetitively, in these expressions. Optimisation based on bending stiffnesses only leads to designs with weal postbuckling performance. In the study by Pandey & Sherbourne [123], optimisation results were obtained for specially orthotropic laminates with a stacking sequence of $[(\theta_1/\text{-}\theta_1/\theta_2/\text{-}\theta_2)_{sym}/(\text{-}\theta_1/\theta_1/\text{-}\theta_2/\theta_2)_{sym}]$ for which $A_{16} = A_{26} = D_{16} = D_{26} = 0$. For uniaxially compressed laminates, optimum ply angles for maximum postbuckling stiffness are given by $(\theta_{1opt}, \theta_{2opt}) = (0^o, 0^o)$ for $a/b = 1$ and 2. The corresponding ply angles for maximum buckling load are $(45^o, 45^o)$. Under a biaxial load with $\lambda = 1$, the corresponding ply angles are $(15^o, 5^o)$ and $(0^o, 90^o)$ for maximum K_p as compared to $(45^o, 45^o)$ and $(70^o, 70^o)$ for maximum N_{cr}. The values of K_p and N_{cr} at these ply angles indicate that a laminate designed with

respect to one criterion will perform quite poorly with respect to another.

Designs can be improved with respect to both criteria by noting that the postbuckling stiffness often reaches its maximum value around 0^o or 90^o ply angles and the values of A_{ij} are independent of the stacking sequence. By introducing 0^o and/or 90^o plies in the core region of the laminates, improved designs can be obtained which have slightly lower buckling loads, but substantially higher postbuckling stiffness.

Chapter 2

Optimal Design Problems

2.1 Introduction

Composite structures often contain components which may be modelled as rectangular plates. A common type of composite plate is the symmetrically laminated angle ply configuration which avoids bending-stretching effects by virtue of mid-plane symmetry. An important failure mode for these plates is buckling under in-plane loading. The buckling resistance of fiber composite plates can be improved by using the ply angle as a design variable, and determining the optimal angles to maximise the buckling load.

The following sections detail five studies, dealing with the optimal design of symmetric rectangular laminated composite plates for maximum buckling load or postbuckling stiffness. The layer fiber angle is used as the optimising variable in all the cases, and either numerical methods, or analytical methods were used to carry out the analysis, in conjunction with the *Golden Section* method [124], which was used to determine the optimal fiber orientations.

2.2 Part 1: Optimal Design of Symmetric Laminates for Maximum Buckling Load Including the Effects of Bending-Twisting Coupling

One phenomenon associated with symmetric angle-ply configurations is the occurrence of bending-twisting coupling which may cause significantly different results as compared to cases in which this coupling is exactly zero [125]. The effect of bending-twisting coupling becomes even more pronounced for laminates with few layers. Due to this coupling, closed-form solutions cannot be obtained for any of the boundary conditions and this situation led to neglecting bending-twisting coupling in several studies involving the optimisation of symmetric laminates under buckling loads. In actual fact, closed-form solutions for symmetric laminates are not available even for the simplified models where this coupling is neglected except if the boundary conditions are simply supported all around. Results obtained using different approaches can be found in the literature. Authors mostly dealt with either simply supported or clamped plate edges, neglecting the effect of bending-twisting coupling. However, the effects of boundary conditions and of bending-twisting coupling on the optimal designs remain mostly unknown. Thus, in general, as there is little reported on the optimal design of laminates with bending-twisting accounted for, and with different boundary conditions, the following optimal design problem was formulated.

2.2.1 Optimal Design Problem

Consider a symmetrically laminated rectangular plate of length a, width b and thickness h which consists of n orthotropic layers with fiber angles θ_k, $k = 1, 2, ..., K$, as shown in Figure 21. The plate is defined in the Cartesian coordinates x, y and z with axes x and y lying on the middle surface of the plate. The plate is subjected to biaxial compressive forces N_x and N_y in the x and y directions, respectively.

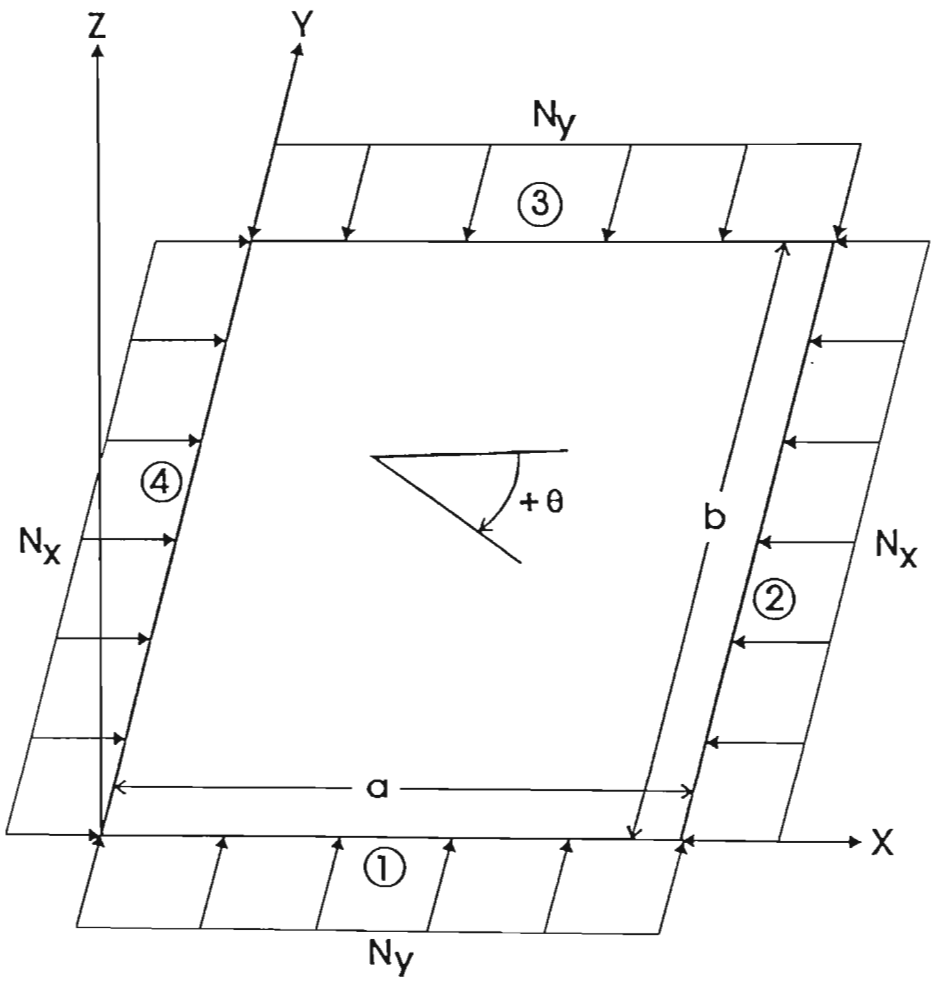

Figure 21. Geometry and loading of the symmetrically laminated plate subject to biaxial loads

The objective of the design problem is to maximise the buckling loads N_x and N_y for a given thickness h by optimally determining the fiber orientations given by $\theta_k = (-1)^{k+1}\theta$ for $k \leq K/2$ and $\theta_k = (-1)^k\theta$ for $k \geq K/2 + 1$. Let $N_x = N$ and $N_y = \lambda N$ where $0 \leq \lambda \leq 1$ is the proportionality constant. The buckling load $N(\theta)$ is given by

$$N(\theta) = \min_{m,n} [N_{mn}(m, n, \theta)] \tag{2.1}$$

where N_{mn} is the buckling load corresponding to the half-wave numbers m and n in the x and y directions, respectively. The design objective is to maximise $N(\theta)$ with respect to θ, viz.

$$N_{\max} \triangleq \max_{\theta} [N(\theta)],\ 0^o \leq \theta \leq 90^o \tag{2.2}$$

where $N(\theta)$ is determined from the finite element solution of the eigenvalue problem given by equation (2.1). The optimisation procedure involves the stages of evaluating the buckling load $N(\theta)$ for a given θ and improving the fiber orientation to maximise N. Thus, the computational solution necessitates successive stages of analysis and optimisation until a convergence is obtained and the optimal angle θ_{opt} is determined within a specified accuracy. The plate may be subjected to any combination of *free*, *simply supported* and *clamped* boundary conditions along the four edges, and may be composed of four layers, such that the bending-twisting effect is not negligible.

2.3 Part 2: Optimal Design of Symmetric Angle-ply Laminates Subject to Nonuniform Buckling Loads and In-plane Restraints

Poisson's effect manifests itself as in-plane loads if the unloaded edges of a uniaxially loaded laminate are restrained from translating freely. This in turn transforms a uniaxial buckling problem into a biaxial one and causes a reduction in the buckling load, as compared to the *classic* case, where the unloaded are free from restraint. Moreover, the optimal values of design variables change as compared to the classic case. In many practical situations, transverse movement of unloaded edges is restricted by adjacent panels, supports or stiffeners, inducing a transverse in-plane compressive force. In these cases, the buckling of uniaxially compressed rectangular plates is affected by the so-called *Poisson Plate Instability* phenomenon [126]. Moreover, it is often the case that the buckling loads are not uniformly distributed along the edges. The use of classic design data for the design of plates subjected to in-plane restraints leads to non-optimal buckling loads, just as an approximation of nonuniform loads by uniform ones also leads to inaccurate buckling loads and non-optimal ply angles. The question of just how much the optimal design of laminated plates subjected to in-plane restraints and non-uniform loads differed from classic designs led to the formulation of the second design problem.

2.3.1 Optimal Design Problem

Consider a symmetrically laminated rectangular plate of length a and width b (Figure 22). The plate is constructed of equal thickness orthotropic layers with fiber angles θ_k and $k = 1, 2, ..., K$ where K denotes the total number of layers. The plate is defined in the Cartesian coordinates x, y and z with axes x and y lying on the middle surface of the plate, and it is subject to uniaxial compression N_x in the x direction. The unloaded edges $y = 0$, $y = a$ are restrained from translating in the y direction giving rise to Poisson's effect, and resulting in compressive forces in this direction. This phenomena leads to a loss of stability under biaxial compressive forces even though the applied load is uniaxial.

The objective of the second design problem is to maximise the buckling load N_x for a given laminate thickness h by optimally determining the fiber orientations given by $\theta_k = (-1)^{k+1}\theta$ for $k \leq K/2$ and $\theta_k = (-1)^k\theta$ for $k \geq K/2 + 1$. The buckling load $N_x(\theta)$ is given by

$$N_x(\theta) = \min_{m,n} [N_{mn}(m, n, \theta)] \tag{2.3}$$

where N_{mn} is the buckling load corresponding to the half-wave numbers m and n in the x and y directions, respectively. The design objective is to maximise $N_x(\theta)$ with respect to θ, viz.

$$N_{\max} \triangleq \max_{\theta} [N_x(\theta)],\ 0^o \leq \theta \leq 90^o \tag{2.4}$$

where $N_x(\theta)$ is determined from the finite element solution of the eigenvalue

problem given by equation (2.3).

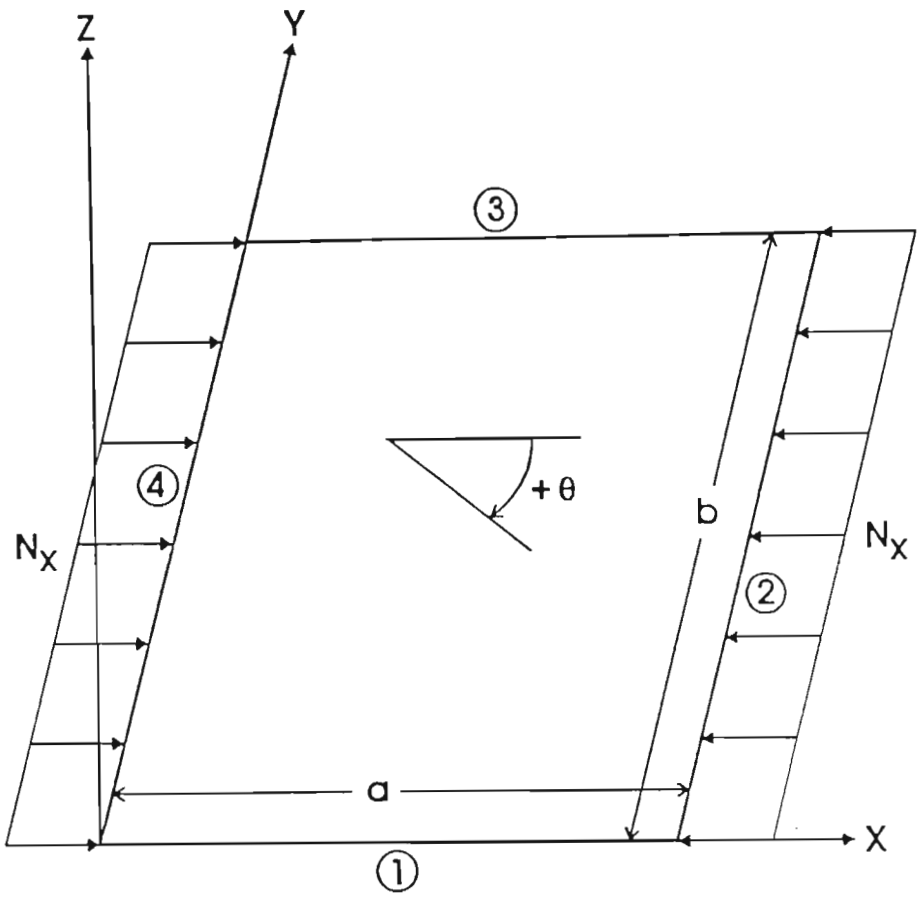

Figure 22. Geometry and loading of the symmetrically laminated plate subject to uniaxial loads and in-plane restraints

The optimisation procedure involves the stages of evaluating the buckling load $N_x(\theta)$ for a given θ and improving the fiber orientation to maximise N_x. Thus, as before, the computational solution necessitates successive stages of analysis and optimisation until a convergence is obtained and the optimal angle θ_{opt} is determined within a specified accuracy. The plate may be subjected to any combination of *free*, *simply supported* and *clamped* boundary conditions along the four edges, and may be composed of four layers, such that the bending-

twisting effect is not negligible. Furthermore, the loading N_x may be nonuniform.

2.4 Part 3: Optimal Design of Symmetric Laminates with Central Circular Cut-outs for Maximum Buckling Load

The presence of holes in laminated plates subjected to in-plane compressive forces results in decreased buckling load values [127]. Although some work has been reported in the literature, these results deal mostly with the effect of the cut-out on the buckling load, and as such, very little has appeared dealing with the optimal design of such plates. This lead to the formulation of the third optimal design problem.

2.4.1 Optimal Design Problem

Consider a symmetrically laminated rectangular plate of length a, width b, central hole diameter d and thickness h which consists of n orthotropic layers with fiber angles θ_k, $k = 1, 2, ..., K$, as shown in Figure 23. The plate is defined in the Cartesian coordinates x, y and z with axes x and y lying on the middle surface of the plate. The plate is subjected to biaxial compressive forces N_x and N_y in the x and y directions, respectively.

As in the first design problem, the objective of the third design problem is to maximise the buckling loads N_x and N_y for a given thickness h by optimally determining the fiber orientations given by $\theta_k = (-1)^{k+1}\theta$ for $k \leq K/2$ and

$\theta_k = (-1)^k\theta$ for $k \geq K/2+1$. Let $N_x = N$ and $N_y = \lambda N$ where $0 \leq \lambda \leq 1$ is the proportionality constant. The buckling load $N(\theta)$ is given by

$$N(\theta) = \min_{m,n} [N_{mn}(m, n, \theta)] \tag{2.5}$$

where N_{mn} is the buckling load corresponding to the half-wave numbers m and n in the x and y directions, respectively. The design objective is to maximise $N(\theta)$ with respect to θ, viz.

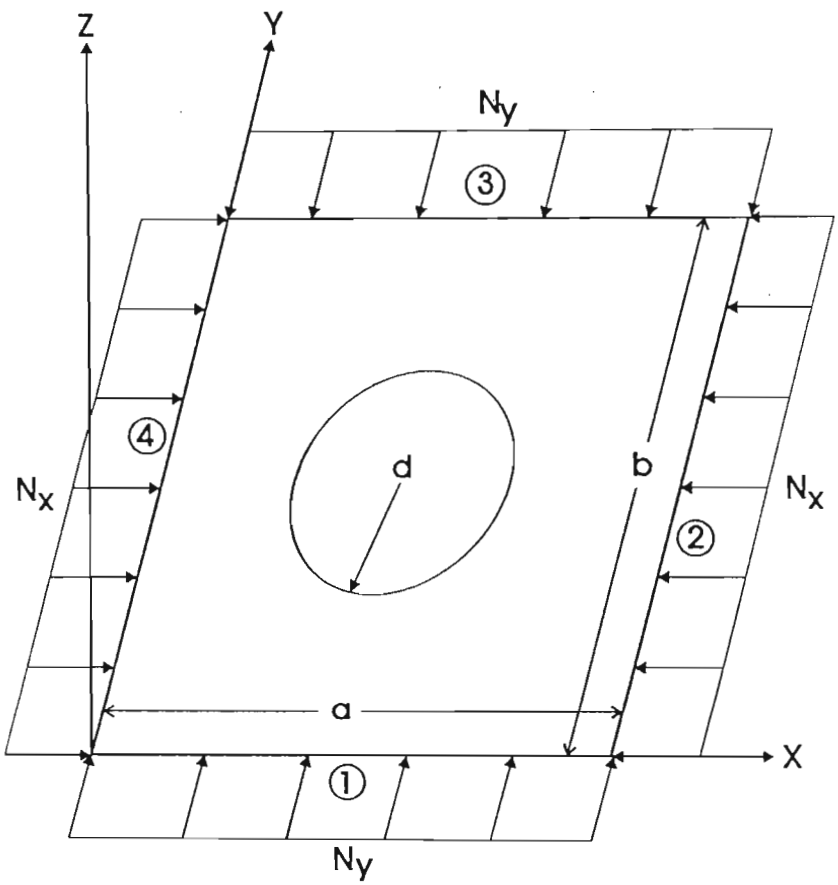

Figure 23. Geometry and loading of the symmetrically laminated plate with central circular cut-out

$$N_{\max} \triangleq \max_{\theta} [N(\theta)],\ 0^o \leq \theta \leq 90^o \tag{2.6}$$

where $N(\theta)$ is determined from the finite element solution of the eigenvalue problem given by equation (2.5).

The optimisation procedure involves the stages of evaluating the buckling load $N(\theta)$ for a given θ and improving the fiber orientation to maximise N. Thus, as before, the computational solution necessitates successive stages of analysis and optimisation until a convergence is obtained and the optimal angle θ_{opt} is determined within a specified accuracy. The plate may be subjected to any combination of *free*, *simply supported* and *clamped* boundary conditions along the four edges, and may be composed of four layers, such that the bending-twisting effect is not negligible.

2.5 Part 4: Optimal Laminate Configurations with Symmetric Lay-ups for Maximum Postbuckling Stiffness

Quite often, composite structures are required to carry loads beyond their buckling limit. In these cases, the postbuckling stiffness has to be maximised to improve the load carrying capability beyond the critical buckling load. Few studies exist on the optimal designs of laminated plates for maximum postbuckling stiffness and the subject remains largely unexplored. In this regard, the

fourth optimal design problem was formulated, and addresses the postbuckling maximisation of symmetrically laminated plates under biaxial compression. In this problem, a method is proposed to determine the optimal fiber orientation and stacking sequence of rectangular laminates by considering the initial postbuckling stiffnesses in *both* the x and y directions [128]. Design optimisation involves the comparison of the postbuckling performance of several laminate configurations with optimal ply angles.

2.5.1 Optimal Design Problem

Consider a laminated rectangular plate of length a, width b and height h laying in the Cartesian $x-y$ plane as shown in Figure 21. The plate is constructed of equal thickness orthotropic layers with fiber angles of θ_k, $k = 1, 2, ..., K$, where K denotes the total number of layers. The coordinate system x y z is located in the mid-plane, and the plate is subject to compressive forces N_x in the x direction, and N_y in the y direction with the load ratio defined as $\lambda = N_y/N_x$. The plate is symmetrically laminated with respect to the mid-plane and simply supported at all edges. Let the initial postbuckling stiffness in the x-direction be denoted by P_x and that in the y-direction by P_y.

The objective of the design optimisation problem is to maximise the initial postbuckling stiffnesses for a given laminate thickness h, and load ratio $\lambda = N_x/N_y$, by optimally determining the fiber orientations with the laminate configurations given by a combination of θ, 0^o and 90^o ply angles. Postbuckling stiffnesses are different in the x and y directions, and the optimal design problem has to be formulated with this situation in mind. A basic requirement is

imposed on the design stipulates that the postbuckling stiffness offered in one direction should be approximately proportional to the load applied in that direction. In this way stiffnesses in both directions will be at an acceptable level, and provide resistance in proportion to the in-plane loads applied in respective directions. It is necessary to maximise the postbuckling stiffness in the higher load direction subject to the requirement that the stiffness in the other direction will be sufficiently large to resist the load in that direction. These considerations are now quantified and used to formulate the optimal design problem in a rigorous manner.

For $\lambda \leq 1$, the in-plane force N_x in the x-direction is larger than that in the y-direction. For this case, the postbuckling stiffness P_x is maximised subject to the requirement that the postbuckling stiffness P_y in the y-direction will not be less than λP_x to ensure that enough postbuckling stiffness exists in the y-direction, noting that $N_y = \lambda N_x$. Thus for $\lambda \leq 1$, the optimal design problem can be stated as

$$\max_{\theta} \; P_x(\theta) \text{ subject to } \frac{P_y}{\lambda} \geq \; P_x \tag{2.7}$$

Similarly for $\lambda \geq 1$, $N_y \geq N_x$ and P_y is maximised subject to the requirement that $P_x \geq P_y/\lambda$ to ensure enough post-buckling stiffness in the x-direction, noting again that $N_x = N_y/\lambda$. Thus for $\lambda \geq 1$, the optimal design problem can be stated as

$$\max_{\theta} \; P_y(\theta) \text{ subject to } \lambda P_x \geq \; P_y \tag{2.8}$$

The maximum values of the stiffnesses are denoted by P_x^* and P_y^*.

These design formulations apply to a given laminate configuration and as

such constitute only a part of the design problem. Due to the specific nature of this problem, several laminate configurations with a combination of ply angles of θ, 0^o and 90^o are considered as candidate designs. More specifically, the configurations of the candidate designs are taken in the form of $(\theta/-\theta/.../0^o/.../90^o/.../0^o/...)_{sym}$. The best design, chosen from among the candidate designs, is that which gives the highest postbuckling stiffness, leading to the optimal laminate configuration.

Next, the optimal configuration problem is formulated. Let P_i^* denote the maximum postbuckling stiffness of the i-th laminate where $P_i^* = P_{xi}^*$ for $\lambda \leq 1$, and $P_i^* = P_{yi}^*$ for $\lambda \geq 1$. The best design is given by the laminate configuration corresponding to the highest P_i^* which is obtained from

$$P^* = \max_i \ P_i^* \tag{2.9}$$

with $i = 1, 2, ..., I$ where I denotes the number of candidate laminates. Thus the complete design optimisation involves the solution of the problem

$$\max_i \ (\max_\theta \ P_{\zeta i}), \ i = 1, 2, ..., I \tag{2.10}$$

$$\text{subject to } \lambda^s P_{\xi i} \geq P_{\zeta i}$$

where $\zeta = x$, $\xi = y$ and $s = -1$ for $\lambda \leq 1$, and $\zeta = y$, $\xi = x$ and $s = 1$ for $\lambda \geq 1$.

For a given laminate configuration, the optimisation procedure involves the stages of evaluating the initial postbuckling stiffnesses $P_x(\theta)$ and $P_y(\theta)$ for a

given θ and improving the fiber orientation iteratively to maximise either of the quantities, depending on the value of λ, subject to the corresponding constraint. Thus, the computational solution consists of successive stages of analysis and optimisation until a convergence is obtained and the optimal ply angle θ_{opt} is determined within a specified accuracy. This procedure is applied to every laminate configuration. Once the design optimisation for each laminate is completed, the best configuration is chosen from amongst the candidate laminates so as to obtain the one with the highest postbuckling stiffness.

2.6 Part 5: Multiobjective Design of Laminated Plates Subject to In-plane Restraints for a Maximum Combination of Prebuckling and Postbuckling Stiffness and Buckling Load

In some instances, when structures are to subjected to loads beyond their buckling limit, they are required to be both strong and stiff before buckling occurs, and stiff after buckling has occurred, in order that catastrophic failure is delayed. The design maximisation of more than a single parameter at a time is termed *multiobjective* design, and can lead to designs which are better in all criteria than the single criteria designs. With this in mind, the last design problem was formulated, with the aim of maximising the prebuckling and postbuckling stiffness, and uniaxial buckling load of symmetrically laminated simply supported plates. In addition, the problem is complicated if the unloaded edges

are subjected to in-plane restraints, such that Poisson's effect becomes an important consideration.

2.6.1 Optimal Design Problem

Consider a symmetrically laminated rectangular plate of length a and width b, as shown in Figure 22. As before, the plate is constructed of equal thickness orthotropic layers with fiber angles θ_k and $k = 1, 2, ..., K$ where K denotes the total number of layers. The plate is defined in the Cartesian coordinates x, y and z with axes x and y lying on the middle surface of the plate, and it is subject to uniaxial compression N_x in the x direction. The unloaded edges $y = 0$, $y = a$ are restrained from translating in the y direction giving rise to Poisson's effect, and resulting in compressive forces in this direction.

The objective of the design optimisation problem is to maximise the weighted sum of the initial postbuckling stiffness P, the prebuckling stiffness K and the critical buckling load N for a given laminate thickness h, by optimally determining the fiber orientations with the laminate configurations given by a combination of θ, 0^o and 90^o ply angles.

The design index to be optimised is thus given as

$$DI = \mu_1 K^* + \mu_2 N^* + \mu_3 P^* \tag{2.11}$$

with $\mu_1 + \mu_2 + \mu_3 = 1$, and the * denoting non-dimensionalised values.

This design formulation applies to a given laminate configuration and as such constitutes only a part of the design problem. Due to the specific na-

ture of this problem, several laminate configurations with a combination of ply angles of θ, 0^o and 90^o are considered as candidate designs. More specifically, the configurations of the candidate designs are taken in the form of $(\theta/-\theta/.../0^o/.../90^o/.../0^o/...)_{sym}$. The best design, chosen from among the candidate designs, is that which gives the highest design index DI, leading to the optimal laminate configuration.

Next, the optimal configuration problem is formulated. Let DI_i designate the maximum design index for laminate i. The best design is given by the laminate configuration corresponding to the highest DI which is obtained from

$$DI^* = \max_i DI_i \tag{2.12}$$

with $i = 1, 2, ..., I$ where I denotes the number of candidate laminates. Thus the complete design optimisation involves the solution of the problem

$$\max_i \ (\max_\theta DI_i), \ i = 1, 2, ..., I \tag{2.13}$$

For a given laminate configuration, the optimisation procedure involves the stages of evaluating $DI(\theta)$ for a given θ and improving the fiber orientation iteratively to maximise this quantity. Thus, as in the previous optimal design problems, the computational solution consists of successive stages of analysis and optimisation until a convergence is obtained and the optimal ply angle θ_{opt} is determined to within a specified accuracy. This procedure is applied to every laminate configuration. Once the design optimisation for each laminate is com-

pleted, the best configuration is chosen from amongst the candidate laminates so as to obtain the one with the highest design index.

Chapter 3

Results and Discussion

3.1 Part 1: Optimal Design of Symmetric Laminates for Maximum Buckling Load Including the Effects of Bending-Twisting Coupling

The biaxially loaded laminates for which optimal designs were sought have different combinations of *free* (F), *simply supported* (S) and *clamped* (C) boundary conditions implemented at the four edges. They are also composed of four symmetric layers, and thus the effects of bending-twisting coupling cannot be neglected. These effects rule out the possibility of an analytical solution and thus the finite element method is used to solve the optimal design problem. The FEM formulation presented is based on Mindlin type theory for thin laminated composite plates and shells.

3.1.1 Finite Element Formulation

With reference to Figure 21, and eqns. (1.120) - (1.122), consider the finite element formulation of the problem [129]. Let the region S of the plate be divided into n sub-regions S_r ($S_r \in S; r = 1, 2, ..., n$) such that

$$\Pi(u) = \sum_{r=1}^{n} \Pi^{S_r}(u) \tag{3.1}$$

where Π and Π^{S_r} are potential energies of the plate and the element, respectively, and u is the displacement vector. Using the same shape functions associated with node i ($i = 1, 2, ..., n$), $S_i(x, y)$, for interpolating the variables in each element, we can write

$$u = \sum_{i=1}^{n} S_i(x, y) u_i \tag{3.2}$$

where u_i is the value of the displacement vector corresponding to node i, and is given by

$$u = \{u_o^{(i)}, v_o^{(i)}, w_o^{(i)}, \psi_x^{(i)}, \psi_y^{(i)}\}^T \tag{3.3}$$

where u_o, v_o and w_o are the displacements of the reference surface in the x, y and z direction, respectively, and ψ_x, ψ_y are the rotations of the transverse normal about the x and y axes.

The static buckling problem reduces to a generalised eigenvalue problem of the conventional form, viz.

$$([K] + \lambda[K_G])\{u\} = 0 \tag{3.4}$$

where $[K]$ is the stiffness matrix and $[K_G]$ is the initial stress matrix. The lowest eigenvalue of the homogeneous system (3.4) yields the buckling load.

3.1.2 Results

Verification

In order to verify the finite element formulation described above, some solutions are compared with those available in the literature. A single-layered simply supported square plate was modeled with $\theta = 30^o$, $\lambda = 0$ (uniaxial compression) and material properties $E_1 = 60.7$ GPa, $E_2 = 24.8$ GPa, $G_{12} = 12$ GPa and $\nu_{12} = 0.23$. The analytical solution for this problem is available in [130]. Table 4 illustrates the effect of the number of finite elements on the non-dimensionalised buckling load N_b where

$$N_b = \frac{N_x a^2}{D_o} \text{ and } D_o = \frac{E_1 h^3}{12(1 - \nu_{12}\nu_{21})}$$

The plate thickness ratio is specified as $h/b = 0.01$. The use of 256 elements for a square plate resulted in an error of less than 0.08% as compared to the analytical solutions [131]. This mesh density was accepted as providing sufficient accuracy. Consequently, in the present study, a square plate is meshed with 256 elements. Plates of aspect ratios other than 1 are meshed with a corresponding proportion of 256 elements.

Number of Elements	N_b
10 x 10	25.57
13 x 13	25.33
16 x 16	25.22
20 x 20	25.14
Exact [Ref. 132]	25.20

Table 4. Effect of the number of elements on the buckling load

Numerical Results

Numerical results are given for a typical T300/5208 graphite/epoxy material with $E_1 = 181$ GPa, $E_2 = 10.3$ GPa, $G_{12} = 7.17$ GPa and $\nu_{12} = 0.28$. The symmetric plate is constructed of four equal thickness layers with $\theta_1 = -\theta_2 = -\theta_3 = \theta_4 = \theta$ and as before, the thickness ratio is specified as $h/b = 0.01$. Different combinations of free (F), simply supported (S) and clamped (C) boundary conditions are implemented at the four edges of the plate. In particular, five different combinations are studied, namely, (F,S,F,S), (F,S,C,S), (S,S,S,S), (C,S,C,S) and (C,C,C,C), where the first letter refers to the first plate edge, and the others follow in the anti-clockwise direction, as shown in Figure 21.

For each of the boundary conditions, three in-plane load cases are considered, namely, uniaxial compression ($N_y = 0$), biaxial compression with $N_y/N_x = 0.5$, and biaxial compression with $N_y/N_x = 1$.

The results presented in this section were obtained for rectangular plates

with aspect ratios varying between 0.5 and 2. The non-dimensionalised buckling parameter N_b is defined as

$$N_b = \frac{Nb^2}{h^3 E_o} \tag{3.5}$$

where N is the critical buckling load, and E_o is a reference value having the dimension of Young's modulus and is taken as E_o = 1GPa.

The dependence of the buckling load N_b on the fiber angle is investigated for the five cases of boundary conditions in Figure 24 for $a/b = r = 0.5$, and in Figure 25 for $r = 1$. With $r = 0.5$ the maximum buckling load occurs at 0° for all the boundary cases, but this is *not* so with $r = 1$. It is clear that the maximum buckling load for a given boundary condition and aspect ratio occurs at a specific value of the fiber angle (referred to as the optimal fiber angle), and this value can be several times higher than the buckling load at other fiber angles. This fact emphasises the importance of carrying out optimisation in design work of this nature to obtain the best performance of fiber composite plates.

Figure 26 shows the effect of the plate aspect ratio $r = a/b$ on θ_{opt} for the five cases of boundary conditions for plates under uniaxial loading. In the case of (F,S,F,S), the optimal fiber angle is 0° for $0.5 \leq r \leq 2$. The case (F,S,C,S) is interesting because the optimal angle remains 0° between $r = 0.5$ and 1.79 at which point θ_{opt} jumps to 47.5°. For the case (S,S,S,S), the jump in the optimal ply angle occurs at $r = 0.8$. With (C,S,C,S), θ_{opt} displays several jumps which occur at $r = 0.67$, 1.27 and 1.88. Finally, for (C,C,C,C), θ_{opt} is non-zero for $r \geq 1.2$ after which the optimal ply angle fluctuates between 29.5° and 47°.

It is noted that the discontinuities that occur in θ_{opt} as the aspect ratio increases from 0.5 to 2 are due to changes in the buckling modes [132].

The values of the maximum buckling load N_b corresponding to the optimal ply angles given in Figure 26 are shown in Figure 27. As expected, the clamped plate gives the highest buckling loads.

The results for biaxial loading with $N_y/N_x = 0.5$ are given in Figure 28. In this case, an interesting situation occurs with discontinuities for *all* the boundary conditions. For (F,S,F,S), the relationship between r and θ_{opt} is worth noting. At $r = 1.33$, θ_{opt} displays a discontinuity jump to 23°, whereupon it remains flat up to $r = 2$. The trends for the cases (C,S,C,S) and (C,C,C,C) show similarities to those shown in Figure 26, although the number of jumps for the case (C,C,C,C) increases. Figure 29 shows the values of N_b corresponding to θ_{opt} shown in Figure 28.

The results for the second biaxial loading case with $N_y/N_x = 1$ are presented in Figure 30. The case (F,S,F,S) does not display any discontinuity, and θ_{opt} remains between 20° and 31°. The cases (C,S,C,S) and (C,C,C,C) show similar trends to those illustrated in Figures 26 and 28. The plates with (F,S,C,S) has an approximate θ_{opt} value of 27° between $r = 0.5$ and $r = 1.43$ at which point the optimal ply angle jumps to 46°, and then increases to $\theta_{opt} = 75°$. Figure 31 gives the values of N_b corresponding to θ_{opt} shown in Figure 30. The trends are similar to those of the other loading cases shown in Figures 27 and 29, but as expected, the values for N_b are less than before due to increased loading.

Finally, Figure 32 compares the optimal ply angles of simply supported laminates with and without bending-twisting coupling. In essence, neglecting

the effect of bending-twisting coupling corresponds to having an infinite number of layers. Figure 32 indicates that this effect is substantial (particularly around $r = 0.75$ and $r = 1.30$) in the case of four-layered plates and its neglect may lead to incorrect optimal fiber orientations, resulting in substantially reduced buckling loads.

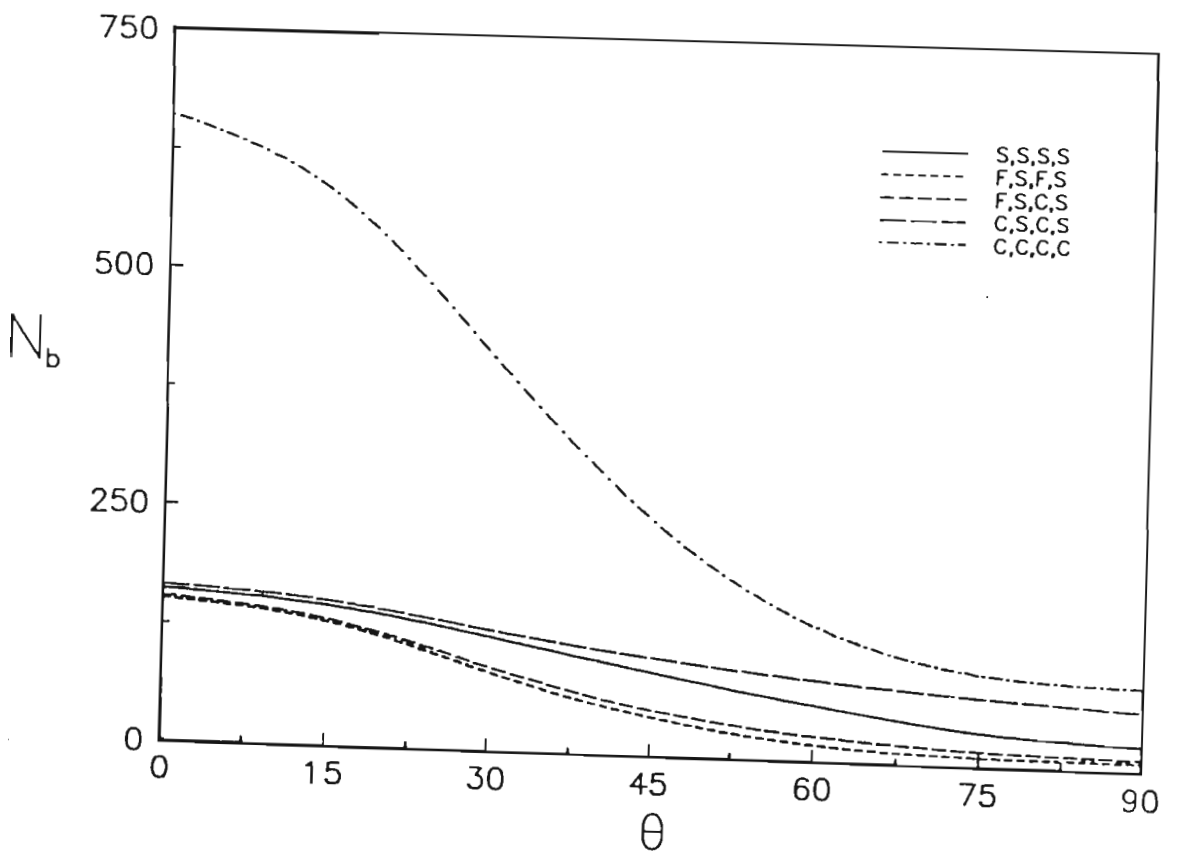

Figure 24. Buckling load plotted against the ply angle for rectangular laminates with $a/b = 0.5$

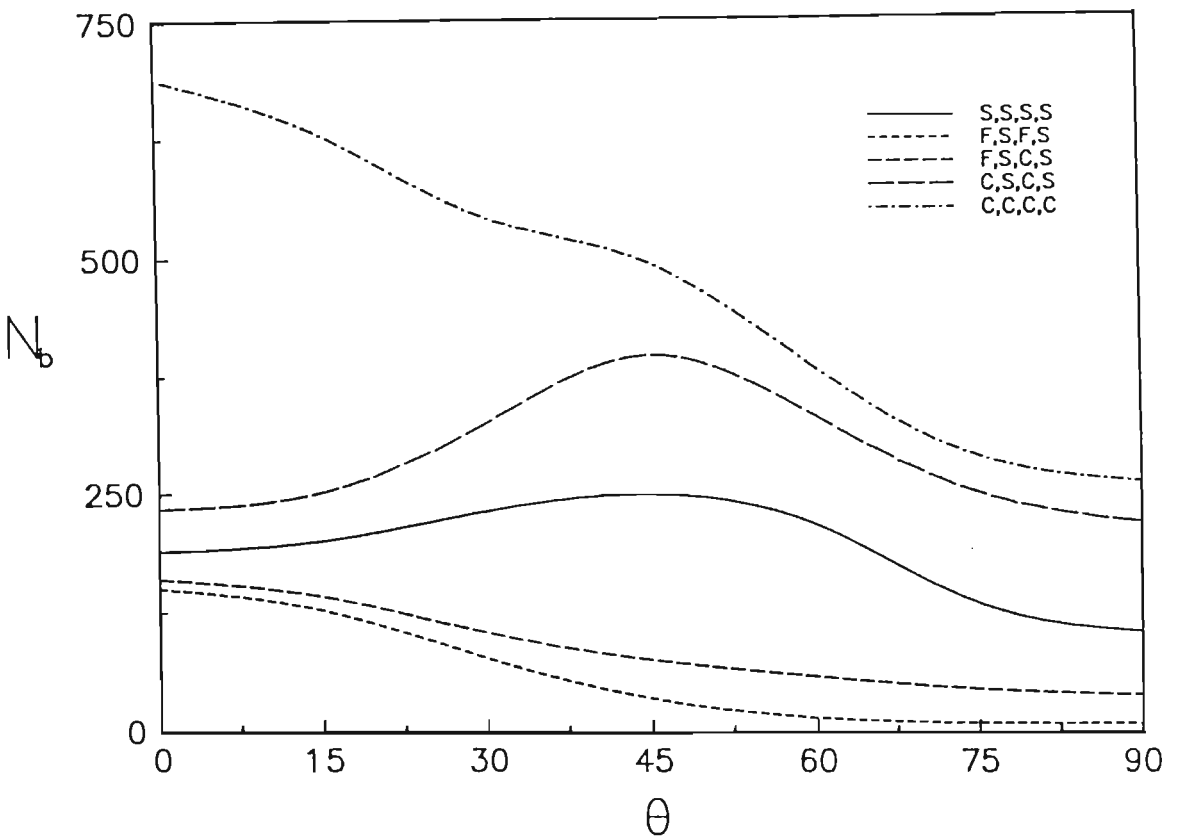

Figure 25. Buckling load plotted against the ply angle for square plates

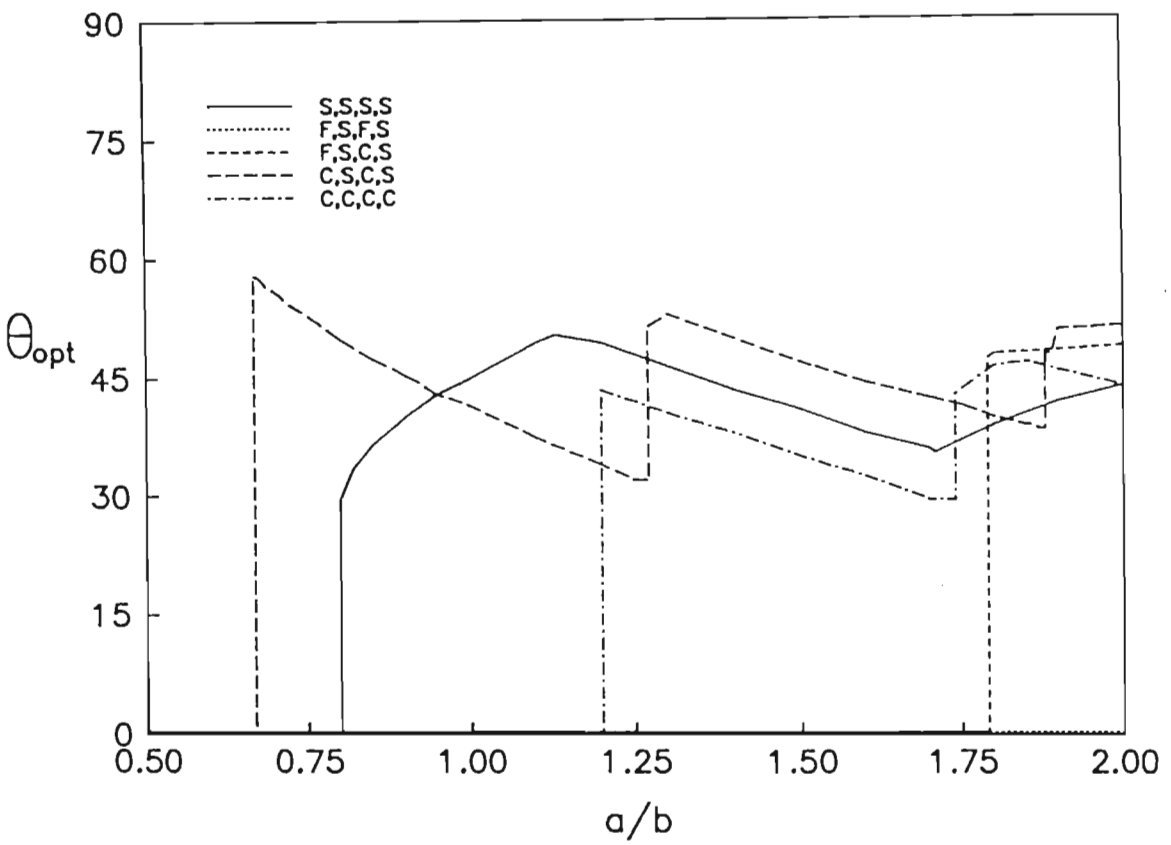

Figure 26. Optimal ply angle plotted against the aspect ratio with $\lambda = 0$,

(uniaxial load)

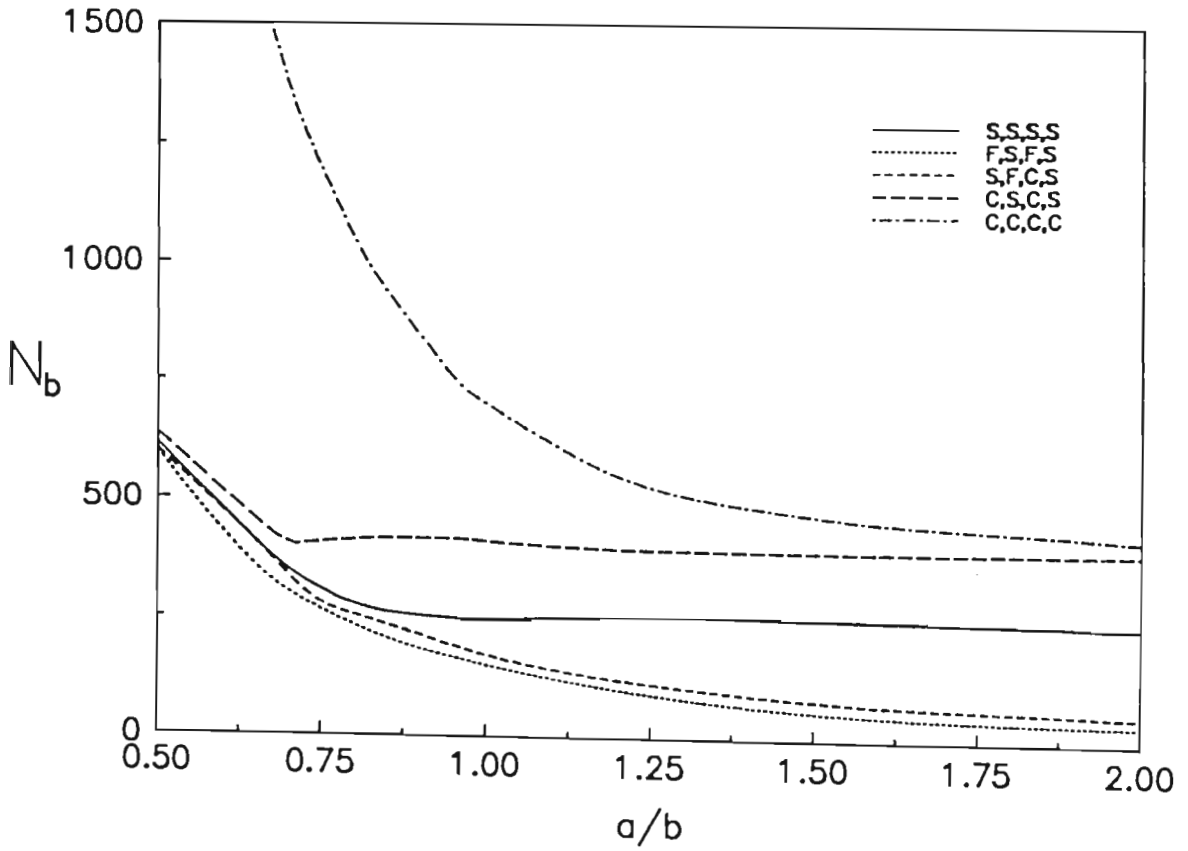

Figure 27. Maximum buckling load plotted against the aspect ratio with

$\lambda = 0$, (uniaxial load)

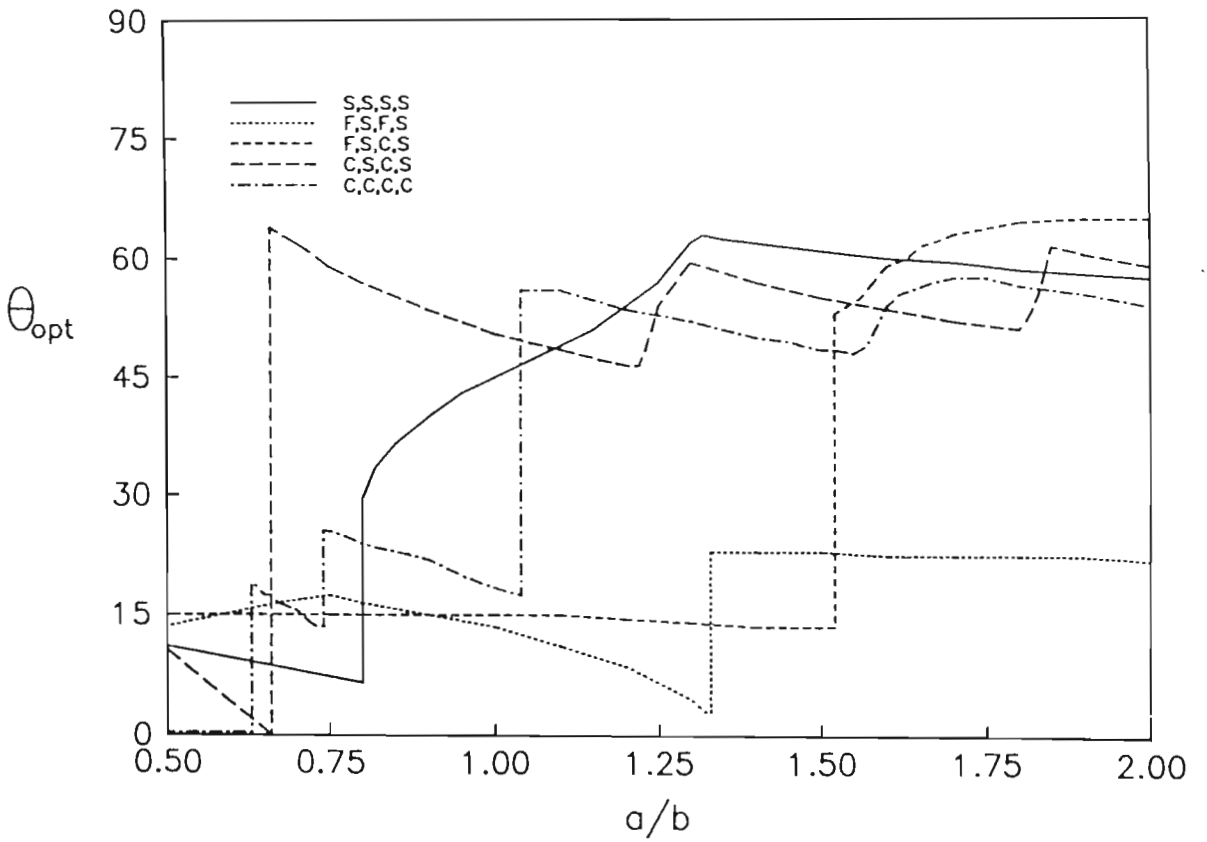

Figure 28. Optimal ply angle plotted against the aspect ratio with $\lambda = 0.5$,

(biaxial load)

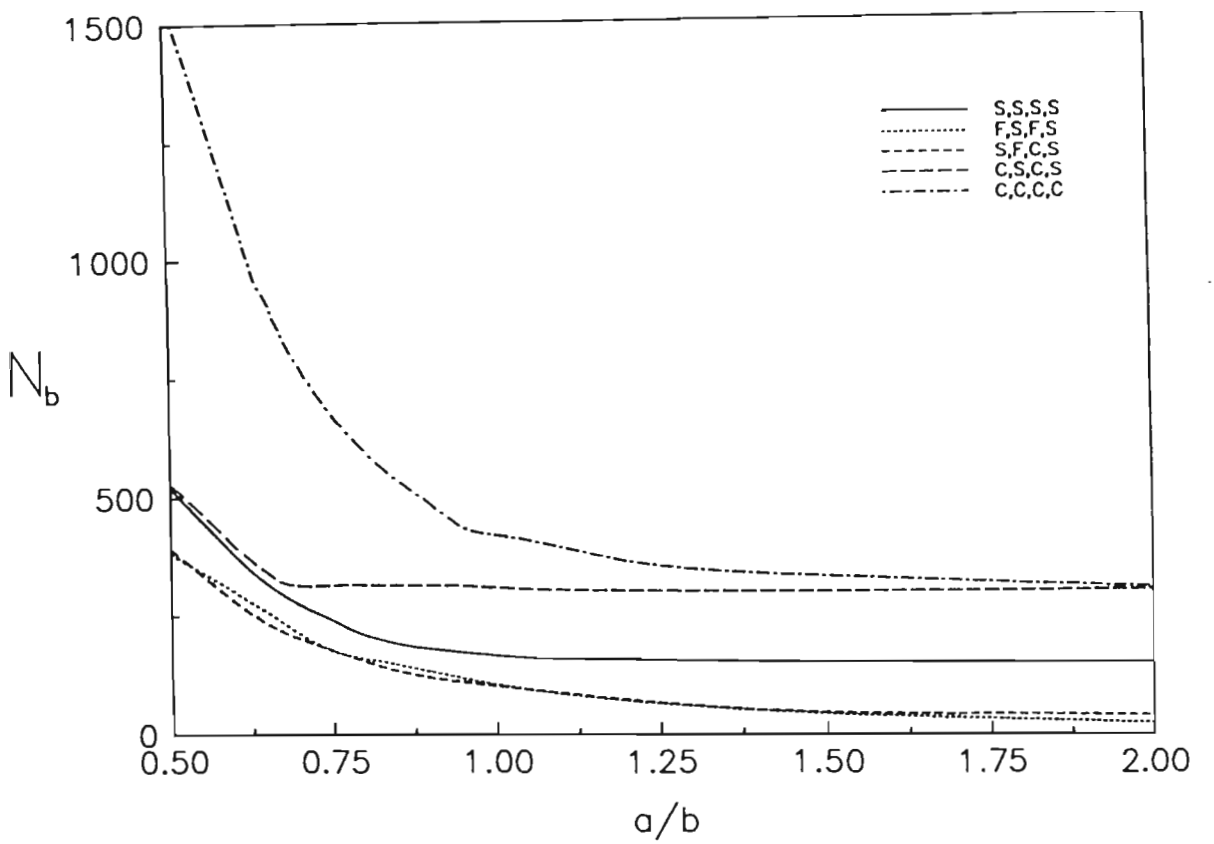

Figure 29. Maximum buckling load plotted against the aspect ratio with

$\lambda = 0.5$, (biaxial load)

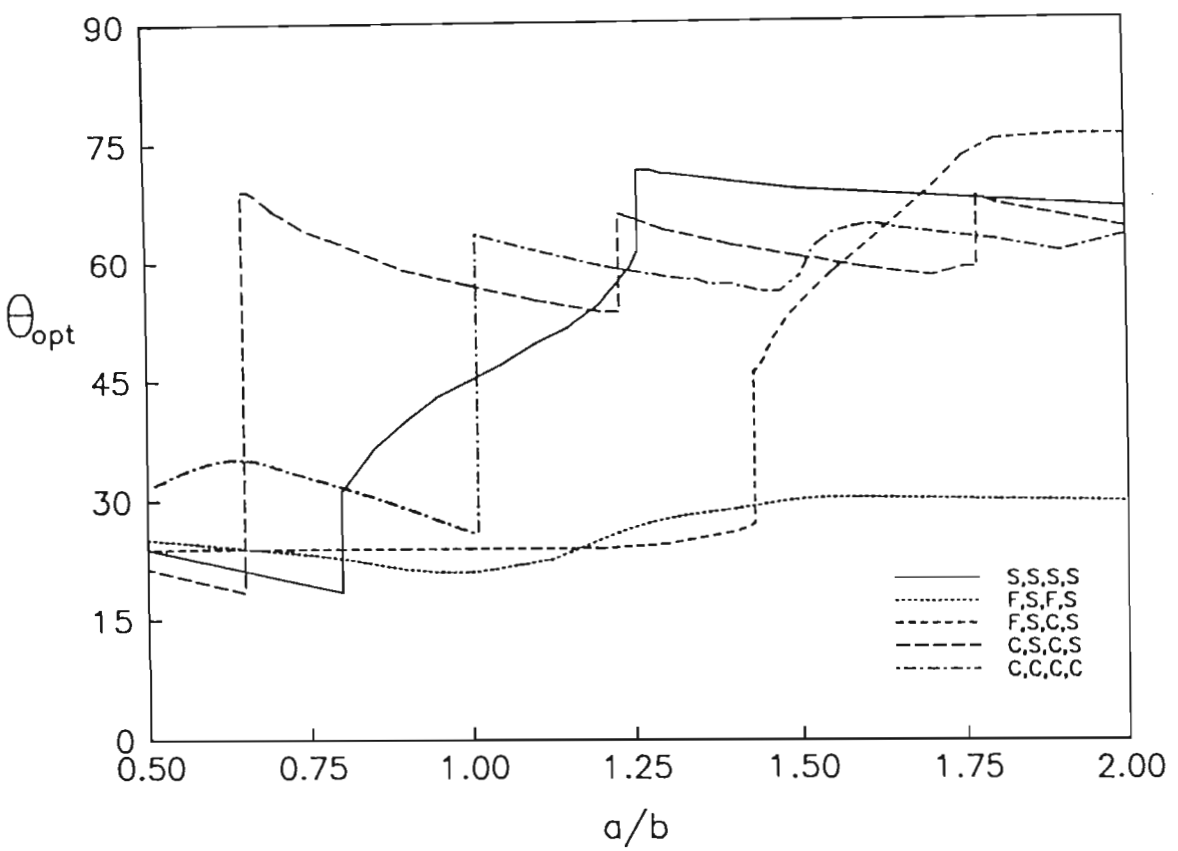

Figure 30. Optimal ply angle plotted against the aspect ratio with $\lambda = 1.0$,

(biaxial load)

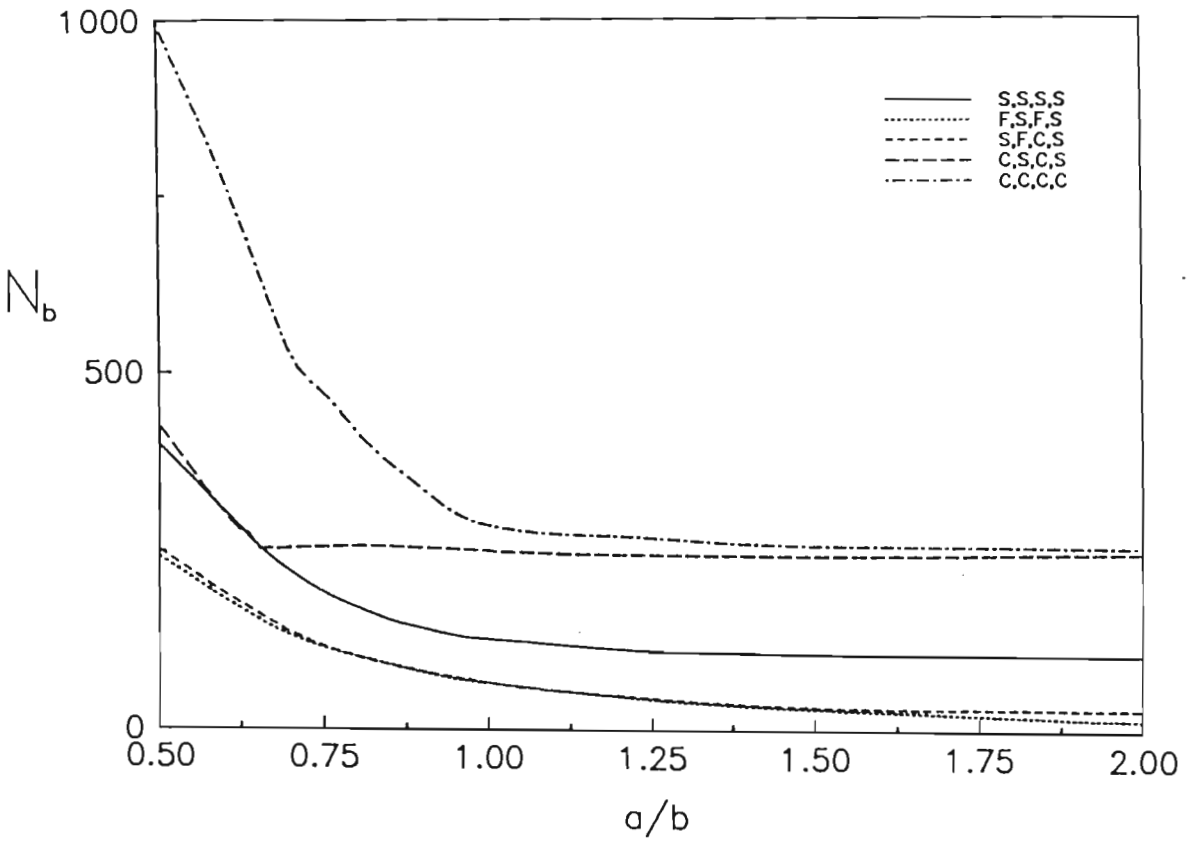

Figure 31. Maximum buckling load plotted against the aspect ratio with

$\lambda = 1.0$, (biaxial load)

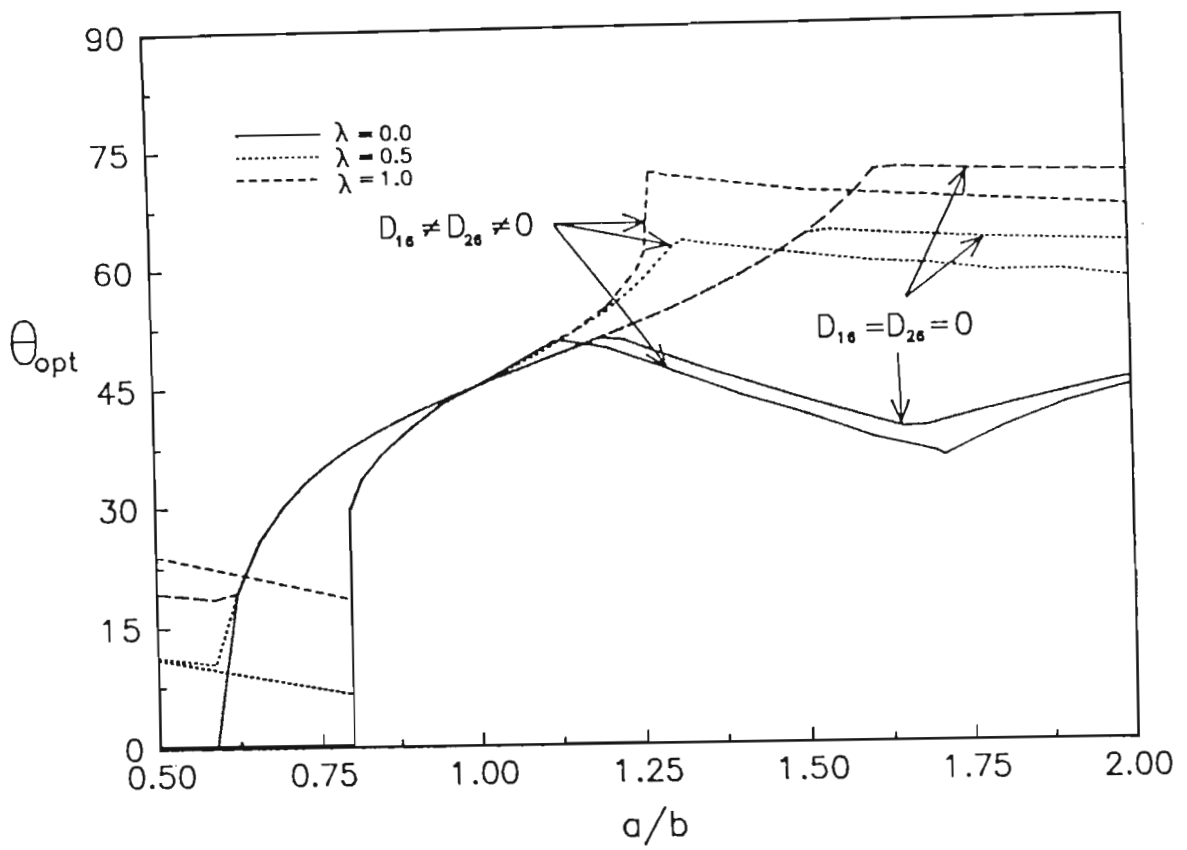

Figure 32. Effect of bending-twisting coupling on the optimal ply angle

3.2 Part 2: Optimal Design of Symmetric Angle-ply Laminates Subject to Nonuniform Buckling Loads and In-plane Restraints

The plates for which optimal designs were sought are uniaxially loaded in the x-axis, as shown in Figure 22, and the unloaded edges $y = 0$, $y = 1$ are restrained from translating in the y-direction. Also, the plates have different combinations of *free* (F), *simply supported* (S) and *clamped* (C) boundary conditions implemented at the four edges, and the loading N_x is not necessarily uniform. As before, they are also composed of four symmetric layers, and thus the effects of bending-twisting coupling cannot be neglected. These effects rule out the possibility of an analytical solution and thus the finite element method is again used to solve the problem. The FEM formulation used for the following results is the same as that given above.

3.2.1 Results

The results which follow were obtained for non-uniformly distributed in-plane loads. In particular, point loads (Figure 33a), partial uniform loads (Figure 33b) and non-uniform loads (Figure 33c) are considered in addition to a full uniform load. Numerical results are given for the same T300/5208 graphite/epoxy material, with E_1 = 181 GPa, E_2 = 10.3 GPa, G_{12} = 7.17 GPa and ν_{12} = 0.28. Also, the plate thickness to length ratio is specified as $h/b = 0.01$, and is constructed of four equal thickness layers with $\theta_1 = -\theta_2 = -\theta_3 = \theta_4 = \theta$. The unloaded edges 1 and 3 are restrained from translation in the y direction. As

mentioned previously, these restraints give rise to Poisson's effect when edges 2 and 4 undergo uniaxial compression (Figures 22 and 33).

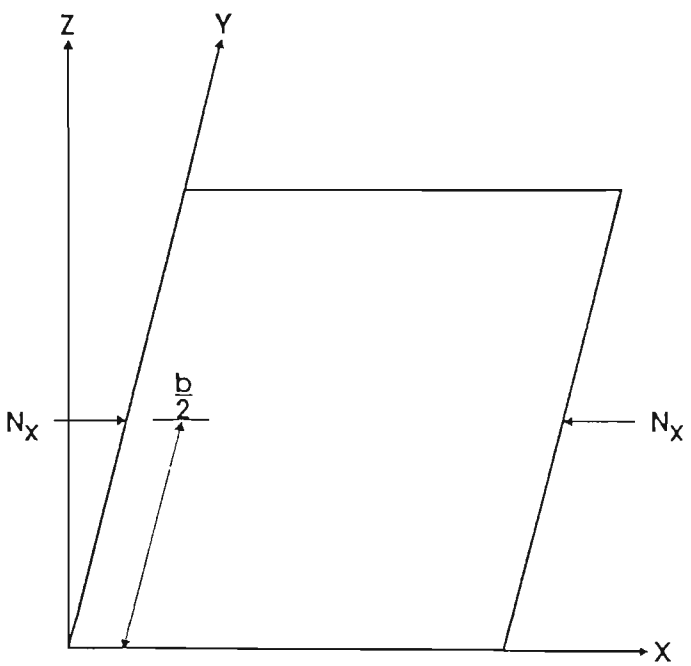

(a)

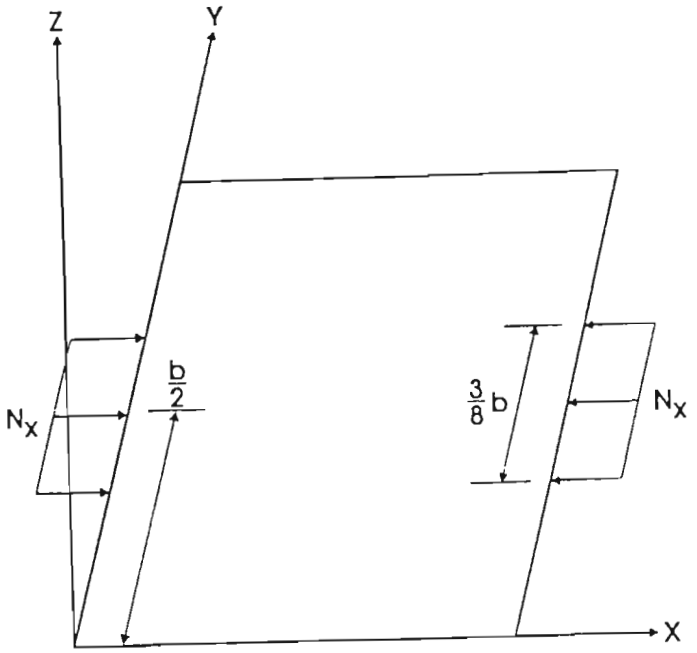

(b)

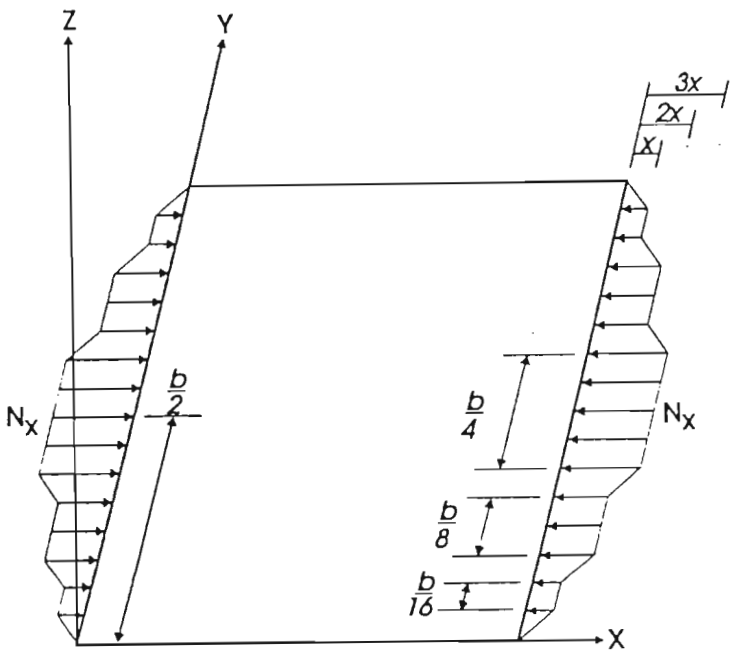

(c)

Figure 33. Nonuniformly distributed buckling loads.

a). Concentrated load b). partial uniform load

c). nonuniformly distributed load (Note: $x = 0.0323$)

The results presented were obtained for plates with aspect ratios varying from 0.5 to 2. The non-dimensionalised buckling parameter N_b is defined in eqn. (3.5).

First, comparative results are given for various loads for laminates with and without in-plane restraints. Tables 5 - 8 show the values of the optimal ply angles and the corresponding maximum buckling loads for simply supported laminates where the subscripts 'c' and 'p' denote the classical (Poisson's effect neglected) and the present (Poisson's effect included) cases respectively [133]. It is observed that as the aspect ratio increases, so the discrepancy between the classic and present results increases. This phenomenon can be clearly seen by checking the ratio $N^p_{\max}/N^c_{\max}$ which drops to less than half as r reaches 2 . The optimal ply angles also show distinct differences. It is observed that θ^p_{opt} for $r \geq 1$ and this difference is even higher for $r = 0.5$ and 0.75. Another interesting fact is that $N^c_{\max}$ fluctuates as r increases while $N^p_{\max}$ decreases steadily. This is due to the biaxial nature of buckling loads in the presence of in-plane restraints. It is seen that the maximum buckling loads are the lowest for point loads and highest for uniformly distributed loads. In fact the buckling loads increase as the compressive forces become more uniformly distributed [134].

r	θ^c_{opt}	$N^c_b(\theta^c_{opt})$	θ^p_{opt}	$N^p_b(\theta^p_{opt})$	N^p_b/N^c_b
0.50	28.6°	212.8	26.0°	205.6	0.97
0.75	54.4°	210.0	38.9°	146.1	0.70
1.00	46.0°	209.4	38.9°	129.8	0.62
1.25	42.0°	202.7	36.6°	117.9	0.58
1.50	44.6°	198.6	35.1°	108.4	0.55
1.75	48.5°	193.7	33.4°	100.6	0.52
2.00	47.7°	189.5	32.2°	94.7	0.50

Table 5. Optimisation results for laminates under a point in-plane load (Figure 33a)

r	θ^c_{opt}	$N^c_b(\theta^c_{opt})$	θ^p_{opt}	$N^p_b(\theta^p_{opt})$	N^p_b/N^c_b
0.50	0°	324.1	0°	323.0	0.99
0.75	53.4°	259.2	0°	165.0	0.64
1.00	47.5°	228.3	36.7°	137.6	0.60
1.25	39.6°	222.5	35.3°	123.1	0.55
1.50	43.4°	214.2	33.6°	112.2	0.52
1.75	48.4°	213.8	32.0°	103.5	0.48
2.00	47.5°	211.3	30.5°	97.1	0.46

Table 6. Optimisation results for laminates under a uniformly distributed partial in-plane load (Figure 33b)

r	θ^c_{opt}	$N^c_b(\theta^c_{opt})$	θ^p_{opt}	$N^p_b(\theta^p_{opt})$	N^p_b/N^c_b
0.50	0°	471.9	0°	470.3	0.99
0.75	41.0°	271.9	0°	227.7	0.84
1.00	51.1°	260.3	31.0°	154.9	0.60
1.25	42.2°	252.9	31.7°	132.2	0.52
1.50	38.9°	238.7	30.5°	119.2	0.50
1.75	44.7°	230.8	29.2°	109.0	0.47
2.00	48.4°	225.7	27.4°	101.8	0.45

Table 7. Optimisation results for laminates under nonuniformly distributed in-plane load (Figure 33c)

r	θ^c_{opt}	$N^c_b(\theta^c_{opt})$	θ^p_{opt}	$N^p_b(\theta^p_{opt})$	N^p_b/N^c_b
0.50	0°	644.5	0°	644.3	1
0.75	0°	300.7	0°	300.6	1
1.00	45.7°	248.3	0°	186.3	0.75
1.25	48.3°	238.4	24.5°	145.6	0.56
1.50	41.2°	225.2	26.5°	128.9	0.50
1.75	33.8°	220.5	24.5°	117.4	0.48
2.00	44.0°	214.7	23.5°	108.3	0.45

Table 8. Optimisation results for laminates under a uniformly distributed in-plane load (Figure 22)

r	θ^c_{opt}	$N^p(\theta^c_{opt})/N^c_b(\theta^c_{opt})$	θ^p_{opt}	$N^p_b(\theta^p_{opt})/N^c_b(\theta^c_{opt})$	$N^p_b(\theta^p_{opt})/N^p(\theta^c_{opt})$
0.5	0°	1	0°	1	1
0.8	0°	1	0°	1	1
1.0	45.7°	0.57	0°	0.75	1.31
1.3	48.3°	0.43	24.5°	0.56	1.32
1.5	41.2°	0.43	26.5°	0.50	1.15
1.8	33.8°	0.42	24.5°	0.48	1.05
2.0	44.0°	0.36	23.5°	0.45	1.23

Table 9. Comparison of θ^c_{opt} and buckling loads for laminates with and without Poisson's effect

Next, the effect of boundary conditions is studied by considering five combinations of free (F), simply supported (S) and clamped (C) boundary conditions. In particular, and as before, the following cases are studied: (F,S,F,S), (F,S,C,S), (S,S,S,S), (C,S,C,S) and (C,C,C,C) where the first letter refers to the first plate edge, and the others follow in anti-clockwise order (Figure 22).

Figure 34 shows the curves of θ_{opt} plotted against the aspect ratio $r = a/b$ for the five boundary conditions with the plates subject to in-plane restraints. For three of the cases, viz. (F,S,F,S), (F,S,C,S) and (C,C,C,C), the optimal fiber angle is 0^o for *all* values of r. For (S,S,S,S), the relationship between r and θ_{opt} is interesting. The optimal angle is 0^o between $r = 0.5$ and $r = 1$, where a jump discontinuity in the value of θ_{opt} occurs. From $r = 1$ to $r = 2$, the graph is smooth, with a peak at $r = 1.5$ of 27^o. The value of the optimal fiber angle at r = 2 is 23.5^o. For the boundary condition (C,S,C,S), the relationship between θ_{opt} and r is similar with the discontinuity occurring at $r = 0.92$. A peak is reached at $r = 1.6$ where θ_{opt} is 42.5^o. At $r = 2$, the optimal fiber angle is 37.5^o.

For comparative purposes, the θ_{opt} values for plates where Poisson's effect is neglected are shown in Figure 35, which is the same as Figure 26. A comparison of Figures 34 and 35 indicates that the θ_{opt} values differ substantially for the cases including and excluding Poisson's effect. Figure 36 shows the maximum buckling load N_b corresponding to the θ_{opt} values shown in Figure 34. Corresponding results for plates with Poisson's effect neglected are shown in Figure 37, which is the same as Figure 27. It is evident from Figures 36 and 37 that plates subject to Poisson's effect will exhibit premature instability, indicating the need to ascertain the presence or absence of restrained edges for design

purposes. The discontinuities in the relationships between r and θ_{opt} shown in Figure 34 are due to changes in the buckling modes [135].

Next, the consequences of neglecting Poisson's effect are studied by comparing the buckling loads at different ply angles, for laminates under uniformly distributed buckling loads. Table 9 clearly illustrates the benefit of taking into account the Poisson effect in the optimisation of laminates which are subject to in-plane restraints by giving a quantitative comparison of present and classical solutions for simply supported (S,S,S,S) laminates. The third column shows the ratio of the buckling loads for laminates with in-plane restraints at the 'classic' optimal fiber angle to the maximum buckling load for classic laminates. As the aspect ratio increases, this ratio decreases, indicating the growing importance of Poisson's effect. The fifth column shows the result of using the classical optimal ply angle instead of the correct optimal ply angle for laminates with in-plane restraints. It is observed that using the classical optimal ply angles may lead to buckling loads which are up to 30% less than the maximum for some aspect ratios [136].

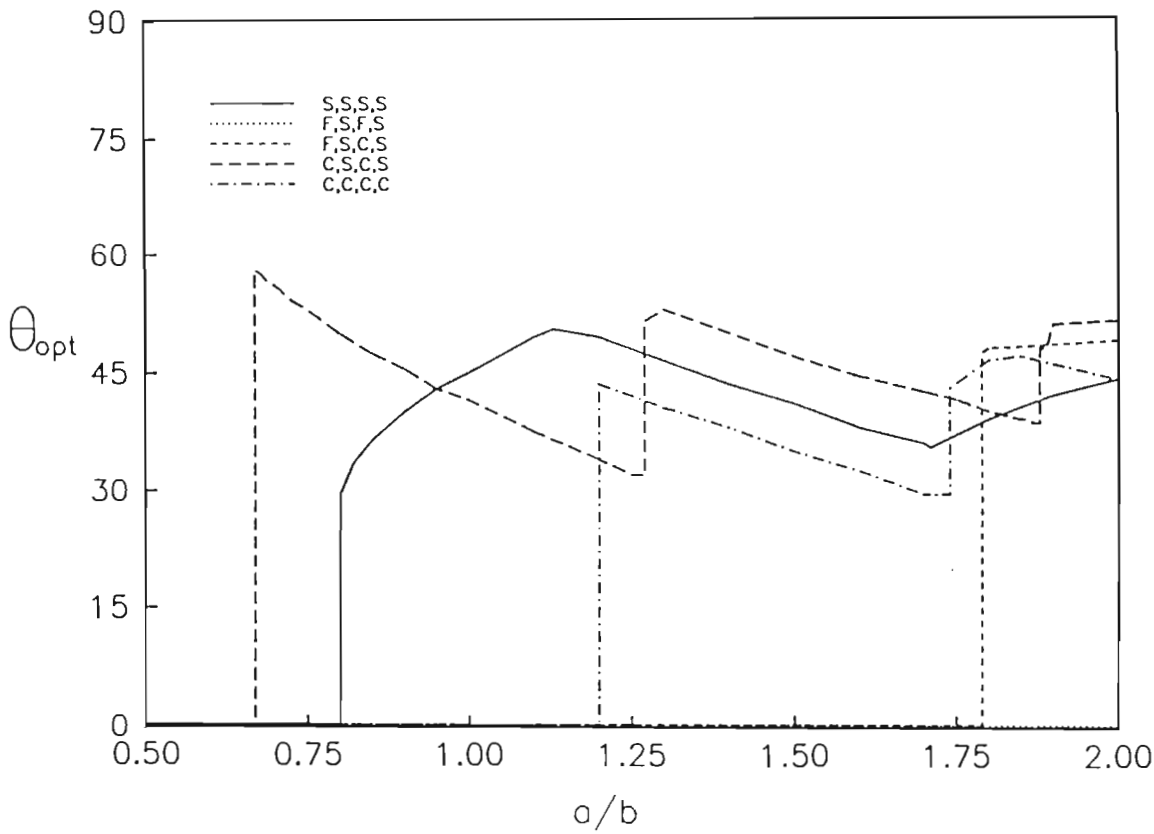

Figure 35. Curves of optimal ply angles versus the aspect ratio with Poisson's effect neglected

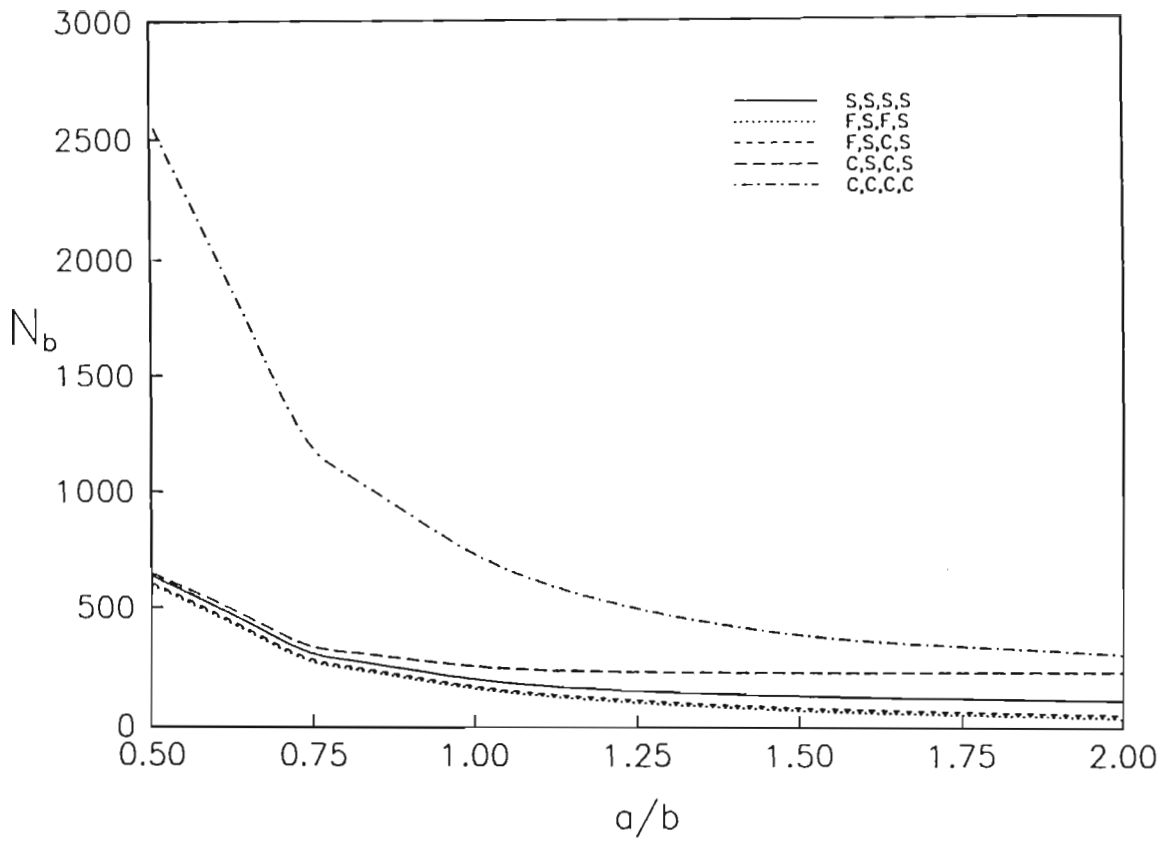

Figure 36. Curves of maximum buckling load versus aspect ratio with Poisson's effect included

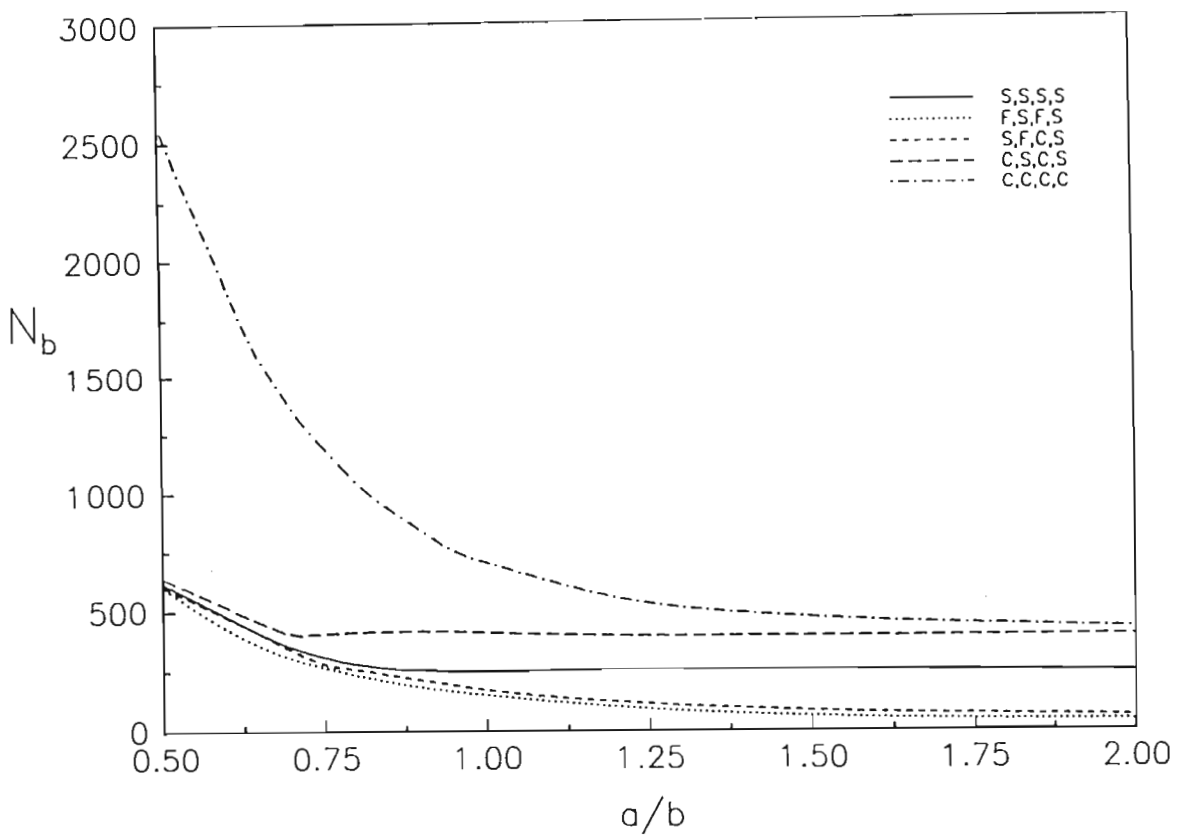

Figure 37. Curves of maximum buckling load versus aspect ratio with Poisson's effect neglected

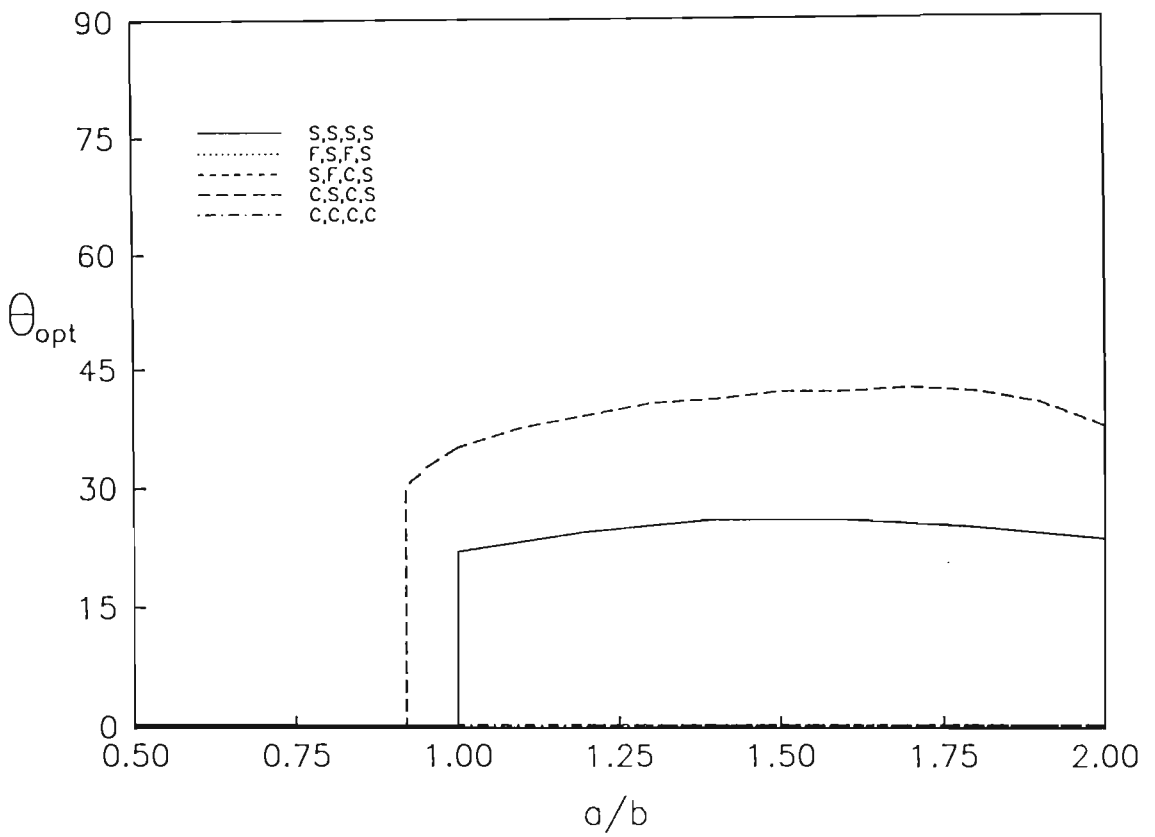

Figure 34. Curves of optimal ply angles versus the aspect ratio with Poisson's effect included

3.3 Part 3: Optimal Design of Symmetric Laminates with Central Circular Cut-outs for Maximum Buckling Load

The biaxially loaded laminates for which optimal designs were sought have central circular holes, and the ratio d/b is prescribed. As before, different combinations of *free* (F), *simply supported* (S) and *clamped* (C) boundary conditions are implemented at the four edges. The plates are also composed of four symmetric layers, and thus the effects of bending-twisting coupling cannot be neglected. These effects rule out the possibility of an analytical solution and thus the same finite element method is once again used to solve the problem.

3.3.1 Results

Numerical results are also given for the T300/5208 graphite/epoxy material. The symmetric plate is constructed of four equal thickness layers with $\theta_1 = -\theta_2 = -\theta_3 = \theta_4 = \theta$ and the thickness ratio is specified as $h/b = 0.01$. Also, $d/b = 0.5$. The same five cases, viz. (F,S,F,S), (F,S,C,S), (S,S,S,S), (C,S,C,S) and (C,C,C,C) are implemented along the four edges. The loading is given by $N_y/N_x = 1$.

The results presented in this section are obtained for rectangular plates with aspect ratios varying between 1 and 3. The non-dimensionalised buckling parameter N_b is used as before, and defined in eqn. (3.5).

Figure 38 shows the dependence of the optimal fiber angle on the laminate aspect ratio, for the five different boundary condition cases. The graphs

for (C,S,C,S) and (C,C,C,C) show discontinuities, for a/b between 1 and 2. The trends show that the effect of the hole is greater when the aspect ratio is small, and diminishes as a/b becomes larger. The jump discontinuities are due to changes in the buckling modes. The remaining three curves show no discontinuities, with that for (S,S,S,S) almost linear and flat.

Figure 39 shows the values of N_b corresponding to θ_{opt} in Figure 38. As before, the curves for (C,S,C,S) and (C,C,C,C) are most interesting, and are not monotonic as are the remaining three cases. For (C,C,C,C), choosing a/b to be approximately 1.3 when $d/b = 0.5$ gives the highest buckling load if the optimal fiber angle is used in the laminate lay-up. As mentioned before, when the aspect ratio is smaller, the effect of the hole is great. When the aspect ratio is large, the laminate becomes weak, offering less buckling resistance, and the effect of the hole is of less importance [138].

For comparative purposes, optimal design curves for laminates subject to similar loads but without central holes are given in Figures 40 and 41 (which are the same as Figures 30 and 31). It should be noted that in these graphs, the aspect ratio varies from 0.5 to 2. None the less, for the values of a/b common to all the figures, it is easily seen that central cut-outs give the laminates very different buckling characteristics, and thus different optimal fiber angles. It is also apparent that the holes reduce the buckling load capacity of the plates.

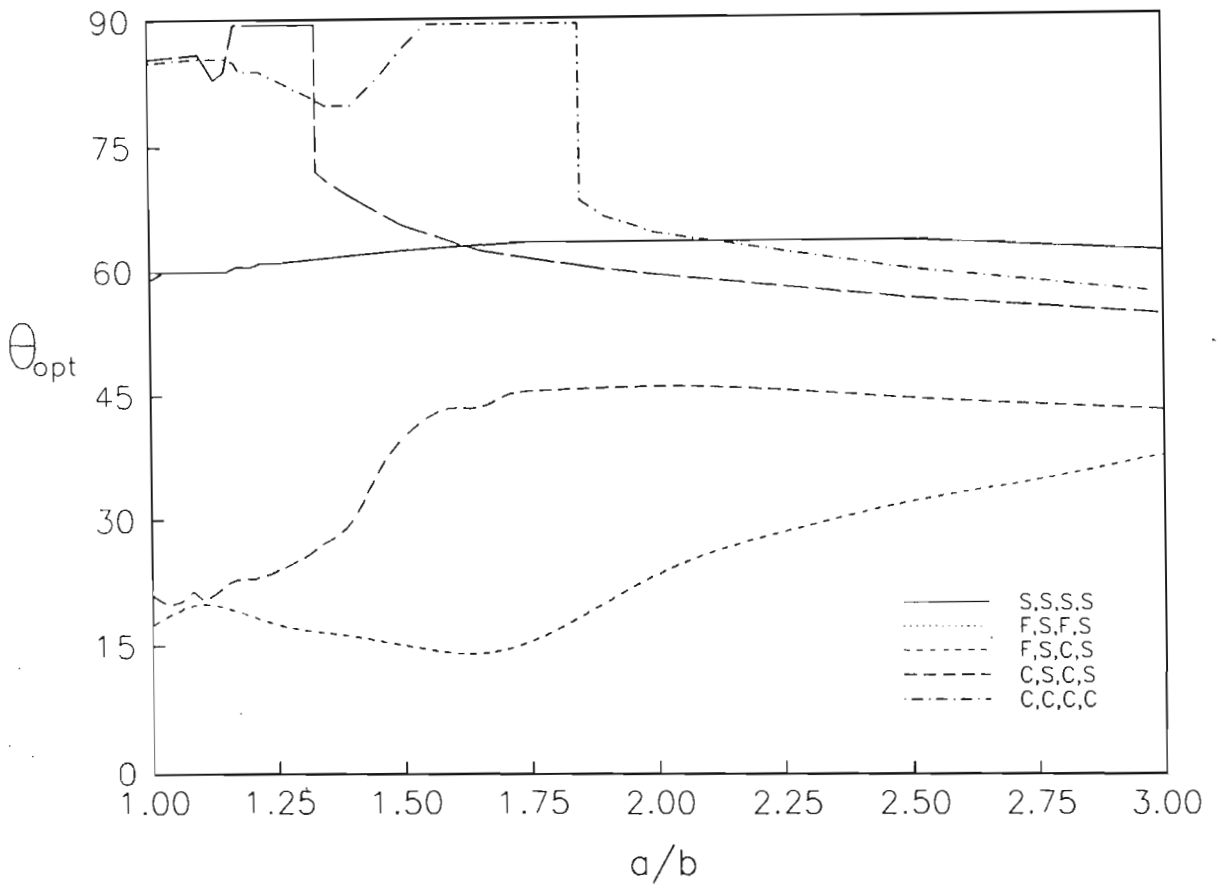

Figure 38. Optimal ply angle plotted against the aspect ratio for plates with holes

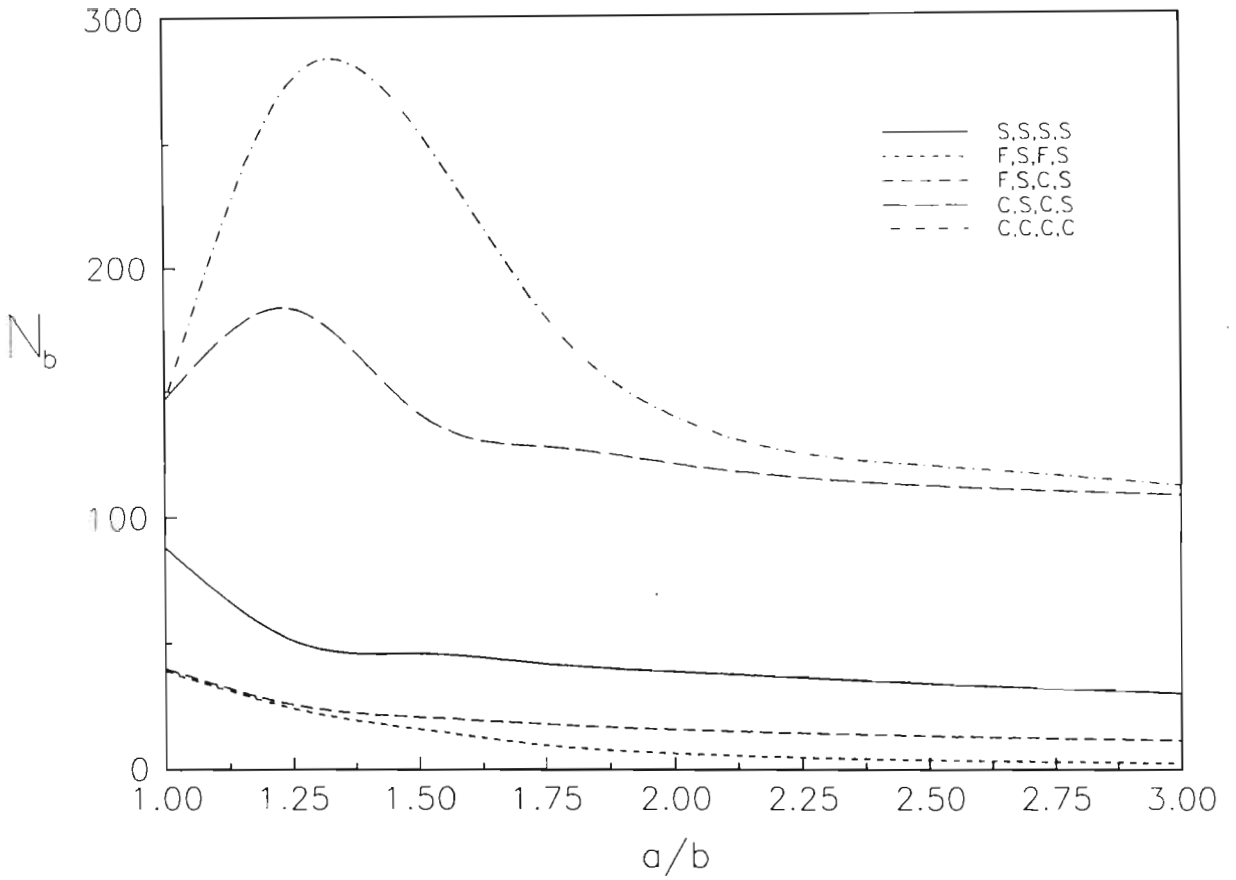

Figure 39. Maximum buckling load plotted against the aspect ratio for plates with holes

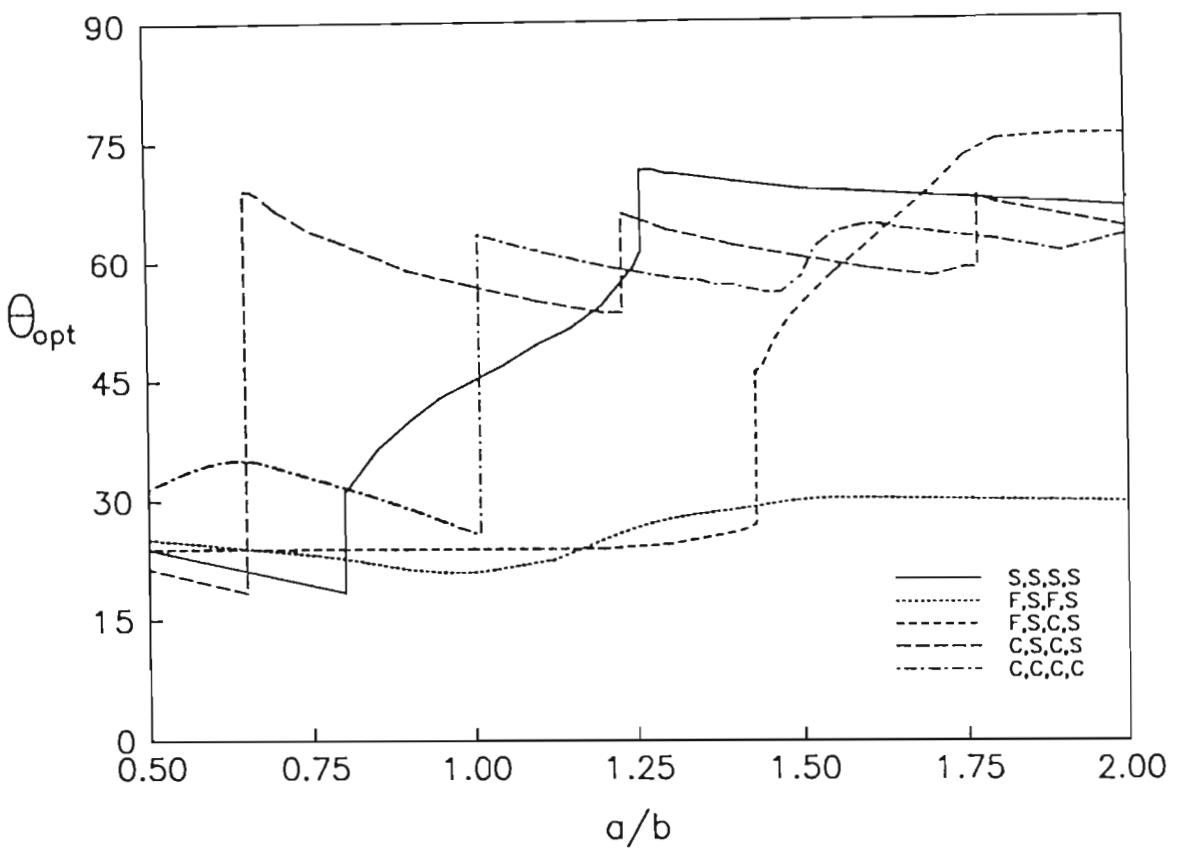

Figure 40. Optimal ply angle plotted against the aspect ratio for plates without holes

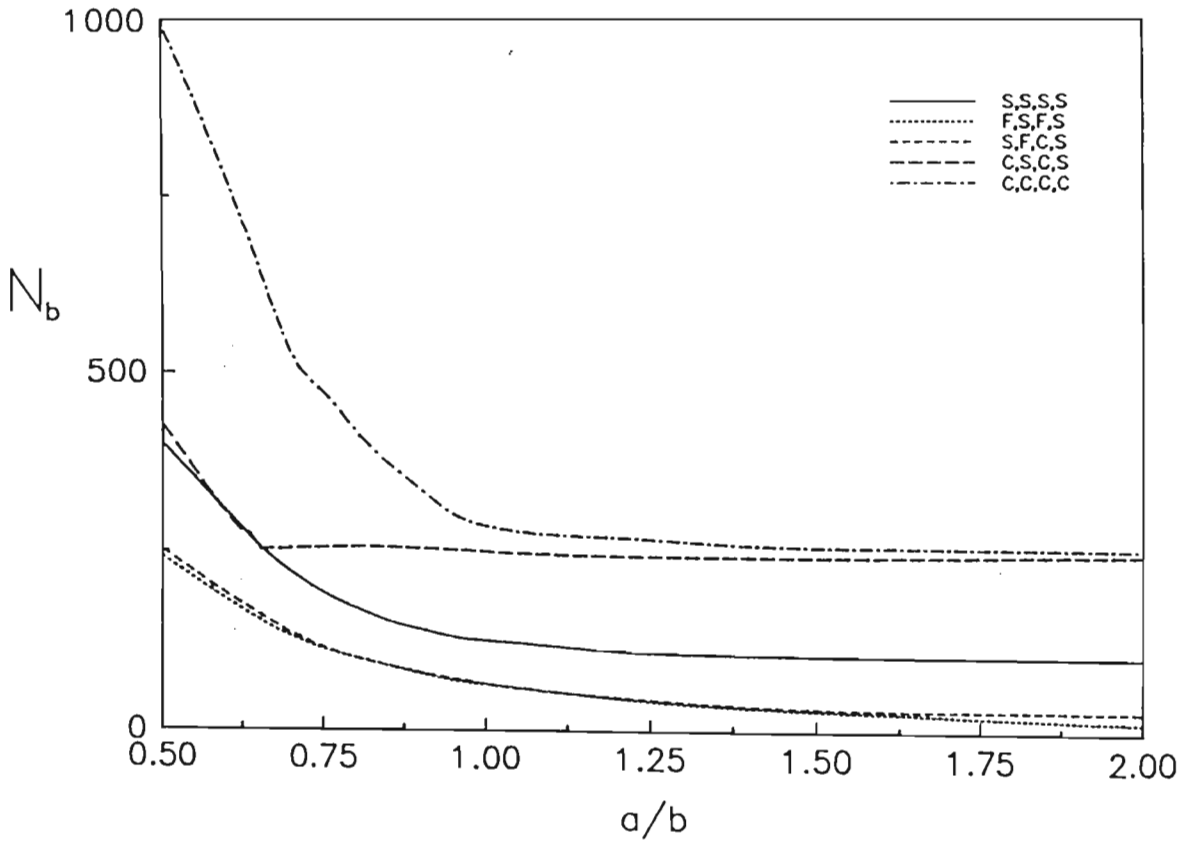

Figure 41. Maximum buckling load plotted against the aspect ratio for plates without holes

3.4 Part 4: Optimal Laminate Configurations with Symmetric Lay-ups for Maximum Postbuckling Stiffness

In order to solve the fourth design optimisation problem, the postbuckling stiffnesses must be derived. Consider the plate subjected to biaxial loading in Figure 21, with λ designating the load ratio N_y/N_x as before. The non-linear differential equations of equilibrium and compatibility in terms of a stress function $F(x,y)$ and the deflection $w(x,y)$ are given by [137]

$$\begin{aligned} L_1 w &= F_{,yy} w_{,xx} - 2F_{,xy} w_{,xy} + F_{,xx} w_{,yy} \\ L_2 F &= (w_{,xy})^2 - w_{,xx} w_{,yy} \end{aligned} \tag{3.6}$$

where the differential operators L_1 and L_2 are defined as

$$\begin{aligned} L_1 &= D_{11}\frac{\partial^4}{\partial x^4} + (D_{12} + D_{33})\frac{\partial^4}{\partial x^2 \partial y^2} + D_{22}\frac{\partial^4}{\partial y^4} \\ L_2 &= a_{22}\frac{\partial^4}{\partial x^4} + (2a_{12} + a_{33})\frac{\partial^4}{\partial x^2 \partial y^2} + a_{11}\frac{\partial^4}{\partial y^4} \end{aligned} \tag{3.7}$$

In equation (3.7), a_{ij} are the in-plane flexibility coefficients obtained as $a_{ij} = A_{ij}^{-1}$, with A_{ij} and D_{ij} denoting the in-plane and bending stiffnesses. The non-linear midplane strains are related to the displacements u, v and w by the following relations:

$$\begin{aligned} \epsilon_x = u_{,x} + \tfrac{1}{2}(w_{,x})^2, \;\; \epsilon_y = v_{,y} + \tfrac{1}{2}(w_{,y})^2 \\ \gamma_{xy} = u_{,y} + w_{,x} w_{,y} \end{aligned} \tag{3.8}$$

The in-plane boundary conditions for uniform boundary displacements and zero applied shear can be expressed as

$$\begin{gathered} u = 0 \ (x = 0), \ \frac{\partial u}{\partial y} = 0 \ (x = a) \\ v = 0 \ (y = 0), \ \frac{\partial v}{\partial x} = 0 \ (y = b) \\ N_{xy} = 0 \ (x = 0, \ y = b) \end{gathered} \tag{3.9}$$

The plate satisfies the simply supported boundary conditions

$$\begin{gathered} w = 0, \ D_{11} w_{xx} + D_{12} w_{xy} = 0, \ x = 0, a \\ w = 0, \ D_{12} w_{xy} + D_{22} w_{yy} = 0, \ y = 0, b \end{gathered} \tag{3.10}$$

The solution of the governing equations subject to boundary conditions (3.9) and (3.10) can be obtained by choosing a force function of the form

$$F = 0.5(N_x y^2 + N_y x^2) + \frac{B_{mn}^2}{32} \left(\frac{\alpha_{mn}^2}{a_{22}} \cos \frac{2m\pi x}{a} + \frac{1}{\alpha_{mn}^2 a_{11}} \cos \frac{2n\pi y}{b} \right) \tag{3.11}$$

where $\alpha_{mn} = na/mb$ is a mode parameter and B_{mn} is an unknown coefficient. The deflection is chosen as

$$w(x, y) = C_{mn} \sin \frac{m\pi x}{a} \sin \frac{n\pi x}{b} \tag{3.12}$$

which satisfies the boundary conditions (3.10).

Force resultants can be written in terms of the stress function as

$$N_x = F_{,yy} \ , \ N_y = F_{,xx} \ , \ N_{xy} = -F_{,xy} \tag{3.13}$$

The principle of virtual displacement, with a virtual displacement of the form given by equation (3.12) can be expressed in the form

$$\int_0^a \int_0^b (L_1 w - F_{,yy}\, w_{,xx} + 2F_{,xy}\, w_{,xy} - F_{,xx}\, w_{,yy}) \times \sin\tfrac{m\pi x}{a} \sin\tfrac{n\pi y}{b} dx dy = 0 \tag{3.14}$$

Substituting the assumed forms of w and F and using a Taylor series expansion in the vicinity of the critical point enables N_x to be expressed in terms of the amplitude of the buckling mode C_{mn} as

$$C_{mn}^2 = -(N_x - N_{cr})\frac{F_{mn}}{G_{mn}} \tag{3.15}$$

where $F_{mn} = (m\pi/a)^2 + \lambda(n\pi/b)^2$ and $G_{mn} = \frac{1}{16}(mn\pi^2/ab)^2(\alpha_{mn}^2/a_{22} + 1/\alpha_{mn}^2 a_{11})$.

Since the in-plane strain ϵ_x is also given by the expression

$$\epsilon_x = a_{11}N_x + a_{12}N_y \tag{3.16}$$

and using (3.8) and (3.12), an expression for $u_{,x}$ is obtained, bearing in mind that in the axial direction

$$\epsilon_x = \frac{u}{a} = \frac{1}{a}\int_0^a u_{,x} dx \tag{3.17}$$

which can be simplified to

$$\epsilon_x = N_x(a_{11} + \lambda a_{12}) - \frac{C_{mn}^2}{8}(\frac{m\pi}{a})^2 \tag{3.18}$$

Then by substituting equation (3.15) into equation (3.18), the expression for ϵ_x becomes

$$\epsilon_x = N_x(a_{11} + \lambda a_{12}) + \frac{1}{8}(\frac{m\pi}{a})^2 \times (N_x - N_{cr})\frac{F_{mn}}{G_{mn}} \tag{3.19}$$

After substituting for F_{mn} and G_{mn} and simplifying, an expression for the initial postbuckling stiffness in the x-direction can be obtained as

$$\frac{dN_x}{d\epsilon_x} = \frac{a_{22} + \alpha_{mn}^4 a_{11}}{2a_{11}a_{22}(1 + \lambda\alpha_{mn}^2) + (a_{22} + \alpha_{mn}^4 a_{11})(a_{11} + \lambda a_{12})} \tag{3.20}$$

where $\lambda = N_y/N_x$ [123].

Similarly, it can be shown that the initial postbuckling stiffness in the y-direction is

$$\frac{dN_y}{d\epsilon_y} = \frac{a_{11} + \alpha_{mn}^4 a_{22}}{2a_{22}a_{11}(1 + \lambda\alpha_{mn}^2) + (a_{11} + \alpha_{mn}^4 a_{22})(a_{22} + \lambda a_{12})} \tag{3.21}$$

The critical wave numbers m and n appearing in these expressions are computed by minimising the expression for the critical buckling load given by

$$N_{cr} = \frac{n^2\pi^2}{b^2(1 + k\alpha_{mn}^2)}[D_{11}\alpha_{mn}^{-2} + 2(D_{12} + 2D_{66}) + D_{22}\alpha_{mn}^2] \tag{3.22}$$

over m and n. These values of m and n are used in equations (3.20) and (3.21) to compute the initial postbuckling stiffnesses.

In the present study, five laminate configurations with eight layers each were considered as candidate designs. These configurations are specified as $\{\theta, -\theta, \theta, -\theta\}_{sym}$, $\{\theta, -\theta, 90, 0\}_{sym}$, $\{\theta, -\theta, 0, 0\}_{sym}$, $\{\theta, -\theta, 0, 90\}_{sym}$ and

$\{\theta, -\theta, 90, 90\}_{sym}$ and referred to as Laminate 1, 2, 3, 4 and 5, respectively. The results are given for a T300/5208 graphite/epoxy material. The plate thickness is specified as $h/b = 0.01$, and all the results are given for square plates. The following non-dimensionalised quantities are defined for postbuckling stiffnesses:

$$P_x = \frac{b^2}{E_o h^3}\frac{dN_x}{d\epsilon_x} \text{ and } P_y = \frac{b^2}{E_o h^3}\frac{dN_y}{d\epsilon_{xy}} \tag{3.23}$$

3.4.1 Results

First the behavior of the postbuckling stiffnesses with respect to the fiber orientation is investigated. Figure 42 shows the curves of P_x and P_y plotted against θ for a type 2 laminate with $\lambda = 0.75$, and $\lambda = 1.75$. This figure may be used to illustrate the method of solution described above. For $\lambda = 0.75$, the intersection of the curves for P_x and P_y/λ occurs at 23^o, and the constraint $P_y/\lambda \geq P_x$ is satisfied for $\theta \in [23^o, 90^o]$. Thus the feasible region for this case is given by $[23^o, 90^o]$. Maximising P_x on this interval gives the optimal angle $\theta_{opt} = 23^o$. Similarly, for $\lambda = 1.75$, the intersection of the curves for λP_x and P_y occurs at 81^o, and $\lambda P_x \geq P_y$ for $\theta \in [0^o, 81^o]$. Maximising P_y on the interval $[0^o, 81^o]$ gives the optimal angle $\theta_{opt} = 81^o$. Occasionally, the maximum occurs at an angle which is not given by the intersection of the stiffness curves. As an example, consider Figure 43 which shows the relationships between P_x and P_y for a type 5 laminate for $\lambda = 1.25$ and 2. The intersection of the curves for $\lambda = 1.25$ occurs at 35^o, and $\lambda P_x \geq P_y$ for $[0^o, 35^o]$. Maximising P_y on the interval $[0^o, 35^o]$ gives the optimal angle at $\theta_{opt} = 0^o$. Actually $\theta_{opt} = 0^o$ with this laminate for $0 \leq \lambda \leq 1.76$, whereupon the optimal fiber orientation jumps

to 48°, as seen from the curves for $\lambda = 2$ in Figure 43 [139].

Figure 44 shows the optimal values of the fiber orientations plotted against λ for the five laminate configurations, with $0 \leq \lambda \leq 4$. The discontinuities in the curves (particularly evident for laminate 5) are due to the optimal fiber orientation jumps, as described above. The curve for laminate 4 is interesting in that θ_{opt} reaches 90° before $\lambda = 1$. Also, the curves for laminates 2 and 4 are identical for $\lambda \leq 1.3$, and they separate for $\lambda > 1.3$.

Figure 45 shows the values of P^*_{xi}, $i = 1, 2, ..., 5$, corresponding to the optimal ply angles θ_{opt} shown in Figure 44, for $\lambda \leq 1$, noting that P_x is maximised for $\lambda \leq 1$. For this range of values, the design solution is given by the uppermost curve formed by the intersection of all five curves. Thus, laminate 1 is the best for $0 \leq \lambda \leq 0.09$, whereupon laminate 3 becomes the best until $\lambda \leq 0.20$ etc.

Similarly, Figure 46 shows the values of P^*_{yi}, $i = 1, 2, ..., 5$ corresponding to θ_{opt} shown in Figure 44, for $1 \leq \lambda \leq 4$. In this case, unlike for $\lambda \leq 1$, not all five laminates are optimal at one stage or another, and the optimal designs are given by type 1, 2 or 5 laminates. Figures 45 and 46 clearly demonstrate the necessity of considering several candidate designs to determine the optimal laminate configuration.

Table 10 shows the optimal laminate configurations for $0 \leq \lambda \leq 4$, the corresponding θ_{opt} and the postbuckling stiffnesses. Laminates 2 and 5 dominate the list for $0.8 \leq \lambda \leq 2.5$, while laminate 1 dominates for $\lambda \geq 3.0$. It is observed that as λ increases, the postbuckling stiffnesses, in general, decrease.

Finally, the postbuckling performance of two fourteen-layer laminates, referred to as laminates 6 and 7, are studied in Tables 11 and 12 for $0 \leq \lambda \leq$

4. These plates also have a thickness ratio of $h/b = 0.01$, are symmetrically laminated and square. The stacking sequence of each laminate is shown in the corresponding table. For these configurations, $A_{16} = A_{26} = D_{12} = D_{26}$ are zero and as such no in-plane or bending-twisting coupling exists [140]. The results in Table 11 show that for laminate 6, $\theta_{opt} = 0^o$ at $\lambda = 0$. θ_{opt} increases rapidly to 90^o as λ increases, and remains at this value for $\lambda \geq 0.6$. θ_{opt} for laminate 7 (Table 12) reaches 90^o only at $\lambda = 3.0$. Postbuckling stiffness in the higher load direction decreases as λ increases for laminate 6, while it fluctuates for laminate 7 .

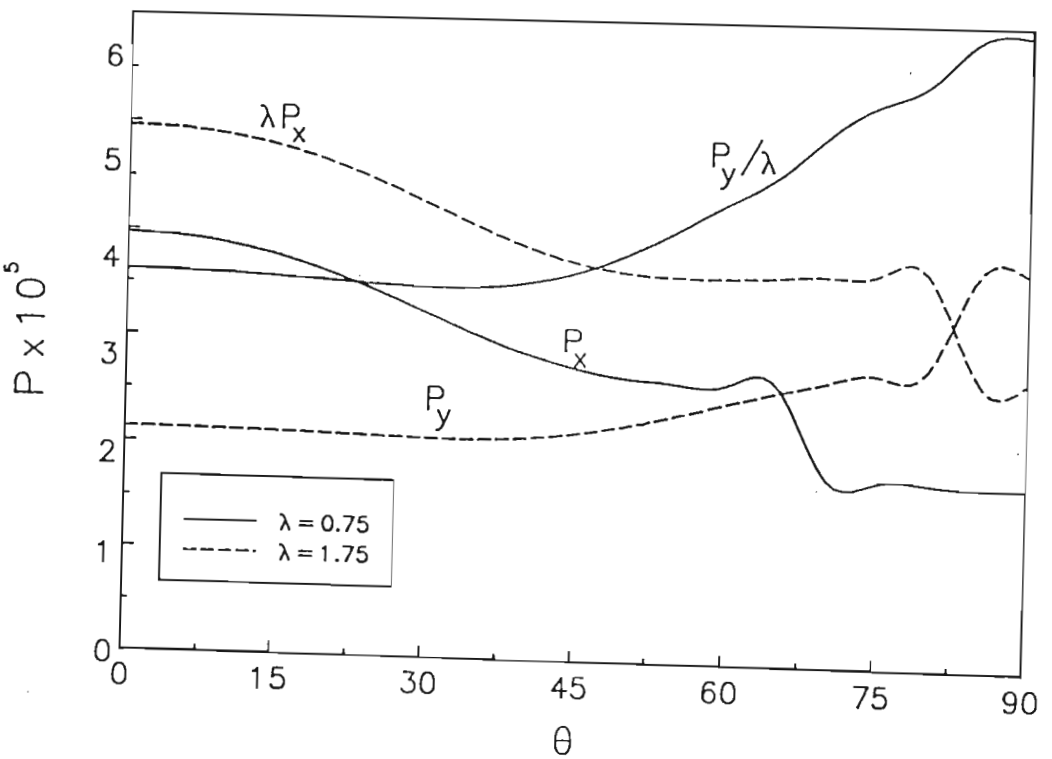

Figure 42. Curves of P_x and P_y versus θ for a type 2 laminate

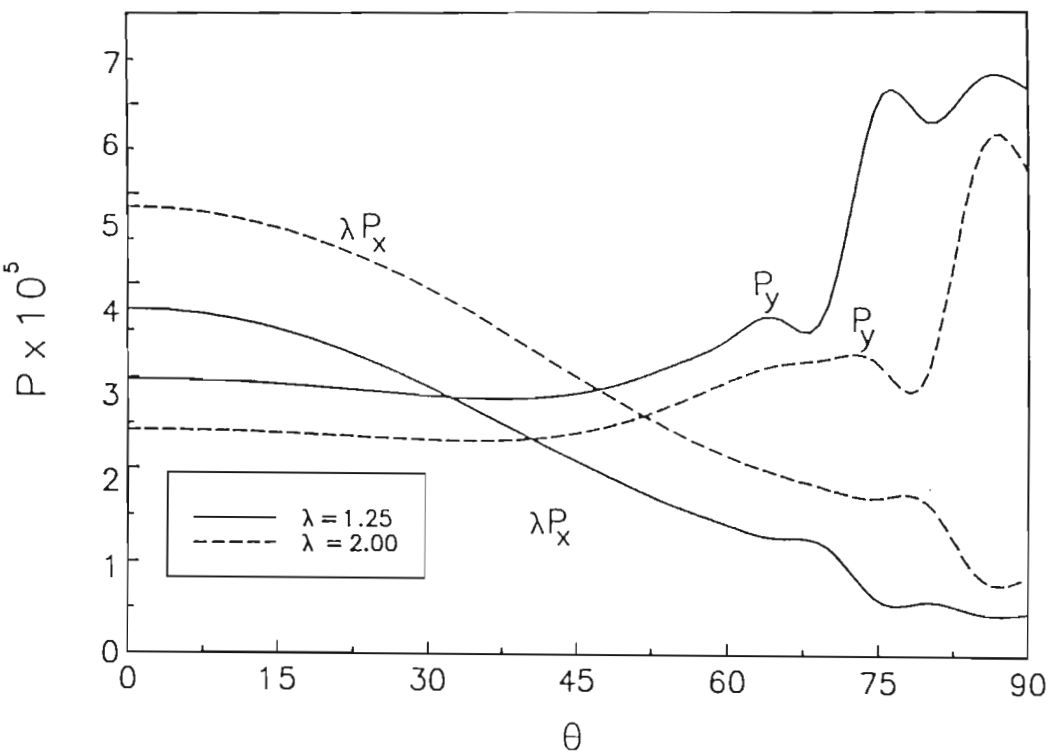

Figure 43. Curves of P_x and P_y versus θ for a type 5 laminate

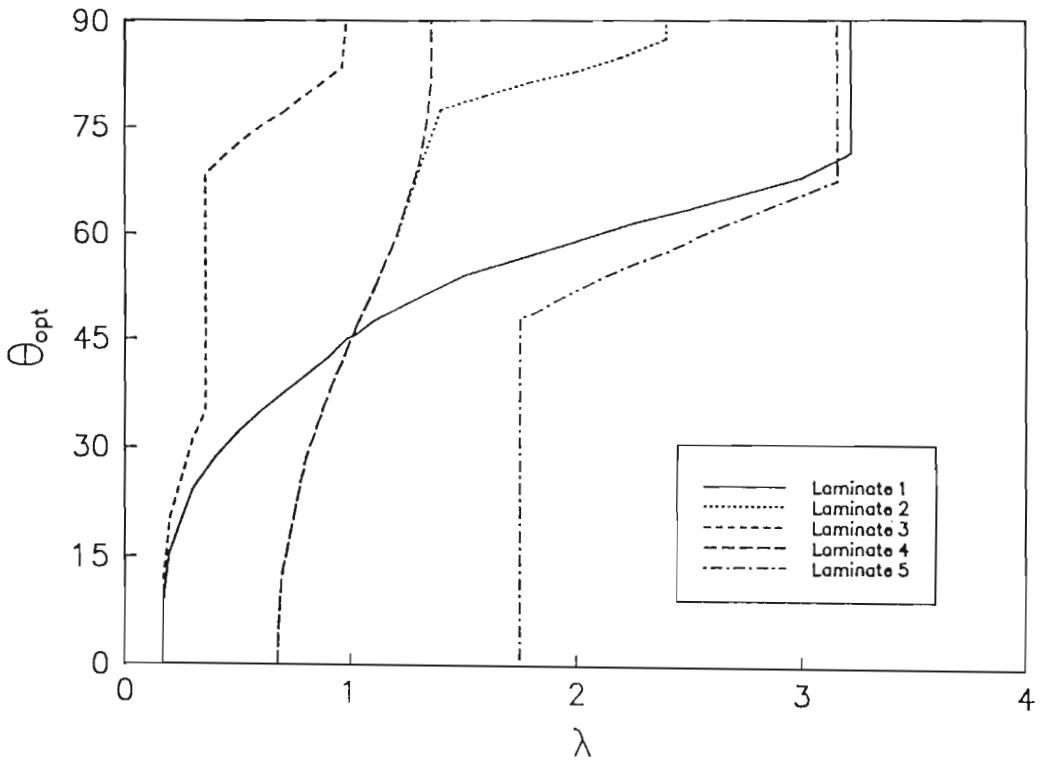

Figure 44. Curves of θ_{opt} versus $\lambda = N_y/N_x$ for five laminate types

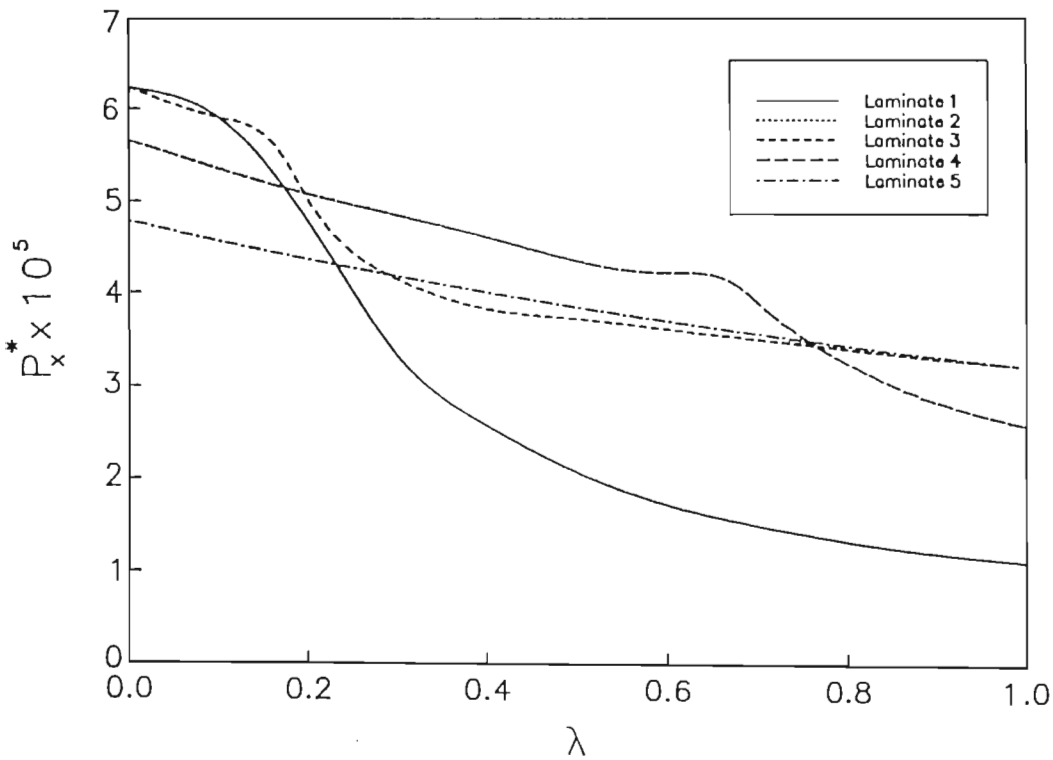

Figure 45. Curves of maximum stiffness P_x^* versus $\lambda = N_y/N_x$

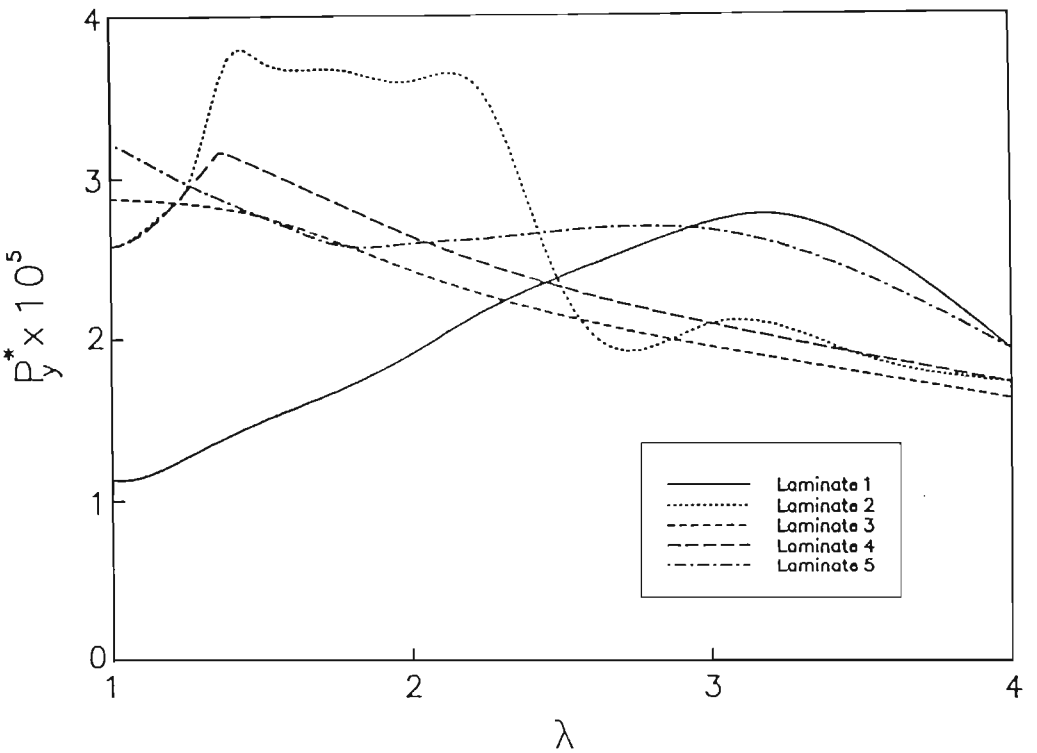

Figure 46. Curves of maximum stiffness P_y^* versus $\lambda = N_y/N_x$

λ	Optimal Laminate	θ_{opt}	P^*_x	P_y/λ
0	1 & 3	0	623409	infinity
0.2	2 & 4	0	507484	1594860
0.4	2 & 4	0	460451	749322
0 6	2 & 4	0	421396	471125
0.8	5	0	344523	430653
1.0	5	0	323078	323078
λ	Optimal Laminate	θ_{opt}	λP_x	P^*_y
1.2	5	0	362738	302282
1.4	2	77.5	394532	375554
1.6	2	79.7	388761	371257
1.8	2	81.4	378402	365868
2.0	2	83.3	403721	359314
2.5	5	59.1	267542	267098
3.0	1	68.2	286530	272233
3.5	1	90	251919	211277
4.0	1 & 5	90	278936	193045

Table 10. Optimal ply angles and laminate configurations for $0 \leq \lambda \leq 4$

λ	θ_{opt}	P^*_x	P_y/λ
0	0	623409	infinity
0.2	0	497808	1045220
0.4	86.2	376739	1045220
0.6	90	350608	645670
0.8	90	327344	448994
1.0	90	306975	334817
λ	θ_{opt}	λP_x	P^*_y
1.2	90	346790	313538
1.4	90	382200	294802
1.6	90	413896	278178
1.8	90	442432	263330
2.0	90	468262	249986
2.5	90	523245	221878
3.0	90	567684	199452
3.5	90	604345	181143
4.0	90	635108	165913

Table 11. Optimal ply angles for the laminate with the stacking sequence

$(\theta/\text{-}\theta/0^{\circ}/\text{-}\theta/0_2^{\circ}/\theta)_{sym}$ (laminate 6)

λ	θ_{opt}	P^*_x	P_y/λ
0	0	623409	infinity
0.2	16.5	482740	482840
0.4	30.6	284951	285444
0.6	37.6	218092	219243
0.8	70.8	207048	437435
1.0	73.2	200830	341346
λ	θ_{opt}	λP_x	P^*_y
1.2	56.6	221678	214402
1.4	63.3	250969	250824
1.6	74.0	289536	289354
1.8	80.5	519675	419518
2.0	82.1	426784	412713
2.5	86.3	404326	392338
3.0	90	434226	214385
3.5	90	472633	193760
4.0	90	506212	176755

Table 12. Optimal ply angles for the laminate with the stacking sequence $(\theta/\text{-}\theta_2/\theta/\text{-}\theta/\theta/0^o)_{sym}$ (laminate 7)

3.5 Part 5: Multiobjective Design of Laminated Plates Subject to In-plane Restraints for a Maximum Combination of Prebuckling and Postbuckling Stiffness and Buckling Load

For the laminated plate which is subjected to axial buckling loads and elastic in-plane restraints along the unloaded edges (as shown in Figure 22),

$$\begin{aligned} N_{xy} &= 0 \\ N_y &= k\nu_{xy}N_x \end{aligned} \tag{3.24}$$

where N_y is the resulting force due to Poisson's effect, k is the elastic constant of the in-plane restraints, and ν_{xy} is Poisson's ratio.

Since

$$\nu_{xy} = \frac{A_{12}A_{33} - A_{13}A_{23}}{A_{11}A_{33} - A_{13}^2} \tag{3.25}$$

and for specially orthotropic laminates $A_{13} = A_{23} = 0$, eqn. (3.25) becomes

$$\nu_{xy} = \frac{A_{12}}{A_{11}} \tag{3.26}$$

and since $\lambda = N_y/N_x$, substituting from eqn. (3.24) gives

$$\lambda = \frac{k\nu_{xy}N_x}{N_x} \tag{3.27}$$

Finally, from (3.26),

$$\lambda = k\frac{A_{12}}{A_{11}} \tag{3.28}$$

Also, from eqn. (1.107)

$$\begin{pmatrix} N_1 \\ N_2 \\ 0 \end{pmatrix} = \begin{pmatrix} A_{11} & A_{12} & 0 \\ A_{12} & A_{22} & 0 \\ 0 & 0 & A_{66} \end{pmatrix} \begin{pmatrix} \epsilon_1 \\ \epsilon_2 \\ \epsilon_{12} \end{pmatrix} \tag{3.29}$$

and $[A]^{-1} = [a]$, thus

$$\begin{pmatrix} \epsilon_1 \\ \epsilon_2 \\ \epsilon_{12} \end{pmatrix} = \begin{pmatrix} a_{11} & a_{12} & 0 \\ a_{12} & a_{22} & 0 \\ 0 & 0 & a_{66} \end{pmatrix} \begin{pmatrix} N_1 \\ N_2 \\ 0 \end{pmatrix} \tag{3.30}$$

Thus, for example

$$\epsilon_1 = a_{11}N_1 + a_{12}N_2 \tag{3.31}$$

But for our plate, $N_1 = N_x = N$, and $N_2 = N_y = \lambda N$, thus

$$\epsilon_1 = N(a_{11} + \lambda a_{12}) \tag{3.32}$$

Since

$$\sigma = E\epsilon \tag{3.33}$$

then

$$K = \frac{N}{\epsilon} = \frac{1}{a_{11} + \lambda a_{12}} \tag{3.34}$$

is the prebuckling stiffness.

The buckling load and postbuckling stiffness have been detailed in eqns. (3.20) and (3.22). In order to account for the in-plane restraints, eqn. (3.28) is substituted into these expressions.

Lastly, the following non-dimensionalised quantities are defined:

$$P^* = \frac{P}{P_o},\ N^* = \frac{N}{N_o},\ K^* = \frac{K}{K_o} \tag{3.35}$$

In the present study, as in the previous, five laminate configurations with eight layers each were considered as candidate designs. These configurations are specified as $\{\theta, -\theta, \theta, -\theta\}_{sym}$, $\{\theta, -\theta, 90, 0\}_{sym}$, $\{\theta, -\theta, 0, 0\}_{sym}$, $\{\theta, -\theta, 0, 90\}_{sym}$ and $\{\theta, -\theta, 90, 90\}_{sym}$ and referred to as Laminate 1, 2, 3, 4 and 5, respectively.

3.5.1 Results

The results are also given for a T300/5208 graphite/epoxy material, and again, the plate thickness is specified as $h/b = 0.01$.

Figure 47 shows the dependence of K^*, N^* and P^*, as well as DI on the fiber orientation θ for a type 2 laminate with an aspect ratio of $a/b = 1$, and $k = 1$. For this example, $\mu_1 = 0.25$, $\mu_2 = 0.5$ and $\mu_3 = 0.25$. Both P^* and K^* have $\theta_{opt} = 0°$, while that for N^* is around $35°$ and $25°$ for DI. It is interesting to note that the curve for P^* is discontinues in two places, between $\theta = 54°$ and $\theta = 60°$.

Similarly, Figure 48 shows the same curves for a type 1 laminate, with $a/b = 1.5$, and $k = 1$. As before, the curve of N^* has the highest values, but

unlike before, that for DI becomes the lowest in value for fiber orientations greater than 48^o. These two figures illustrate the importance of optimal design.

The dependence of DI on the fiber angle for all 5 laminate types is shown in Figure 49, for a plate aspect ratio of 1 and $k = 1$. In this case, the best laminate is always type 2, except at $\theta = 0^o$ when a type 5 laminate is also best. It is interesting to note that laminate types 1 and 3 share similar DI characteristics for $0^o \leq \theta \leq 55^o$, whereupon type 3 becomes the better of the two. This trend also occurs with laminates 4 and 5, although only when $\theta \geq 77^o$. Prior to this fiber orientation, laminate 5 is the better of the two for values of θ ranging between 0^o and 47^o, whereupon type 4 becomes better [141].

Similar curves are plotted in Figure 50, with $a/b = 1.5$, and $k = 1$. In this case, laminate 1 is optimal for $0^o \leq \theta \leq 24^o$, whereafter laminate 2 becomes best. From Figures 49 and 50 it is obvious that the laminate which gives the highest design index DI in both cases is laminate 2, with $\theta_{opt} = 27^o$ for $a/b = 1$ and $\theta_{opt} = 49^o$ for $a/b = 1$.

The effect of k on the optimal fiber orientation are shown in Table 13, for different plate aspect ratios, with $DI = 0.25K^* + 0.5N^* + 0.25P^*$. The choice of μ_1 and μ_2 here gives greater weighting to the buckling load N^*, and would be used where this factor is twice as important as the prebuckling and post-buckling stiffnesses, design wise. When the plate is narrow ($a/b \leq 0.8$), θ_{opt} is 0^o, and in these cases, the optimal laminate is either types 1 or 3. When $a/b = 0.8$, the optimal fiber orientation becomes nonzero, with the value increasing as the plate aspect ratio increases to $a/b = 1.25$. The value of θ_{opt} then tapers off slightly as a/b increases to 3. The corresponding values of

$K^*/K_{\max}$, $N^*/N_{\max}$ and $P^*/P_{\max}$ are listed in columns 4, 5 and 6 of Table 13, respectively. It is intersecting to note that for low aspect ratios, these three values are approximately/exactly 1. Generally, as a/b increases, so the values for $K^*/K_{\max}$and $P^*/P_{\max}$ decrease, while that for $N^*/N_{\max}$ remains approximately 1. This trend is followed until $a/b = 1.25$, where, as for θ_{opt}, the values for the prebuckling and postbuckling stiffnesses increase slightly. The last three columns of this column show the ratios of values of the individual optimal pre- and postbuckling stiffnesses, as well as the buckling load to the collective maximum found using the multiobjective scheme. This demonstrates the amount of stiffness/load lost as a result of using multiobjective design. The ideal would be to have the results in columns 3 - 6 all as high as possible, but obviously this is not the case. Table 14 illustrates similar results for $k = 0$.

In order to demonstrate the effect of varying values for μ_1, μ_2, and μ_3 on the design index, trade-off curves are given for four cases. In the first two cases, $\mu_1 + \mu_2 = 1$, with the influence of P^* neglected. Figure 51 shows the trade-off for $k = 0$ and $a/b = 1$. With $\mu_2 = 0$, K^* is approximately 1.7 whereas with $\mu_1 = 0$, N^* is approximately 1.0. Figure 52 likewise is the trade-off curve for $\mu_1 + \mu_2 = 1$ with $k = 1$ and $a/b = 1$. In this case when $\mu_2 = 0$, K^* is approximately 1.37 in value. Thus the effect of increasing value of k is to decrease that of K^*. The value of N^* when $\mu_1 = 0$ is the same as that for when $k = 0$.

Trade-off curves with the effect of P^* neglected are shown in Figures 53 and 54. As before the effect of increasing k is to depress the value of P^* whereas as before, that for N^* remains almost constant.

Finally a trade-off curve of μ_2 versus θ_{opt} is given in Figure 55, for $\mu_1 + \mu_2 = 1$, $k = 0, 1$ and $\mu_2 + \mu_3 = 1$, $k = 0, 1$. In all four cases, as μ_2 increases in value, the optimal fiber angle similarly increases. It is interesting to note that for $\mu_2 = 1$ the optimal fiber angles for all four cases lie between the values 42^o and 48^o.

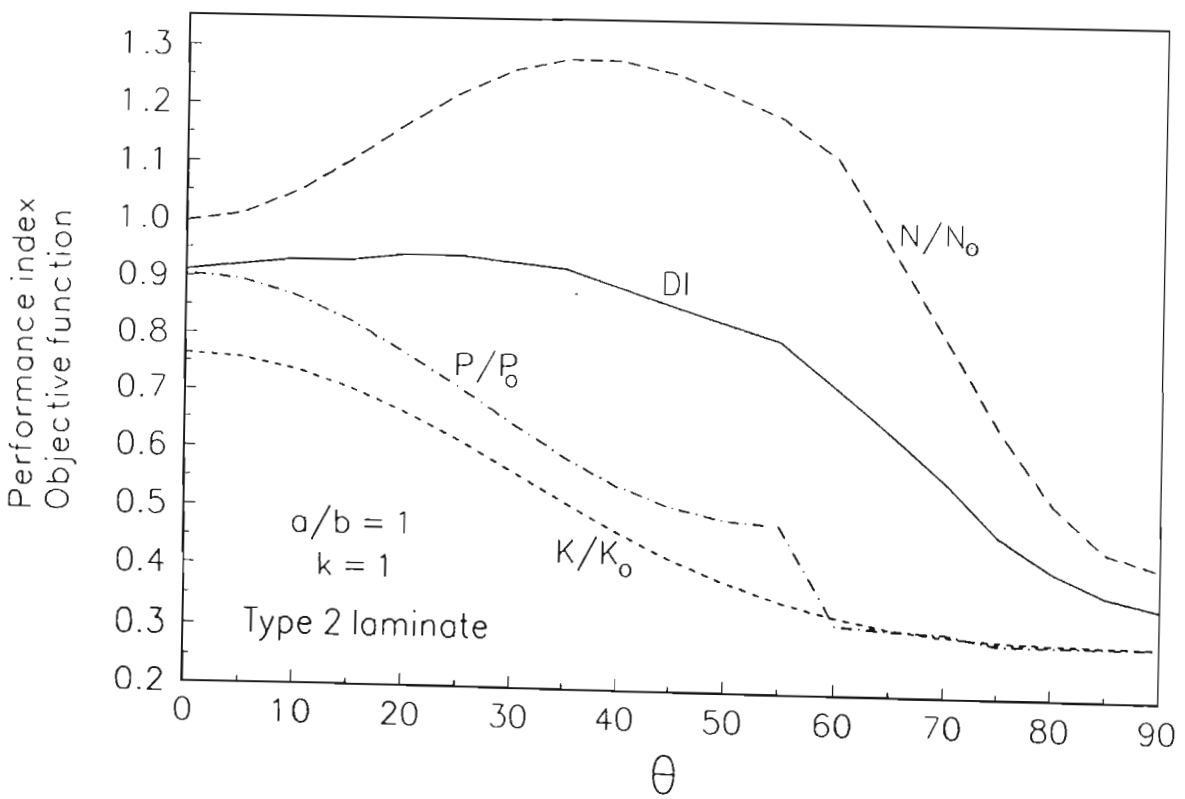

Figure 47. Dependence of K^*, N^*, P^* and DI on the fiber angle for a type 2 laminate

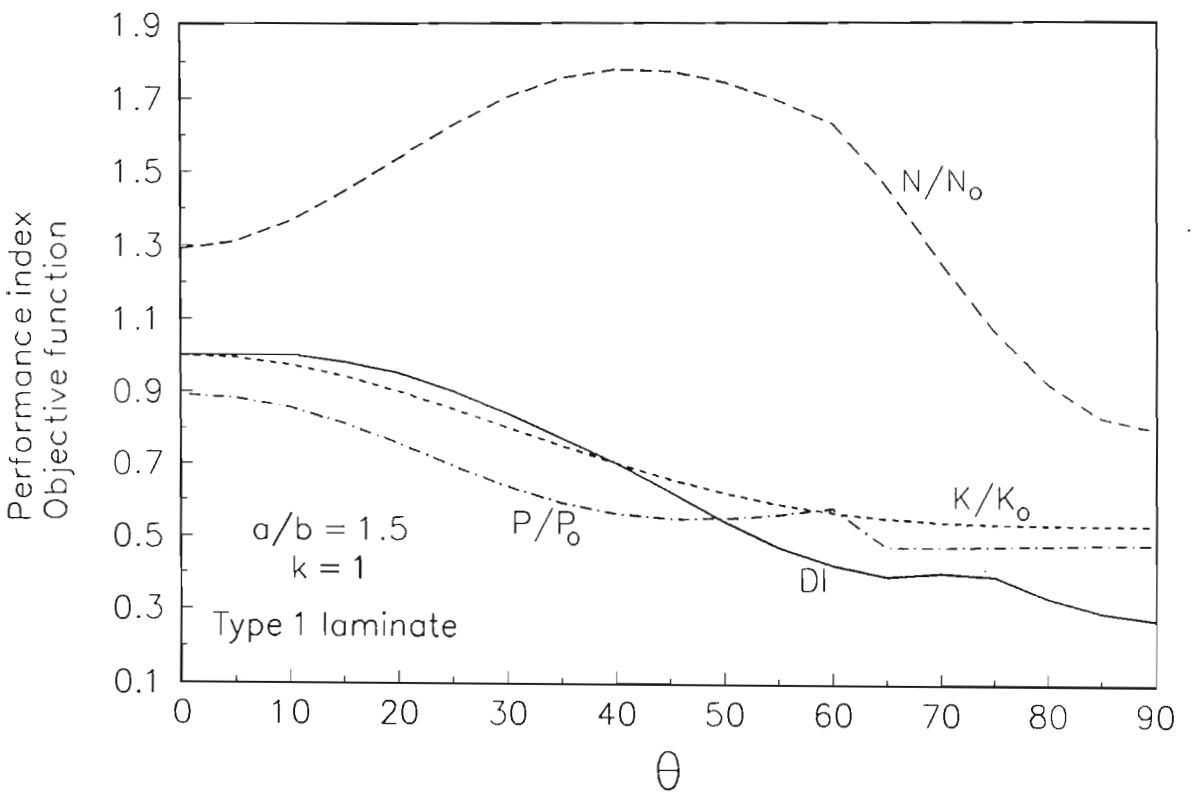

Figure 48. Dependence of K^*, N^*, P^* and DI on the fiber angle for a type 5 laminate

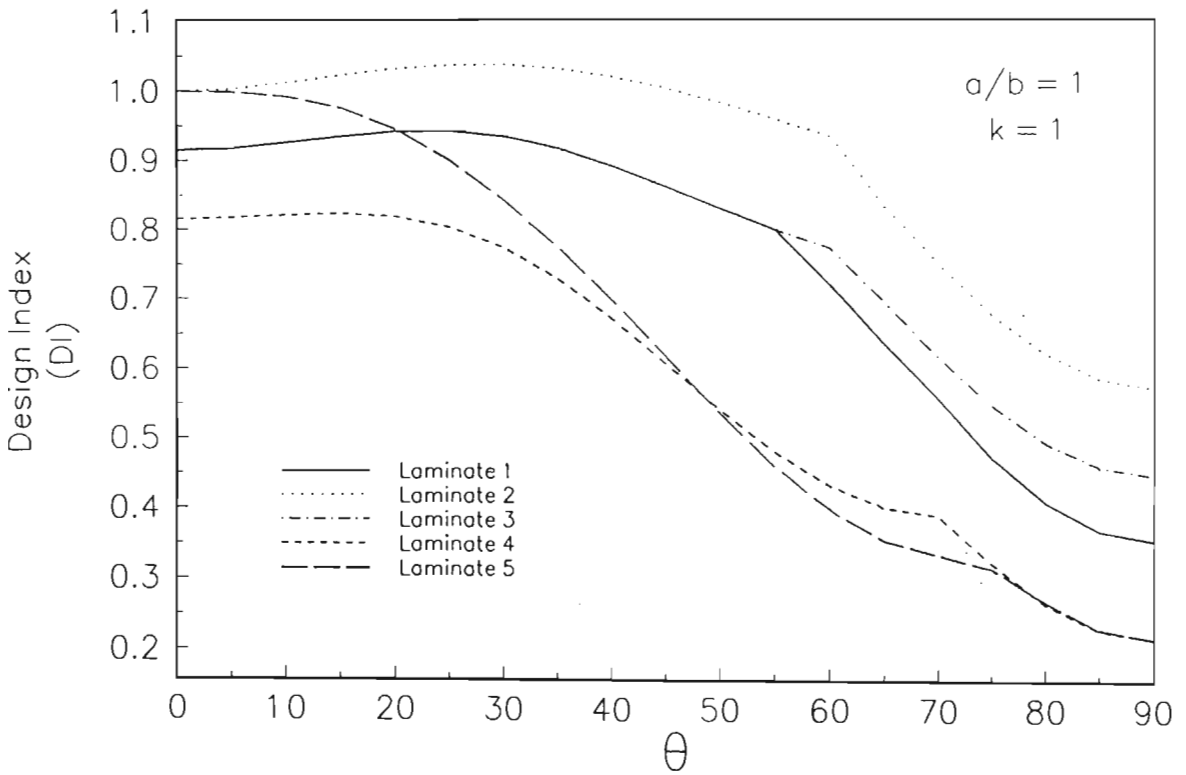

Figure 49. Dependence of DI on the fiber angle for all five laminate types, with $a/b = 1$

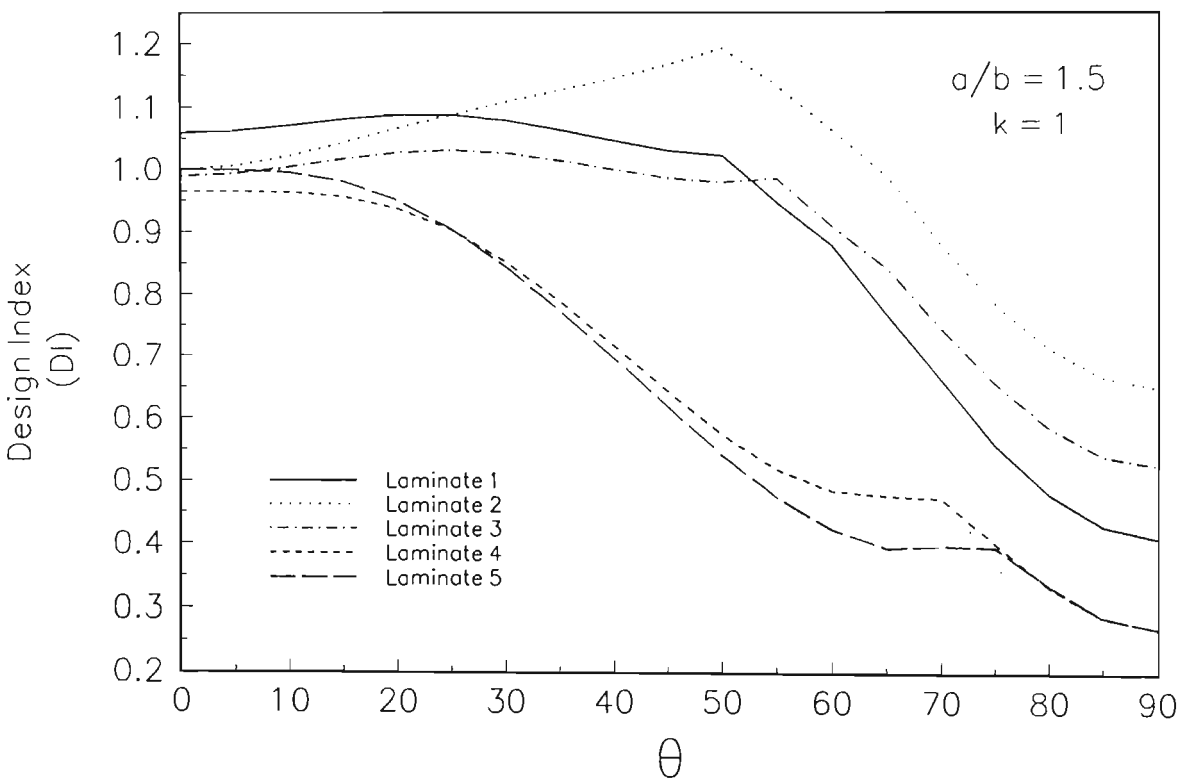

Figure 50. Dependence of DI on the fiber angle for all five laminate types, with $a/b = 1.5$

a/b	Lam No	θ_{opt}	K^*/K_{max}	N^*/N_{max}	P^*/P_{max}	$K(\theta^N_{opt})/K_{max}$	$N(\theta^N_{opt})/N_{max}$	$P(\theta^N_{opt})/P_{max}$
0.2	1&3	0	1	1	1	1	1	1
0.4	1&3	0	1	0.985	1	0.846	0.985	0.846
0.6	1&3	0	1	0.841	1	0.650	0.841	0.655
0.8	3	20.1	0.848	0.860	0.852	0.600	0.729	0.625
1.0	3	42.6	0.587	0.997	0.651	0.575	0.622	0.649
1.25	3	44.6	0.577	1	0.723	0.577	0.519	0.723
1.50	3	38.5	0.614	0.999	0.777	0.609	0.481	0.540
1.75	3	33.3	0.663	0.965	0.820	0.590	0.467	0.493
2	3	43.61	0.581	0.999	0.459	0.575	0.458	0.459
3	3	43.4	0.582	0.999	0.573	0.575	0.491	0.573

Table 13. Optimal laminate configurations with

$$DI = 0.25K^* + 0.5N^* + 0.25P^*,\ k = 0$$

a/b	Lam No	θ_{opt}	K^*/K_{max}	N^*/N_{max}	P^*/P_{max}	$K(\theta^N_{opt})/K_{max}$	$N(\theta^N_{opt})/N_{max}$	$P(\theta^N_{opt})/P_{max}$
0.2	1&3	0	1	1	1	1	1	1
0.4	1&3	0	1	0.994	1	0.929	0.994	0.903
0.6	1&3	0	1	0.896	1	0.783	0.896	0.697
0.8	3	17.6	0.921	0.892	0.884	0.727	0.800	0.637
1.0	3	27.6	0.826	0.938	0.742	0.685	0.726	0.622
1.25	3	56.9	0.578	1	0.730	0.578	0.647	0.730
1.50	3	54.2	0.592	0.999	0.797	0.592	0.574	0.495
1.75	3	52.4	0.603	1	0.834	0.603	0.538	0.834
2	3	51.1	0.611	1	0.838	0.611	0.523	0.838
3	3	48.1	0.632	0.971	0.729	0.602	0.554	0.298

Table 14. Optimal laminate configurations with

$$DI = 0.25K^* + 0.5N^* + 0.25P^*,\ k = 1$$

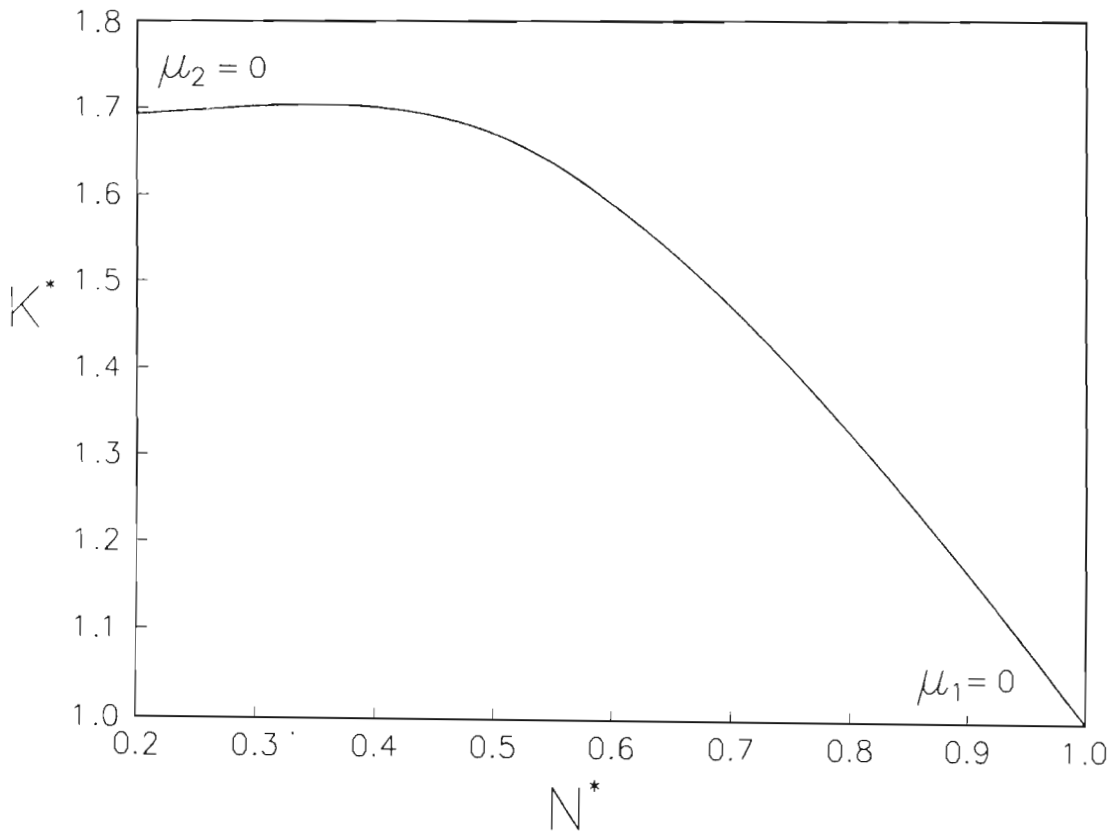

Figure 51. Trade-off curve for $\mu_1 + \mu_2 = 1$, with $k = 0$ and $a/b = 1$

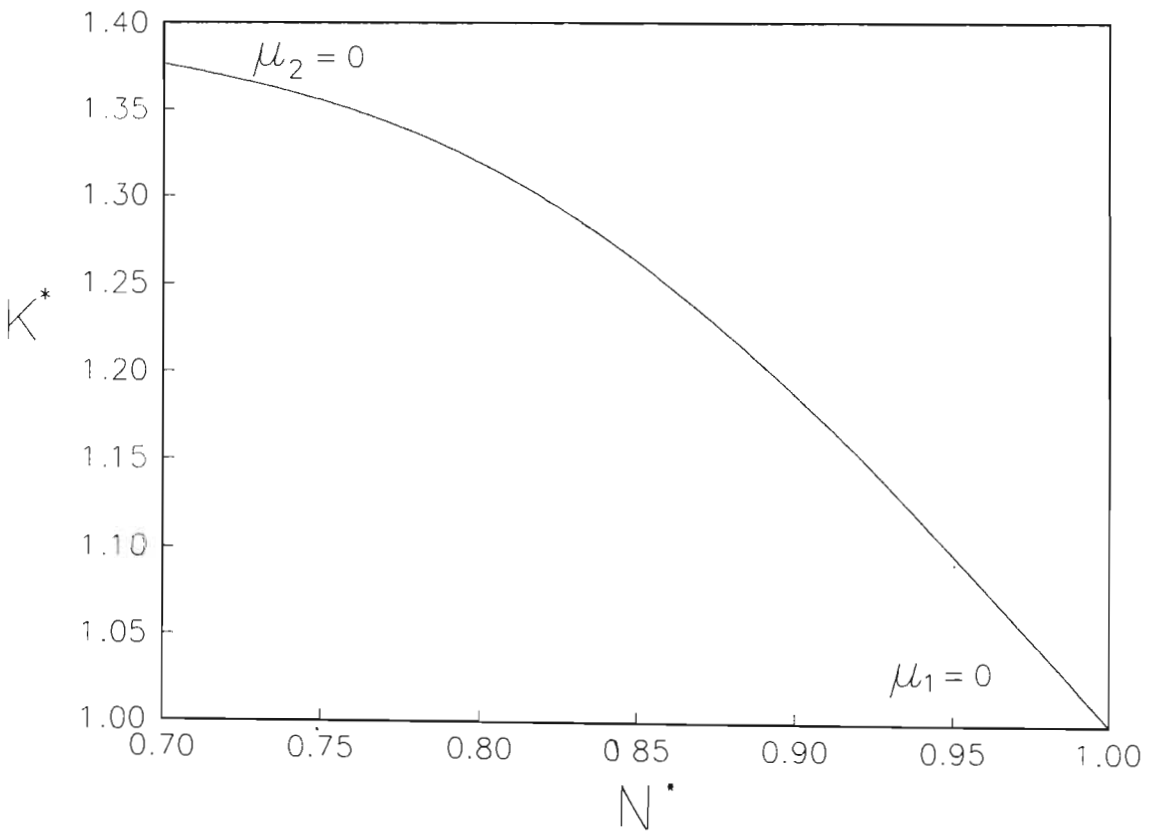

Figure 52. Trade-off curve for $\mu_1 + \mu_2 = 1$, with $k = 1$ and $a/b = 1$

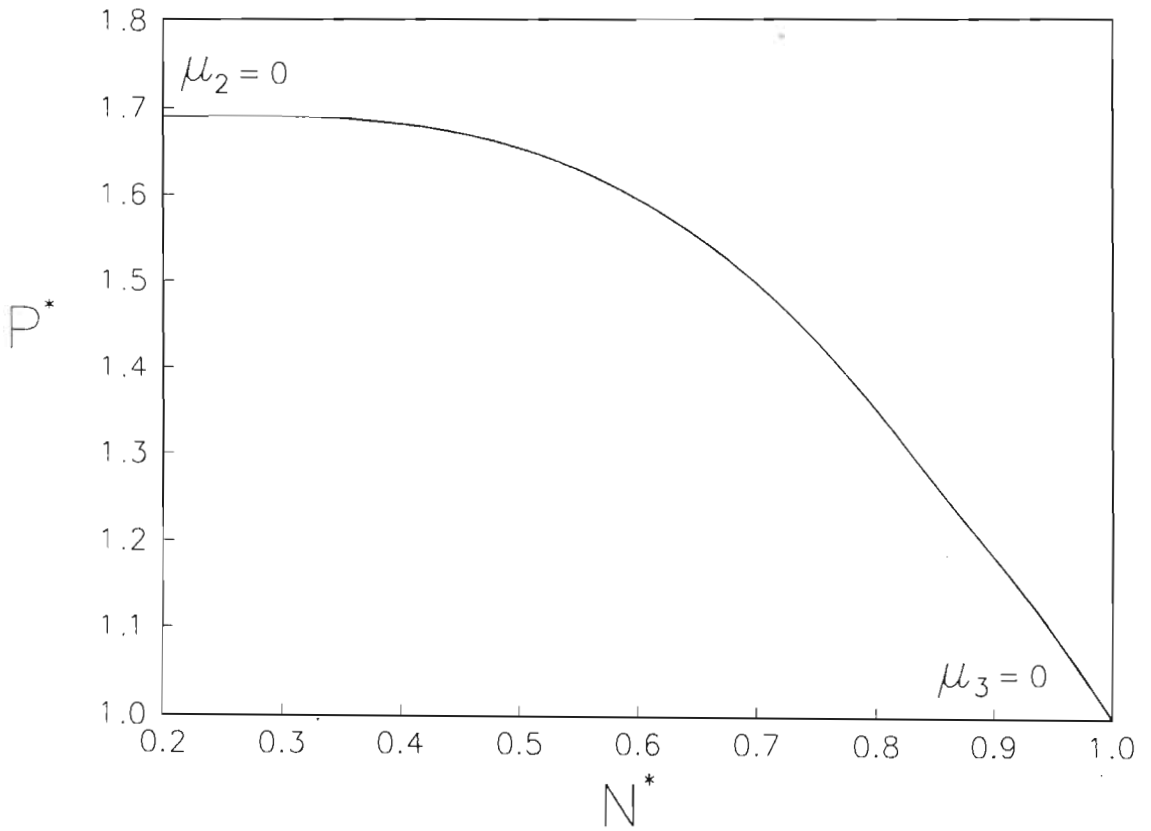

Figure 53. Trade-off curve for $\mu_2 + \mu_3 = 1$, with $k = 0$ and $a/b = 1$

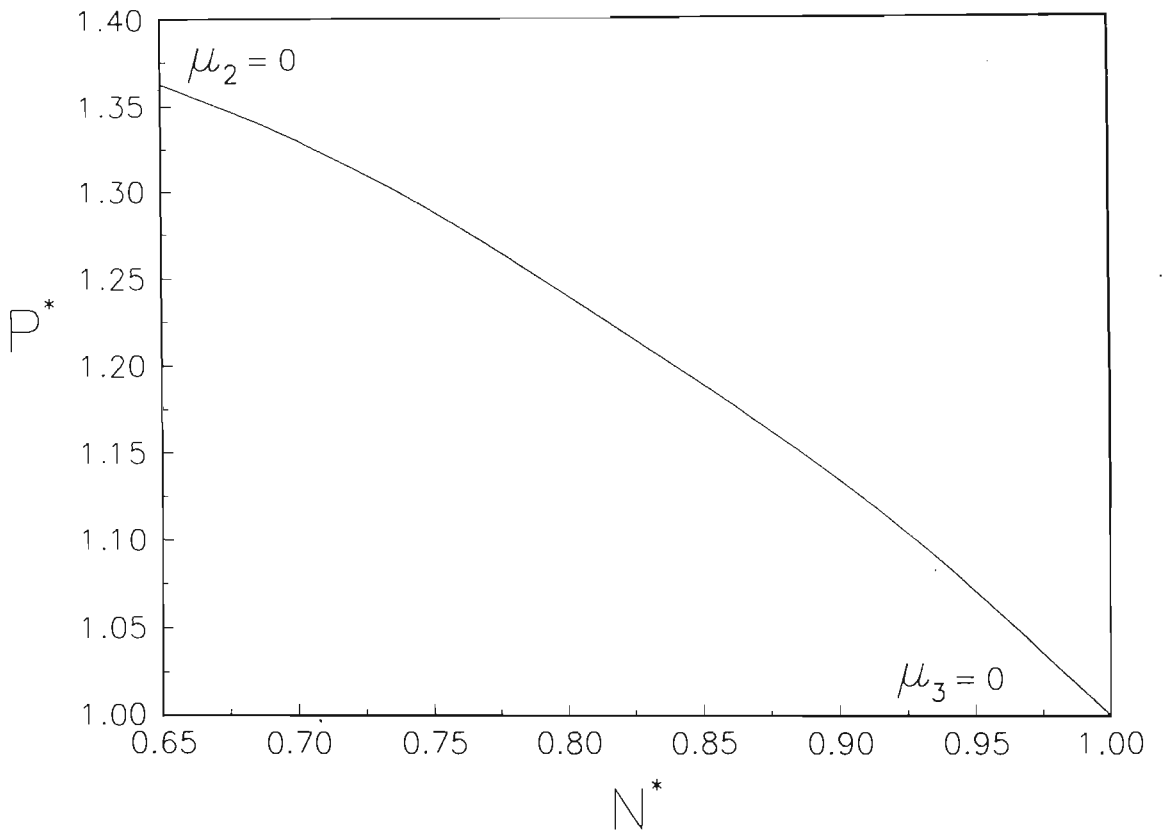

Figure 54. Trade-off curve for $\mu_2 + \mu_3 = 1$, with $k = 1$ and $a/b = 1$

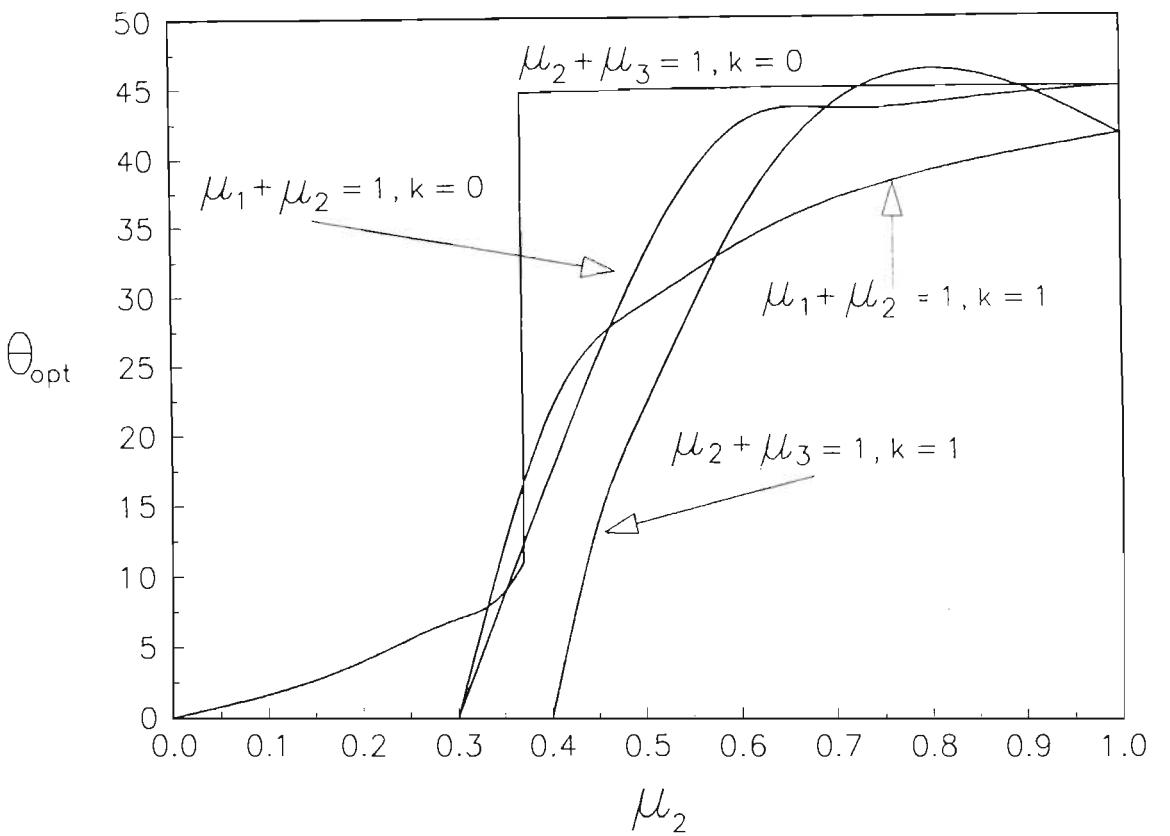

Figure 55. Trade-off curve for $\mu_1 + \mu_2 = 1$, $k = 0$, 1 and $\mu_2 + \mu_3 = 1$, $k = 0$, 1

Chapter 4

Conclusions

Five problems dealing with the optimal design of rectangular symmetrically laminated plates were investigated. In all cases, the layer fiber angle was the optimising variable, and the objective was the maximisation of either the buckling load (design problems 1 - 3), the postbuckling stiffnesses (problem 4) or a weighted combination of the prebuckling and postbuckling stiffness, and the buckling load (problem 5). Their relevance in practical design situations are emphesized, and important findings in each case are discussed.

For the first three problems, the finite element method was used in conjunction with an optimising routine to determine the optimal designs, since the complexity of the problems investigated ruled out the use of analytical methods. This formulation was based on Mindlin-type laminated thin plate and shell theory. The fourth and fifth problems allowed the use of analytical methods for analysis and optimisation purposes.

4.1 Part 1: Optimal Design of Symmetric Laminates for Maximum Buckling Load Including the Effects of Bending-Twisting Coupling

The effect of optimisation on the buckling load was investigated by plotting the buckling load against the design variable (Figures 24 and 25). The results show that the difference in the buckling loads of optimal and non-optimal plates could be quite substantial, emphasising the importance of optimisation for fiber composite structures.

It is observed that optimal fiber angles display several jump discontinuities when plotted against the aspect ratio. The present study shows that the number and location of these discontinuities caused by the changes in the buckling mode depend on the specific boundary conditions and the biaxial loading ratio N_y/N_x. In most cases the optimal fiber angle is quite sensitive to the value of the aspect ratio with (F,S,F,S) plates exhibiting the least sensitivity, and (C,S,C,S) plates exhibiting the most sensitivity.

A comparison of optimal fiber angles with and without bending-twisting coupling (Figure 32) showed that this effect cannot be neglected at certain aspect ratios. It is noted that the effect can be minimised by using a large number of layers in the laminate construction.

4.2 Part 2: Optimal Design of Symmetric Angle-ply Laminates Subject to Nonuniform Buckling Loads and In-plane Restraints

In this section, a comparative study is undertaken to investigate the effects of in-plane restraints and nonuniformity of load distributions.

In-plane restraints give rise to Poisson's effect and lead to buckling under biaxial compression for a uniaxially loaded plate, causing premature instability. The results show that the reduction in the buckling load depends on the aspect ratio and can be substantial for higher aspect ratios. In all cases of buckling loads, this reduction is more than 50% for an aspect ratio of 2. It is found that the differences in the optimal values of the ply angles are also considerable and increase as the aspect ratio becomes larger. These results clearly illustrate the extent of error which will be introduced into the analysis and design of composite laminates in the presence of in-plane restraints if Poisson's effect is not accounted for.

An interesting outcome of the study is the results pertaining to the effects of distributions of in-plane compressive loads on the optimal designs. Tables 5 - 8 indicate that, in general, θ_{opt} becomes smaller and the buckling load larger as the in-plane loads become more evenly distributed. Moreover, the differences in the θ_{opt} values of classical and present cases, in general, also increase as the compressive loads become more uniform. However, the ratio N_b^p/N_b^c does not show a clear trend.

Results are presented for combinations of simply-supported, clamped and free boundary conditions. Significant differences in the optimal fiber orientations and buckling loads are observed for the cases with and without Poisson's effect. Similarly, if the compressive loads are nonuniform, a uniform approximation will lead to nonconservative estimates of the buckling load.

4.3 Part 3: Optimal Design of Symmetric Laminates with Central Circular Cut-outs for Maximum Buckling Load

Optimal designs for laminated plates with central circular holes are presented, and compared to results found for plates without holes. The plates are subjected to biaxial loads, and combinations of boundary conditions at the edges. The effect of the cut-outs is greatest when the aspect ratio of the plate is small. In all cases, the buckling load capacity of the laminates containing holes is lower than those without holes, and the optimal fiber angles differ when holes are present. When the aspect ratio is large, the laminate becomes weak, offering less buckling resistance, and the effect of the hole is of less importance. The use of values determined in optimal design studies of laminated plates without holes can thus lead to non-optimal results for laminates containing holes.

4.4 Part 4: Optimal Laminate Configurations with Symmetric Lay-ups for Maximum Postbuckling Stiffness

A method is given for the optimal postbuckling design of symmetrically laminated angle-ply plates. The design objective is specified as the maximisation of the initial postbuckling stiffness in the higher load direction subject to a stiffness constraint in the other direction. This formulation ensures sufficient stiffness in both directions. Due to the special nature of the problem the optimal design is chosen from among several candidate configurations with angle-ply and cross-ply layers. It is shown that the optimal configuration depends on the ratio of the in-plane loads in the x and y directions. The postbuckling stiffnesses may fluctuate as the load ratio increases, but the general tendency is to decrease with increasing load ratio. Results are given for two additional configurations in which no in-plane or bending-twisting coupling occurs by virtue of the special choice of the stacking sequences. These configurations exhibit lower postbuckling stiffnesses as compared to the optimal designs chosen from among candidate designs.

4.5 Part 5: Multiobjective Design of Laminated Plates Subject to In-plane Restraints for a Maximum Combination of Prebuckling and Postbuckling Stiffness and Buckling Load

A multiobjective design study is carried out with the objective being the maximisation of the weighted sum of the prebuckling and postbuckling stiffnesses, and the buckling load, for uniaxially loaded plates with in-plane restraints along the unloaded edges. The optimal design process presented is applied to five candidate laminate configurations, and the best is chosen under the given biaxial loading and geometric parameters.

In general, it is usually the case that the buckling load is the most important design criteria, with the prebuckling and the postbuckling stiffnesses playing lesser roles. Thus, the study concentrates on a weighting scheme that gives twice as much prominence to the non-dimensionalised buckling load than the non-dimensionalised prebuckling and postbuckling stiffnesses. In this case, when the plate aspect ration is small ($a/b \leq 0.8$), the multiobjective design gives individual stiffnesses and buckling loads which are almost as high as in cases that would be obtained in single objective designs, but as the aspect ratio increases, these individual values decrease. Nonetheless, the multiobjective design shows that laminate types 1 and 3 are the best choices for cases where high prebuckling and postbuckling stiffness and buckling load are required.

Chapter 5

Suggestions and Further Research

The literature reflects that although much investigation has been carried out concerning the buckling of laminated plates and the optimal design of such plates, there still remains much to be done. Five optimal design problems were tackled here, but they actually create more avenues for research than they close. As composite materials become more popular in more applications, and correspondingly, as they become economically viable for these applications, so more funds will become available for research into their applicabilty. Slowly but surely, a greater reserve of knowledge of composites will be developed.

From the work that was carried out here, the following research problems spring to mind, and some of them have been tackled:

1. Optimal design of laminated plates subjected to varying thermal loads and combinations of boundary conditions. This type of problem is termed

coupled, since the first part involves solving for the heat distribution, and the second the determination of the optimal design in order to maximise the buckling temperature. This investigation is almost finished.

2. Optimal design of laminated plates subjected to varying in-plane and thermal loads and combinations of boundary conditions. This problem is more complicated than that described above, since the there is now a combination of temperature loading and pressure loading along the edges. None the less, the problem will be tackled in the near future, and should prove interesting.

3. Optimal design of biaxially laminated plates subjected to a weighted combination of the prebuckling and postbuckling stiffness, and buckling load. Since this problem, unlike the problem solved in Part 4 of this thesis, includes biaxial loads, the postbuckling stiffnesses P_x and P_y in *both* directions will have to be accounted for.

4. Optimal design of laminated plates with central circular cut-outs subjected to thermal loads and combinations of boundary conditions.

Bibliography

[1] Forsythe, G. E. and Wasow, W. R., (1960), '*Finite Difference Methods for Partial Differential Equations*', John Wiley and Sons, New York.

[2] Richtmeyer, R. D. and Morton, K. W., (1967), '*Difference Methods for Initial-Value Problems*', Second Edition, Wiley-Interscience, New York.

[3] Huebner, K. H. and Thornton, E. A., (1982), '*The Finite Element Method for Engineers*', John Wiley and Sons, Toronto.

[4] Kapkowski, J., (1968), '*A Finite Element Study of Elastic Plastic Stress Distributions in Notched Specimens under Tension*', Meddelelse SKB II/M 13, Department of Ship Structures, The Technical University of Norway.

[5] Gallagher, R. H., Gellatly, R. A., Padlog, J. and Mallett, R. H., (1967), 'A Discrete Element Procedure for Thin-Shell Instability Analysis', *AIAA J.*, Vol. 5, 1.

[6] Zienkiewicz, O. C., (1968), '*The Finite Element Method in Structural and Continuum Mechanics*', McGraw-Hill Book Company, New York.

[7] Courant, R., (1943), 'Variational Methods for the Solutions of Problems of Equilibrium and Vibrations", *Bull. Am. Math. Soc.*, Vol. 49.

[8] Euler, L., (1774), '*Methods Inveniendi Lineas Curvas Maximi Minimine Proprietate Gaudentes*', M. Bousquet, Lausanne and Geneva.

[9] Polya, G., (1952), 'Sur une Interpretation de la Methode des Differences Fines Qui Peut Fournir des Bornes Superieures ou Inferieures', *C. R. Acad. Sci.*, Vol. 235.

[10] Polya, G., (1954), '*Estimates for Eigenvalues: Studies Presented to Richard von Mises*', Academic Press, New York.

[11] Hersch, J., (1955), 'Equations Differentielles et Fonctions de Cellules', *C. R. Acad. Sci.*, Vol. 240.

[12] Weinberger, H. F., (1956), 'Upper and Lower Bounds for Eigenvalues by Finite Difference Methods', *Commun. Pure Appl. Math.*, Vol. 9.

[13] Weinberger, H. F., (1958), 'Lower Bounds for Higher Eigenvalues by Finite Difference Methods', *Pac. J. Math.*, Vol. 8.

[14] Greenstadt, J., (1959), 'On the Reduction of Continuous Problems to Discrete Form', *IBM J. Res. Dev.*, Vol. 3.

[15] Morse, P. M. and Feshback, H., (1953), '*Methods of Theoretical Physics*', McGraw-Hill Book Company, New York, Section 9.4.

[16] White, G. N., (1962), '*Difference Equations for Plane Thermal Elasticity*', LAMS-2745, Los Alamos Scientific Laboratory, Los Alamos, New Mexico.

[17] Friedrichs, K. O., (1962), '*A Finite Difference Scheme for the Neumann and the Dirichlet Problem*', NYO-9760, Courant of Mathematical Sciences, New York University, New York.

[18] Cea, J., (1964), 'Approximation Variationnelle des Problemes aux Limites', *Ann. Inst. Fourier*, Vol. 14.

[19] Kellogg, R. B., (1964), 'Difference Equations on a Mesh Arising from a General Triangulation', *Math. Comp.*, Vol. 18.

[20] Kellogg, R. B., (1965), 'Ritz Difference Equations on a Triangulation', *Proceedings of the Conference on the Application of Computing Methods to Reactor Problems*, Argonne National Laboratory.

[21] Ciarlet, P. G., (1966), '*Variational Methods for Non-Linear Boundary Value Problems*', Thesis, Case Institute of Technology, Cleveland, Ohio.

[22] Oganesjan, L. A., (1966), 'Convergence of Difference Schemes in Case of Improved Approximation of the Boundary', *Zh. Vychisl. Mat. Mat. Fiz.*, Vol. 6.

[23] Varga, R. S., (1967), '*Hermite Interpolation-Type Ritz Methods for Two-Point Boundary Value Problems*', in Numerical Solutions of Partial Differential Equations, Academic Press, New York.

[24] Friedrichs, K. O. and Keller, H. B., (1967), '*A Finite Difference Scheme for Generalized Neumann Problems*', in Numerical Solutions of Partial Differential Equations, J. H. Bramble (ed.), Academic Press, New York.

[25] Aubin, J. P., (1967), 'Approximation des Espaces de Distributions et des Operateurs Differentiels', *Bull. soc. Math. Fr.*, Mem. 12.

[26] Ciarlet, P. G., Schultz, M. H. and Varga, R. S., (1967), 'Numerical Methods of High-Order Accuracy for Non-Linear Boundary Value Problems. I: One-Dimensional Problem', *Numer. Math.*, Vol. 9.

[27] Goel, J.J., (1968), 'Construction of Basic Functions for Numerical Utilization of Ritz's Method', *Numer. Math.*, Vol. 12.

[28] Zlamal, M., (1968), 'On the Finite Element Method', *Numer. Math.*, Vol. 12.

[29] Birkhoff, G., Schultz, M. H. and Varga, R. S., (1968), 'Piecewise Hermite Interpolation in One and Two Variables with Applications to Partial Differential Equations', *Numer. Math.*, Vol. 11.

[30] Schultz, M. H., (1969), 'L-Multivariate Approximation Theory', *SIAM J. Numer. Anal.*, Vol. 6, 2.

[31] Zenisek, A., (1970), 'Interpolation Polynomials on the Triangle', *Numer. Math.*, Vol. 15.

[32] Bramble, J. H. and Zlamal, M., (1970), 'Triangular Elements in the Finite Element Method', *Math. Comp.*, Vol. 24, 112.

[33] Carlson, R. E. and Hall, C. A., (1971), 'Ritz Approximation to Two-Dimensional Boundary Value Problems', *Numer. Math.*, Vol. 18.

[34] Babuska, I., (1971), 'The Rate of Convergence for the Finite Element Method', *SIAM J. Numer. Anal.*, Vol. 8.

[35] Babuska, I., (1971), 'Error Bounds for the Finite Element Method', *Numer. Math.*, Vol. 16.

[36] Fix, G. and Nassif, N., (1972), 'On Finite Element Approximations to Time-Dependent Problems', *Numer. Math.*, Vol. 19.

[37] Yamamoto, Y. and Tukuda, N., 'A Note on the Convergence of Finite Element Solutions', *Int. J. Numer. Methods,* Vol. 6.

[38] Fried, I., (1972), 'Discretization and Computational Errors in High- Order Finite Elements', *AIAA J.*, Vol. 9, 10.

[39] Fried, I., (1972), 'Accuracy of Complex Finite Elements', *AIAA J.*, Vol. 10, 3.

[40] Oden, J. T., (1972), '*Finite Elements of Nonlinear Continua*', McGraw-Hill Book Company, New York.

[41] Birkhoff, G. and Garabedian, H. L., (1960), 'Smooth Surface Interpolation', *J. Math. Phys.*, Vol. 39.

[42] De Boor, C., (1962), 'Bi-cubic Spline Interpolation', *J. Math. Phys.*, Vol. 41.

[43] Birkhoff, G. and De Boor, C., (1965), '*Piecewise Polynomial Interpolation and Approximation*', in Approximation of Functions, Elsevier Publishing Company, Amsterdam.

[44] Ahlberg, J. H., Nilson, E. N. and Walsh, J. L., (1967), '*The Theory of Splines and Their Applications*', Academic Press, New York.

[45] Prenter, P. M., (1975), '*Splines and Variational Methods*', John Wiley and Sons, New York.

[46] Gordon, W. J., (1969), 'Distributive Lattices and the Approximation of Multivariate Functions', *Proceedings of the Symposium on Approximation with Special Emphasis on Spline Functions*, University of Wisconsin, May 5-7, Academic Press, New York.

[47] Schoenberg, I. J., (1969), '*Approximations with Special Emphasis on Spline Functions*', Academic Press, New York.

[48] Gordon, W. J., (1969), 'Spline-Blended Surface Interpolation Through Curve Networks', *J. Math. Mech.*, Vol. 19, 10.

[49] Greville, T. N. E., (1969), '*Theory and Applications of Spline Functions*', Academic Press, New York.

[50] Varga, R. S., (1971), 'Functional Analysis and Approximation Theory in Numerical Analysis', *SIAM (Regular Conference Series in Applied Mechanics)*, Philadelphia.

[51] Strang, W. G. and Fix, G., (1974), '*An Analysis of the Finite Element Method*', Prentice-Hall, Englewood Cliffs, New Jersey.

[52] Babuska, I. and Aziz, A. K., (1973), '*The Mathematical Foundations of the Finite Element Method - With Applications to Partial Differential Equations*', Academic Press, New York.

[53] Whiteman, J. (ed.), (1973), '*The Mathematics of Finite Elements and Applications*', Academic Press, New York.

[54] Oden, J. T., (1972), 'Some Aspects of Recent Contributions to the Mathematical Theory of Finite Elements', *Advances in Computational Methods in Structural Mechanics and Design, Proceedings of the 2nd U.S.-Japan Seminar*, University of Alabama Press, Huntsville, Alaska.

[55] Hrenikoff, A., (1941), 'Solution of Problems in Elasticity by the Framework Method', *J. Appl. Mech.*, Vol. 8.

[56] McHenry, D., (1943), 'A Lattice Analogy for the Solution of Plane Stress Problems', *J. Inst. Civ. Eng.*, Vol. 21.

[57] Newmark, N. M.(1949), in *Numerical Methods of Analysis in Engineering*, L. E. Grinter (ed.), Macmillan Company, New York.

[58] Argyris, J. H., (1954), 'Energy Theorems and Structural Analysis', *Aircraft Eng.*, Vol. 26.

[59] Argyris, J. H., (1955), 'Energy Theorems and Structural Analysis', *Aircraft Eng.*, Vol. 27.

[60] Argyris, J. H., (1956), 'The Matrix Analysis of Structures with Cut-Outs and Modifications', *Proceedings of the 9th International Congress on Applied Mechanics, Section II: Mechanics of Solids.*

[61] Argyris, J. H. and Kelsey, S., (1956), 'Structural Analysis by the Matrix Force Method with Applications to Aircraft Wings', *Wiss. Ges. Luftfahrt Jahrb.*

[62] Argyris, J. H., (1957), 'The Matrix Theory of Statics', *Ing. Arch.*, Vol. 25.

[63] Argyris, J. H. and Kelsey, S., (1959), 'The Analysis of Fuselages of Arbitrary Cross-Section and Taper', *Aircraft Eng.*, Vol. 31.

[64] Argyris, J. H. and Kelsey, S., (1960), '*Energy Theorems and Structural Analysis*', Butterworth and Company, London.

[65] Turner, M. J., Clough, R. W., Martin, H. C. and Topp, L. C., (1956), 'Stiffness and Deflection Analysis of Complex Structures', *J. Aeronaut. Sci.*, Vol. 23, 9.

[66] Clough, R. W., (1960), 'The Finite Element Method in Plane Stress Analysis', *Proceedings of 2nd ASCE Conference on Electronic Computation*, Pittsburgh.

[67] Besseling, J. F., (1963), 'The Complete Analogy Between the Matrix Equations and the Continuous Field Equations of Structural Analysis', *International Symposium on Analogue and Digital Techniques Applied to Aeronautics*, Liege, Belgium.

[68] Melosh, R. J., (1963), 'Basis for the Derivation of Matrices for the Direct Stiffness Method', *AIAA J.*, Vol. 1.

[69] De Veubeke, B. F., (1964), '*Upper and Lower Bounds in Matrix Structural Analysis*', in AGARD-ograph 72, Pergamon Press, New York.

[70] Jones, R. E., (1965), 'A Generalization of the Direct-Stiffness Method of Structural Analysis', *AIAA J.*, Vol. 220.

[71] Zienkiewicz, O. C. and Cheung, Y. K., (1965), 'Finite Elements in the Solution of Field Problems', *Engineer*, Vol. 220.

[72] Oden, J. T. and Reddy, J. N., (1976), '*An Introduction to the Mathematical Theory of Finite Elements*', John Wiley and Sons, New York.

[73] Hildebrand, F. B., (1965), '*Methods of Applied Mathematics*', Prentice-Hall, Englewood Cliffs, New Jersey.

[74] Oden, J. T. and Somogyi, D., (1969), 'Finite Element Applications in Fluid Dynamics', *Proc. ASCE J. Eng. Mech. Div.*, Vol. 95, EM3.

[75] Zienkiewicz, O. C., (1977), '*The Finite Element Method*', Third Edition, McGraw-Hill Book Company, New York.

[76] Felippa, C. A. and Clough, R. W., (1970), 'The Finite Element Method in Solid Mechanics', in *SIAM-AMS Proceedings*, Vol. 2, American Mathematical Society, Providence, pp. 210-252.

[77] Oliveira, E. R. A., (1968), 'Theoretical Foundations of the Finite Element Method', *Int. J. Solids Struct.*, Vol. 4, pp. 929-952.

[78] Pian, T.H.H. and Tong, P., (1969), 'Basis of Finite Element Methods for Solid Continua', *Int. J. Numer. Methods Eng.*, Vol. 1, 1, p. 26.

[79] Case, J., Lord Chilver & Ross, C. T. F., (1993), '*Strength of Materials and Structures, with and introduction to Finite Element Methods*', Third Edition, Edward Arnold Publishers, Kent, UK.

[80] Tsai, S. & Hahn, W., (1980), *Introduction to Composite Materials*, Technomic Publishing Company, Westport, USA.

[81] Whitney, J. M., (1987), 'Structural Analysis of Laminated Anisotropic Plates', Technomic Publishing Co., Inc., Lancaster, Pennsylvania.

[82] Noor, A. K., Mathers, M. D. & Anderson, M. S. (1977), 'Exploiting symmetries for efficient postbuckling analysis of composite plates', *AIAA Journal*, 15, pp. 24-32.

[83] Nemeth, M. P., (1986), 'Importance of anisotropy on buckling of compression-loaded symmetric composite plates', *AIAA Journal*, 24, pp. 1831-1835.

[84] Whitney, J. M., (1987), 'The effect of shear deformation on the bending and buckling of anisotropic laminated plates', In *Composite Structures 4*, edited by I. H. Marshall. Elsevier Applied Science, London, pp. 1.109-1.121.

[85] Grenestedt, J. L., (1989), 'A study of the effect of bending-twisting coupling on buckling strength', *Composite Structures*, 12, pp. 271-290.

[86] Nemeth, M. P., (1992), 'Buckling of symmetrically laminated plates with compression, shear and in-plane bending', *AIAl Journal*, 30, pp. 2959-2965.

[87] Rohwer, K., (1988), 'Bending-twisting coupling effects on the buckling load of symmetrically stacked plates', In *Composite Materials and Structures, Proceedings of the Int. Conf. on Composite Materials and Structures*, 6-9 January, Madras, India, edited by K. A. V. Pandalai and S. K. Malhotra, Tata McGraw-Hill Publishing Company Ltd., New Delhi, pp. 313-323.

[88] Sherbourne, A. N. & Pandey, M. D., (1991), 'Differential quadrature method in the buckling analysis of beams and composite plates', *Computers and Structures*, 40, pp. 903-913.

[89] Adali, S., (1994), 'Lay-up optimisation of laminated plates under buckling loads', In *Buckling and Postbuckling of Composite Plates*, edited by G. J. Turvey and I. H. Marshall, Chapman & Hall Publishing Company Ltd., London, pp. 334-370.

[90] Chen, T. L. C. & Bert, C. W., (1976), 'Design of composite material plates for maximum uniaxial compressive buckling load', *Proceedings of the Oklahoma academy of Science*, 56, pp. 104-107.

[91] Bert, C. W. & Chen, T. L. C., (1976), 'Optimal design of composite material plates to resist buckling under biaxial compression', *Transactions of the Japan Society for Composite Materials*, 2, pp. 7-10.

[92] Hirano, Y., (1979), 'Optimum design of laminated plates under axial compression'. *AIAA Journal*, 17, pp. 1017-1019.

[93] Hirano, Y., (1983), 'Optimization of laminated composite plates and shells', *Mechanics of Composite Materials: Recent Advances, Proceedings of the IUTAM Symposium on Mechanics of Composite Materials*, 16-19 August 1982, Blacksburg, Virginia, edited by Z. Hashin and C. T. Herakovich, Pergamon Press, New York, pp. 355-365.

[94] Joshi, S. P. & Iyengar, N. G. R., (1982), 'Studies on optimisation, of laminated composite plates', *Proceedings of the 13th Congress of the International Council of the Aeronautical Sciences/AIIA Aircraft Systems and Technology Conference*, 22-27 August, Seattle, Washington, pp. 607-614.

[95] Joshi, S. P. & Iyengar, N. G. R., (1985), 'Optimal design of laminated composite plates under axial compression', *Transactions of the Canadian Society of Mechanical Engineers*, 9, pp. 45-50.

[96] Nakagiri, S. & Takabatake, H., (1986), 'Buckling strength optimization of FRP laminated plates by use of the Hessian matrix', *Computational Mechanics '86, Theory and Applications. Proceedings of International Conference on Computational Mechanics*, edited by G. Yagawa and S. N. Atluri, May 25-29, Tokyo, 2, pp. X71-X76.

[97] Muc, A., (1988), 'Optimal fibre orientation for simply-supported, angle-ply plates under biaxial compression', *Composite Structures*, 9, 161-172.

[98] Hirano, Y., (1979), 'Optimum design of laminated plates under shear', *Journal of Composite Materials*, 13, 329-334.

[99] Housner, J. M. & Stein, M., (1975), 'Numerical analysis and parametric studies of the buckling of composite orthotropic compression and shear panels', *Technical Note*, NASA IN 0-7996, 103 pp.

[100] Grenestedt, J. L., (1991), 'Layup optimization against buckling of shear panels', *Structural Optimization*, 3, pp. 115-120.

[101] Chao, C. C., Koh, S. L. & Sun, C. T., (1975), 'Optimization of buckling and yield strengths of laminated composites', *AIAA Journal*, 13, pp. 1131-1132.

[102] Crouzet-Pascal, J., (1984), 'Buckling analysis of laminated composite plates', *Fibre Science and Technology*, 11, pp. 413-446.

[103] Tang, J., (1984), 'On optimum design of laminated plates and the effect of coupling between bending and extension', *Computational Structural Mechanics and Applications*, 1, pp. 75-84.

[104] Tang, J., (1967), 'On optimum design of laminated plates under bidirectional axial compression', *Acta Mechanica Sinica*, 19, pp. 268-272.

[105] Tang, J., (1989), 'On optimum analysis of laminated plates under shear', *Acta Material Composite Sinica*, 6, pp. 48-55.

[106] Pedersen, P., (1987), 'On sensitivity analysis and optimal design of specially orthotropic laminates', *Engineering Optimization*, 11, pp. 305-316.

[107] Pedersen, P., (1987), 'On sensitivity analysis and optimal design for laminates', *Mechanical Behaviour of Composites and Laminates*, edited by W. A. Green and M. Micunovic, Elsevier Applied Science, London, pp. 274-283.

[108] Grenestedt, J. L., (1990), 'Composite plate optimization only requires one parameter', *Structural Optimization*, 2, pp. 29-37.

[109] Grenestedt, J. L. & Gudmundson, P., (1992), 'Lay-up optimization of composite material structures', *Lay-up Optimization of Composite Structures*, Report No. 92-24, Royal Institute of Technology, Stockholm, Sweden, C1-C32. Paper presented at *IUTAM Symposium on Optimal Design with Advanced Materials*, 18-20 August, Lyngby, Denmark, 16.

[110] Cheng, G. & Tang, J., (1992), 'Optimum design of laminated plates with respect to eigenvalues', Paper presented at *IUTAM Symposium on Optimal Design with Advanced Materials*, 18-20 August, Lyngby, Denmark, 12.

[111] Leissa, A. W., (1987), 'An overview of composite plate buckling', *Composite Structures 4*, edited by I.H. Marshall. Elsevier Applied Science, London, pp. 110-129.

[112] Leissa, A. W., (1987), 'A review of laminated composite plate buckling', *Applied Mechanics Reviews*, Vol. 40, 5, pp. 575-595.

[113] Kassimaly, A., Craddock, N. J. & Matinrad, M., (1986), 'Stability of fibre composite plates with various support conditions', *Proceedings of Inter-*

national Symposium on Composite Materials and Structures, edited by T.T. Loo and C.T. Sun, Technomic Publishing Company, Inc., Lancaster, Pennsylvania, pp. 267-273.

[114] Sawyer, J. W., (1977), 'Flutter and buckling of general laminated plates', *Journal of Aircraft*, 14, pp. 387-393.

[115] Qian, B., Reiss, B. & Aung, W., (1989), 'Optimum single modal and bimodal buckling design of symmetric laminates', *Recent Developments in Buckling of Structures*, edited by D. Hui, V. Birman and D. Bushnell, ASME, New York, New York, pp. 25-29.

[116] Obraztsov, I. F. & Vasil'ev, V. V., (1989), '*Optimal design of composite structures. In Handbook of Composites, Vol.2 - Structures and Design*', edited by C. T. Herakovich and Y. M. Tarnopolskii, North Holland, Amsterdam, pp. 3-84.

[117] Sherbourne, A. N. & Pandey, M. D. (1992), 'Effects of in-plane restraints on the stability of laminated composite plates'. *Composite Structures*, 20, pp. 73-81.

[118] Pandey, M. D. & Sherbourne, A. N., (1991), 'Buckling of anisotropic composite plates under stress gradient', *Journal of Engineering Mechanics*, 117, pp. 260-275.

[119] Srivatsa, K. S. & Krishna Murty, A. V., (1992), 'Stability of laminated composite plates with cut-outs', *Computers and Structures*, 43, pp. 273-279.

[120] Nemeth, M. P., (1988), 'Buckling behaviour of compression-loaded symmetrically laminated angle-ply plates with holes', *AIAA Journal*, 26, pp. 330-336.

[121] Hyer, M. W. & Lee, H. H., (1991), 'The use of curvilinear fibre format to improve buckling resistance of composite plates with central circular holes', *Composite Structures*, 18, pp. 239-261.

[122] Frauenthal, J. C., (1973), 'Initial postbuckling behaviour of optimally designed columns and plates', *International Journal of Solids and Structures*, 9, pp. 115-127.

[123] Pandey, M. D. & Sherbourne, A. N., (1993), 'Postbuckling behaviour of optimized rectangular composite laminates', *Composite Structures*, 23, pp. 27-38.

[124] Haftka, R. T. & Gürdal, Z., (1992), '*Elements of Structural Optimisation*', 3rd Edition, Kluwer Academic Publishers, Dordrecht.

[125] Walker, M. & Adali, S., (1992) 'Maximisation of eigenvalues using finite element methods with applications to the optimal design of laminates', *Proceedings of the Eighteenth South African Symposuim on Numerical Mathematics,* 7-9 July, Durban, pp.107.

[126] Walker, M., Adali, S. & Verijenko, V., (1994) 'Optimal design of laminated composite plates for maximum buckling load subject to in-plane restraints using the FEM', *Proceedings of CADCOMP-94*, 29 June - 1 July, Southampton, UK, pp. 119-128.

[127] Walker, M., Adali, S., Verijenko, V. & McClure, C., (1994) 'Maximisation of eigenvalues for the optimal buckling design of symmetrically laminated composite plates using the finite element method', *Proceedings of the Twenteeth South African Symposuim on Numerical Mathematics,* 15-17 July, Durban, pp.89.

[128] Adali, S., Walker, M. & Verijenko, V., (1994) 'Optimal laminate configurations with symmetric lay-ups for maximum postbuckling stiffness', *Proceedings of the First International Conference on Composites Engineering*, 29-31 August, New Orleans, Louisiana, USA, pp. 345-350.

[129] Walker, M., Adali, S. & Verijenko, V., 'Optimisation of symmetric laminates for maximum buckling load including the effects of bending-twisting coupling', Submitted to *Computers & Structures.*

[130] Narita, Y. & Leissa, A. W., (1990), 'Buckling studies for simply supported symmetrically laminated rectangular plates', *International Journal of Mechanical Science,* 32, 11, pp. 909-924.

[131] Walker, M., Verijenko, V. & Adali, S., (1994), 'Pitfalls in the use of finite element method software to solve practical engineering problems', *Mechanical Technology*, pp. 27-30.

[132] Walker, M., Adali, S. & Verijenko, V., (1993) 'Maximisation of eigenvalues with applications to the optimal design of composite laminates using the finite element method', *Proceedings of the Nineteenth South African Symposuim on Numerical Mathematics,* 12-14 July, San Lameer, pp.177.

[133] Walker, M., Adali, S. & Verijenko, V., 'Optimal design of symmetric angle-ply laminates subject to nonuniform buckling loads and in-plane restraints', Submitted to *Thin-Walled Structures.*

[134] Walker, M., Adali, S. & Verijenko, V., (1994) 'Poisson's effect on the optimal buckling design of composite laminates with bending twisting coupling', *Proceedings of the Third World Congress on Computational Mechanics*, 1-5 August, Chiba, Japan, Vol. 2, pp. 1124-1125.

[135] Walker, M., (1994), 'Maximisation of eigenvalues with applications to the optimal buckling design of symmetrically laminated plates, *Proceedings of the Sixth Natal-KwaZulu Mathematics Conference*, 7-9 May, Durban, pp. 21-30.

[136] Walker, M., Adali, S. & Verijenko, V., (1993) 'Design optimisation of laminated composite plates using the finite element method', *Proceedings of FEMSA'93 - The Twelfth Symposuim on Finite Element Methods in South Africa,* 7-9 July, Pretoria, pp. 78-81.

[137] Chia, C. Y., (1980), '*Nonlinear Analysis of Plates'*, McGraw-Hill, New York, New York.

[138] Walker, M., Adali, S. & Verijenko, V., 'Optimal design of laminated composite plates with central cut-outs for maximum buckling load using the FEM', to be presented at *FEMSA'95 - The Thirteenth Symposuim on Finite Element Methods in South Africa.*

[139] Adali, S., Walker, M. & Verijenko, V., 'Optimal laminate configurations with symmetric lay-ups for maximum postbuckling stiffness', To appear in *Composites Engineering.*

[140] Bartholomew, P., (1977), 'Ply stacking sequences for laminated plates having in-plane and bending orthotropy', *Fibre Science and Technology,* 10, pp. 239-254.

[141] Walker, M. & Adali, S., 'Optimal design of symmetric laminates for a maximum combination of prebuckling and postbuckling stiffness and buckling load', *In preperation.*